UNIVERSITÀ
DEGLI STUDI
DI PADOVA

Sede Amministrativa: Università degli Studi di Padova

Dipartimento **TERRITORIO E SISTEMI AGRO-FORESTALI**

SCUOLA DI DOTTORATO DI RICERCA IN:

"TERRITORIO, AMBIENTE, RISORSE E SALUTE"

CICLO: XXVI

HYDROLOGIC CONTROL ON THE TRIGGERING AND MAGNITUDE OF DEBRIS FLOWS IN ALPINE CATCHMENTS

Direttore della Scuola: Ch.mo Prof. Mario Aristide Lenzi

Supervisore: Dr. Lorenzo Marchi

Co-supervisore: Ch.mo Prof. Marco Borga

Dottorando: Stefano Crema

...to whom
in Heaven and on Earth
has made possible
all this...
...and to those
who transmit passion
for research...

Riassunto

Il presente lavoro ha analizzato le condizioni idrologiche associate all'innesco di colate detritiche in una regione alpina.
L'analisi è stata suddivisa in due rami principali: la prima parte è stata effettuata a scala regionale e decennale (2000-2010) per approfondire le tematica delle soglie pluviometriche per l'innesco di colate e delle incertezze legate alla determinazione della pioggia nelle zone di innesco delle colate detritiche. Si è cercato, inoltre, di caratterizzare, dal punto di vista morfometrico, le zone di innesco delle colate stesse. Uno studio approfondito è stato dedicato successivamente all'analisi della risposta idrologica di alcuni bacini, per tre eventi di piena avvenuti fra il 2006 ed il 2009
L'area di studio è l'intera Provincia Autonoma di Bolzano (Alto Adige, Nord Italia). Tale area occupa una nicchia idrometereologica peculiare, caratterizzata da un'elevata frequenza di fenomeni temporaleschi con forzante orografica, che, specialmente nel periodo estivo, possono attivare colate detritiche e piene improvvise.

La caratterizzazione morfometrica dei siti di innesco è stata effettuata esaminando l'area contribuente e la pendenza locale dei punti stessi. La caratterizzazione è stata effettuata dividendo il dataset in classi di durata di precipitazione, introducendo ulteriori filtri sull'intensità di pioggia e considerando anche la relazione con le principali litologie.
Un'altra questione in esame è legata alla stima di soglie pluviometriche per l'innesco di colate detritiche unitamente all'incertezza legata a questa stima.
In primo luogo, un insieme di soglie pluviometriche è stato derivato mediante un approccio frequentista. La procedura di stima di precipitazione per l'identificazione della soglia è basata su due fattori principali: dato del pluviometro più vicino e una interpolazione (Inverse Distance) di tutti i dati orari disponibili a scala regionale e decennale. Le soglie sono state analizzate prendendo in considerazione tutti i punti disponibili ed anche cercando di raggrup-

pare i fenomeni di colata in base alla stagionalità, alle diverse caratteristiche dell'evento meteorico ed in base a zone geologicamente omogenee.
Il livello di incertezza relativo alla stima di soglie di pioggia è stato analizzato in dettaglio. Il problema della stima di risulta essere particolarmente importante proprio a causa della posizione delle zone di innesco di colate detritiche, con pluviometri che sono comunemente situati a bassa quota (e.g., nei fondovalle) e colate detritiche che hanno origine ad altitudini elevate, nella parte di testata di bacini montani.
La procedura di stima di precipitazioni adottata per la valutazione dell'incertezza, è quella basata sull'utilizzo del pluviometro più vicino, che viene considerato come *proxy* per stimare la pioggia innescante sul sito di colata.
L'obiettivo è quello di studiare l'impatto dell'incertezza insita nella stima delle precipitazioni sulla definizione di una soglia per l'innesco di colate detritiche, e l'uso operativo della soglia per scopi di previsione. Due sono le condizioni che maggiormente influenzano l'icertezza di stima: la variabilità spazio temporale delle precipitazioni e le distanze tra le zone d'innesco ed i relativi pluviometri più prossimi sia sul piano orizzontale che sul piano verticale. Tre sono gli effetti principali considerati: (i) l'effetto del campionamento delle precipitazioni sulla stima dei parametri del modello di soglia, (ii) l'effetto dell'applicazione di una serie di procedure per filtrare le informazioni di precipitazione sul modello di stima della soglia, e (iii) l'incidenza del campionamento della precipitazione sulle performance della soglia come predittore di accadimento di colate. Questi aspetti vengono esaminati mediante una simulazione condotta a scala regionale.
La metodologia adottata esamina le soglie di intensità-durata mediante la selezione di una serie di pluviometri che si assumono rappresentare un sito di innesco di colata, denominati DFR, ed una serie di pluviometri prossimi a questi (in rapporto 1:1), denominati MR, che vengono usati per stimare la precipitazione sul sito DFR. Una serie di soglie pluviometriche di riferimento viene utilizzate per identificare gli eventi di precipitazione che "innescano" colate detritiche su DFR (cioè eventi che superano la soglia). Per questi stessi eventi, le corrispondenti soglie pluviometriche sono derivate da osservazioni MR. Il

confronto tra le soglie pluviometriche derivate da DFR e MR, ha rivelato che l'incertezza nella stima di precipitazione ha un impatto importante sulle soglie di intensità-durata. In particolare, i risultati hanno mostrato che le soglie stimate dalle osservazioni MR presentano stime in difetto. La valutazione delle soglie stimate per procedure di allarme, ha mostrato che, mentre la probabilità di rilevamento è alta, il problema principale è l'elevato rapporto di falsi allarmi, che limita la precisione complessiva del procedimento. Le performance generali sulla previsione di colate detritiche si sono dimostrate buone per soglie pluviometriche moderate e scarse per soglie elevate.

Infine, diverse tecniche di interpolazione sono state applicate ad una selezione di pluviometri prossimi al DFR per valutare l'eventuale miglioramento portato dagli interpolatori. I risultati hanno dimostrato che l'interpolazione può migliorare le stime, in particolare i miglioramenti più significativi si sono notati nei casi di correlazione debole tra DFR e MR, mentre per gli altri casi ed in particolare considerando eventi intensi e/o localizzati, i benefici derivanti dal considerare i valori interpolati rispetto al valore del pluviometro più prossimo non sono così significativi.

Nella seconda parte della tesi viene esaminata la forzante idrometeorologica ed idrologica relativa all'innesco di colate, attraverso l'analisi dei tre eventi meteorici avvenuti il 3-4 ottobre 2006, 20-21 giugno 2007 e 3-4 Settembre 2009 per capire come la variabilità meteorologica si rifletta nelle diverse risposte dei bacini. Il primo evento ha generato infatti piene improvvise di modesta intensità lungo le aste torrentizie principali con quasi nessuna colata registrata nei corsi d'acqua secondari, il secondo ha innescato un gran numero di colate in bacini secondari ed è stato caratterizzato da una risposta idrica minore nei collettori principale, il terzo ha visto sia piene improvvise importanti che colate detritiche diffuse. Tali eventi sono stati studiati utilizzando dati di pioggia calibrati da radar sul singolo evento, fornendo un input importante per la calibrazione di un modello idrologico distribuito, ed utilizzando inoltre informazioni derivanti dall'analisi di un ampio database di fenomeni di instabilità (incluse le colate detritiche) che copre l'intero territorio provinciale e che viene mantenuto costan-

temente aggiornato. L'integrazione di dati radar e da rete pluviometrica, dati di portata, informazioni spaziali e volumetriche sugli eventi di colata assieme ad osservazioni sul campo sono usati, unitamente al modello idrologico distribuito, per analizzare le risposte idrologiche e geomorfologiche agli eventi innescanti. Il forte contrasto in termini di risposta idrica ed effetti morfologici fra le tre piene risulta legato a differenze nelle condizioni di umidità antecedenti e nella struttura spazio-temporale degli eventi innescanti. La modellazione afflussi-deflussi ha permesso la stima e di portate al picco e di volumi di deflusso in una serie di piccoli bacini non strumentati in cui i volumi depositati dalle colate sono stati stimati mediante indagini post-evento. Il calcolo della concentrazione volumetrica di sedimento eseguito utilizzando i risultati dell'approccio di modellazione scalato ai bacini da colata ha portato a valori realistici. Le relazioni tra portate al picco e volumi mobilizzati dalle colate mostrano coefficienti di correlazione più elevati di quelli che considerano le variabili morfometriche ed i volumi di precipitazione.

Summary

The present work analyzes the hydrologic conditions leading to the triggering of debris flows in an alpine region.
The overall analysis has been split in two parts: the first part of the analysis has been carried out at a regional and decadal scale to improve our knowledge of rainfall thresholds for debris-flow occurrences, of the uncertainty related to rainfall estimation at debris-flow initiation sites, and of the main morphometric characteristics of debris-flow triggering locations; in the second part a focus has been devoted to the analysis of the hydrologic response of some watersheds for a selection of events with the help of detailed input information, both topographic and hydrological.
The study area is upper Adige River basin (Northern Italy), which occupies a distinctive hydrometeorological niche, characterized by high frequency of orographic thunderstorms.

The first part of the thesis analyzes the debris-flow triggering issue at regional and decadal-scale (2000-2010).
A morphometric characterization of debris-flow triggering locations has been carried out in terms of slope-area analysis. The characterization was carried out dividing considered debris flows in classes of rainfall duration, rainfall intensity and considering also the potential relation with the different geologic settings.
Another issue under investigation is related to rainfall threshold estimation (from raingauges network) for debris-flow occurrence and the uncertainty related to this estimation.
First, a set of rainfall thresholds has been derived adopting a frequentist approach. The rainfall estimation procedure used for threshold identification was based on two major sources: records from the nearest gauge and an Inverse Distance interpolation of all the available records at regional and decadal scale. Thresholds have been analyzed considering all the available points and also trying to group debris-flow occurrences according to seasonal occurrence, different storm characteristics and homogeneous geologic setting.
The level of uncertainty related to rainfall threshold estimation has been analyzed in detail The estimation problem is especially severe for the location of the debris flows, with raingauges that are commonly located at low elevation (e.g., in the valley floors) and debris flows that originate at high elevations, in the head part of the mountain catchments.
The rainfall estimation procedure used for the uncertainty assessment, is the one based on the nearest raingauge, which is used as a proxy to estimate the rainfall that has resulted in debris flows.
The objective is to investigate the impact of the uncertainty inherent in the estimation of rainfall on the definition of a threshold for possible debris-flow occurrence, and on the operational use of the threshold for prediction purposes. These effects are likely to depend on two factors: the space-time rainfall variability and the distances between the debris-flow locations and the raingauges

on both the horizontal and the vertical planes. Three main problems are considered: (i) the effect of the rainfall sampling problem on the estimation of the parameters of the threshold model, (ii) the effect of applying a number of procedures to filter the rainfall information on the threshold model estimation, and (iii) the examination of the impact of the precipitation sampling problem on the performance of the threshold as a predictor of debris-flow occurrence. These aspects are examined here based on a simulation experiment.
The methodology examines the intensity-duration thresholds derived from a set of raingauge locations that is assumed to represent debris flow/landslide points (DFR) and an equivalent set of raingauges assumed to have the role of closest available measurement (MR). A set of reference rainfall thresholds is used to identify the rainfall events at DFR that "triggered debris flows (i.e. exceed the threshold). For these same events, the corresponding rainfall thresholds are derived from MR observations. Comparison between the rainfall thresholds derived from DFR and MR, revealed that uncertainty in rainfall estimation has a major impact on estimated intensity-duration thresholds. Specifically, results showed that thresholds estimated from MR observations are consistently underestimated. Evaluation of the estimated thresholds for warning procedures, showed that while detection is high, the main issue is the high false alarm ratio, which limits the overall accuracy of the procedure. Overall performance on debris-flow prediction was shown to be good for low rainfall thresholds and poor for high rainfall thresholds examined.
Finally different interpolation techniques have been applied to a set of gauges close to the DFR to assess the eventual improvement brought by the interpolation procedure. Results on this showed that interpolation can improve estimates specifically in the case of poor DFR-MR correlation, while in the other cases, especially considering intense and/or localized storms, the benefits of considering interpolated value in respect to only one near gauge is not so significant.

In the second part of the thesis the hydrometeorological and hydrological controls of these events are examined through analyses of three storm systems occurred on October 3-4, 2006, June 20-21 2007 and September 3-4, 2009. The

first storm system generated a moderate flash flood along the main streams with almost no debris flows in the tributaries, the second triggered a large number of debris flows and was characterized by a minor runoff response for the major streams, and the third resulted in both a relevant flash flood response and widespread debris flows. These events have been examined by using per-event calibrated radar rainfall data, providing an important input for the evaluation of a distributed hydrological model, and by using a database reporting location and information related to the events. Raingauge and streamflow data, debris flow spatial information and observations are used along with the distributed model to analyze the hydrological and geomorphic responses to these rainstorms. The striking contrast in flood and geomorphic responses between the three floods is related to contrasts in the antecedent moisture conditions and in the space-time structure of the triggering storm. Rainfall-runoff modeling has permitted estimating discharge and runoff volumes in a number of small ungauged catchments in which debris-flow volumes had been assessed by means of just-post-event surveys. The computation of sediment concentration by volume using model-estimated water runoff has resulted in realistic values. The relations between water peak discharge and debris-flow volumes show higher correlation coefficients than those involving morphometric variables and rainfall amounts.

Index

1 Introduction

1.1 Debris flows: general features and triggering conditions

Debris flows are commonly recognized as geomorphic processes strongly influencing and shaping the mountain territory. In inhabited regions, debris flows constitute a serious risk for the population. Iverson et al. (1997) describes debris flows as *"masses of poorly sorted sediment, agitated and saturated with water, surging down slopes in response to gravitational attraction"*. Another attempt at the definition of debris flows is the following: *"Debris flows are gravity-driven torrential paroxysmal mass movements, mainly concentrated at steep stream channels"* (Scheidl et al., 2013).

Debris flows typically occur in steep and small mountainous catchments. A debris flow starts within an initiation zone, evolves down along the transportation zone and accumulates the transported material in the deposition zone, often corresponding to an alluvial fan (Fig. 1.1).

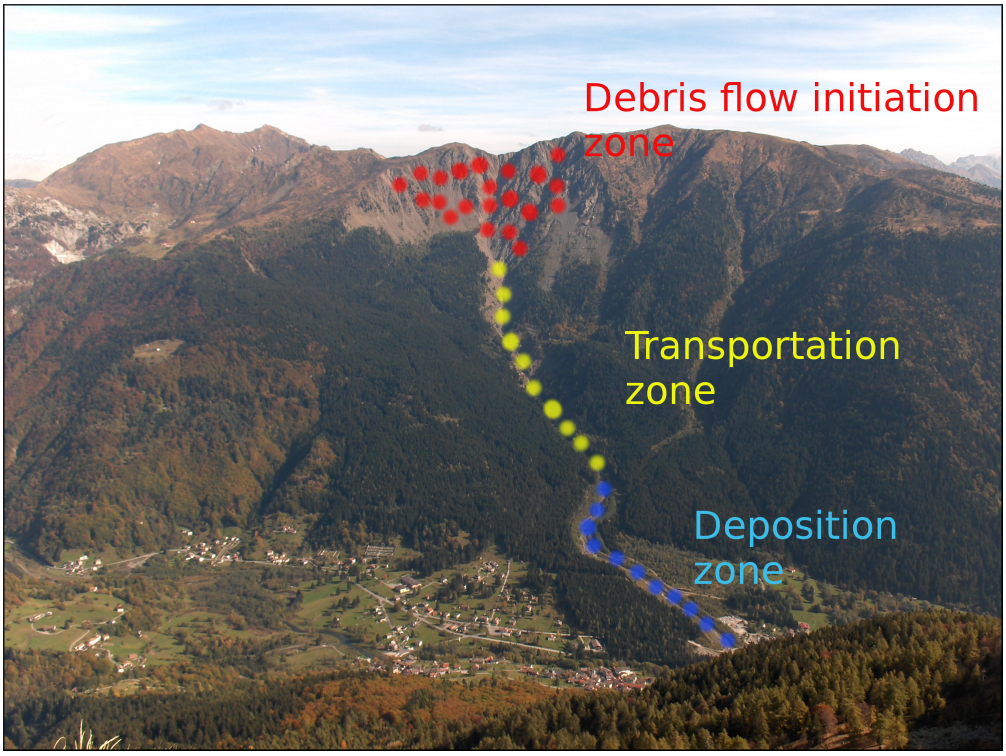

Figure 1.1: Zones of a debris-flow process within a catchment. The figure gives an overview of the Moscardo Torrent basin (Carnic Alps, Northern Italy). *Courtesy of: Michela Dini*

The volumes of the largest debris flows may attain some hundred thousand or millions of cubic meters. In debris flows, the coarse sediment is usually concentrated in the upper layers and at the front of the flow. Prerequisite conditions for most debris flows include an abundant source of unconsolidated fine-grained rock and soil debris, steep slopes, a large source of water, and sparse vegetation (Costa, 1984). The front of a debris-flow can reach velocities up to 30 m/s (Costa, 1984; Rickenmann, 1999) and peak discharges tens of times greater than for floods occurring in the same catchment (Hungr et al., 1984). The flow is characterized as unsteady and non-uniform, and typically

debris flows occur in one or several surges. In order to define the granular and fine phases characterizing a debris-flow, Fig. 1.2 shows the phase diagram for torrential mass movements including the competence area of debris flows and indicating the fine component, the coarse component and the water content of most typical debris flows.

Figure 1.2: Phase diagram of mass movements, modified after Phillips and Davies (1991)

Another well-known classification scheme is provided by Coussot and Meunier (1996). The classification regards in general *"mass movements and flows occurring on natural steep slopes"* (Coussot and Meunier, 1996).Two main criteria are take in consideration:

- the solid fraction type

- the solid (volume or weight) fraction

Fig. 1.3 summarizes, it the form of an ellipse, the limits, conceptual and qualitative.

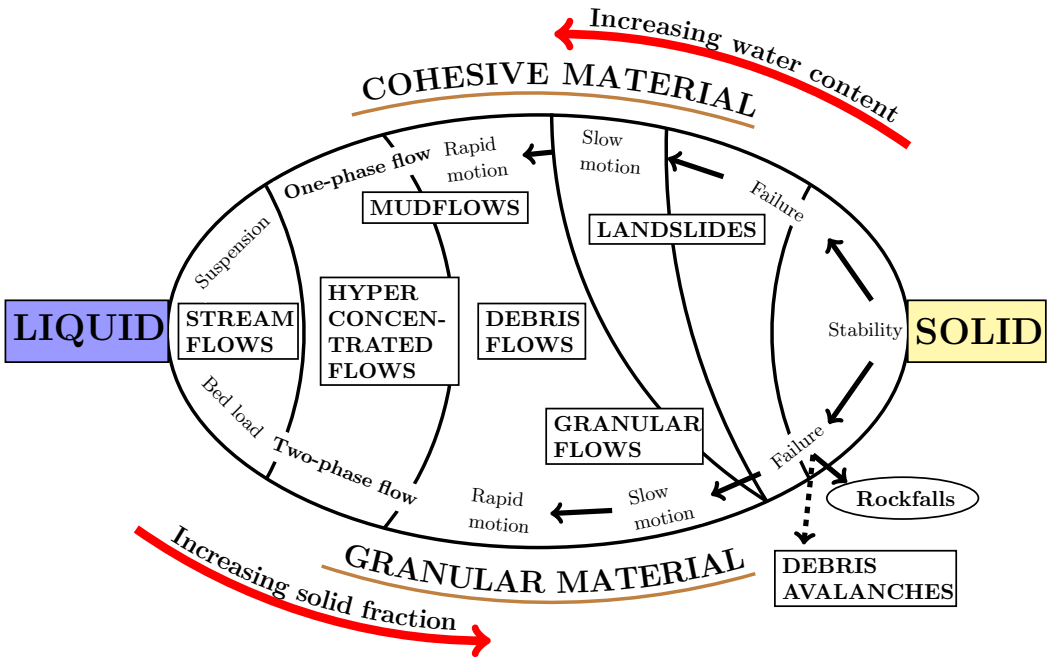

Figure 1.3: Coussot-Meunier flow classification diagram divided into solid and water content, reconstructed and modified after Coussot and Meunier (1996).

Among many other different classification criteria the size classification method (Jakob, 2005) is herein reported (Tab. 1).

Table 1: Size classification for debris flows from Jakob (2005)

Size class	V, range (m^3)	Q_b, range (m^3/s)	Q_v, range (m^3/s)	B_b (m^2)	B_v (m^2)	Potential consequences
1	$<10^2$	<5	<1	$<4\times10^2$	$<4\times10^3$	Very localized damage, known to have killed forestry workers in small gullies, damage small buildings
2	10^2–10^3	5–30	1–3	4×10^2–2×10^3	4×10^3–2×10^4	Could bury cars, destroy a small wooden building, break trees, block culverts, derail trains
3	10^3–10^4	30–200	3–30	2×10^3–9×10^3	2×10^4–9×10^4	Could destroy larger buildings, damage concrete bridge piers, block or damage highways and pipelines
4	10^4–10^5	200–1500	30–300	9×10^3–4×10^4	9×10^4–4×10^5	Could destroy parts of villages, destroy sections of infrastructure corridors, bridges, could block creeks
5	10^5–10^6	1500–12,000	300–3×10^3	4×10^4–2×10^5	4×10^5–2×10^6	Could destroy parts of towns, destroy forests of 2 km^2 in area, block creeks and small rivers
6	10^5–10^6	N/A	3×10^3–3×10^4	$>2\times10^5$	2×10^6–3×10^7	Could destroy towns, obliterate valleys or fans up to several tens of km^2 in size, dam rivers
7	10^6–10^7	N/A	3×10^4–3×10^5	N/A	3×10^7–3×10^8	Could destroy parts of cities, obliterate valleys or fans up to several tens of km^2 in size, dam large rivers
8	10^7–10^8	N/A	3×10^5–3×10^6	N/A	3×10^8–3×10^9	Could destroy cities, inundate large valleys up to 100 km^2 in size, dam large rivers
9	10^8–10^9	N/A	3×10^6–3×10^7	N/A	3×10^9–3×10^{10}	Vast and complete destruction over hundreds of km^2
10	$>10^9$	N/A	3×10^7–3×10^8	N/A	$>3\times10^{10}$	Vast and complete destruction over hundreds of km^2

V is the total volume, Q_b and Q_v are the peak discharge for bouldery and volcanic debris flows, respectively, B_b and B_v are the area inundated by bouldery and volcanic debris flows. N/A signifies that bouldery debris flows of this magnitude have not been observed. The constant in Eq. (2) was rounded so that B by non-volcanic debris flows is 10 times smaller than that of volcanic debris flows.

The above-mentioned method classifies debris flows using the total deposited volume V, peak discharge Q (for bouldery or volcanic debris flows) and the inundated area B.

1.2 Hydrologic triggering of debris flows

Intense rainstorms and rapid ice/snowmelt can be considered primary climatic factors while antecedent or pre-event rainfall conditions are usually seen as secondary climatic factors for debris-flow initiation (Jakob, 2005).
It is generally recognized that a combination of hydrologic, topographic and material properties factors is required for debris flow to happen (Fig. 1.4), in this work, the rainfall triggering of debris flows has been the purpose of intensive study. Researches have included assessments of empirical relations between debris-flow occurrence and rainfall causing slope failures.
Even though shallow slope failures may be caused under wholly unsaturated conditions by infiltration that increases the soil weight or decreases the ambient soil moisture suction (Brand, 1981), most studies point out that debris flows result from development of positive pore pressures in locally saturated conditions. Positive pore pressures in hillslope soil can develop by two means; direct infiltration of water at the slope surface, and groundwater inflow from the neighboring soil or rock. Infiltration generally involves unsaturated flow in vertical direction, though lateral unsaturated flow may rearrange the moisture. Side inflow may occur by saturated groundwater flow from adjacent materials. An inclined water table, topographic convergence, and other factors can help direct the saturated flow laterally (Anderson and Burt, 1978).

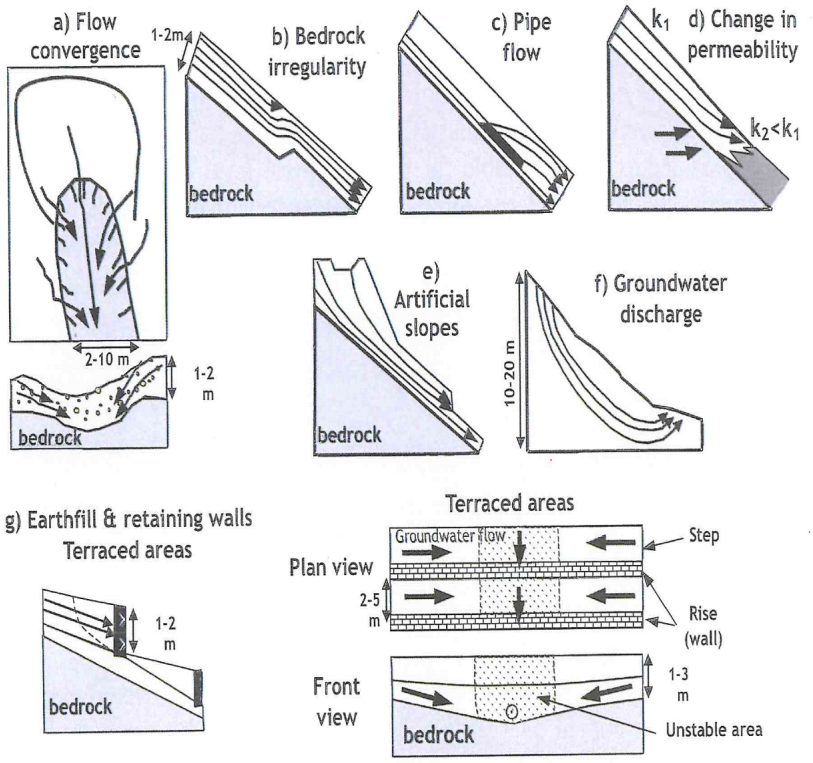

Figure 1.4: Sketches of the main morphological and hydrological conditions connected with soil slips, from Crosta and Frattini (2001)

Antecedent soil moisture condition needs to be included into the hydrologic factors in order to modify soil pore pressure. Antecedent soil moisture influences indeed strength characteristic of the soil and determines the quantity of water needed to saturate the terrain profile, so it directly affects slope stability. While rainfall measurements are quite simple to obtain, soil moisture is usually derived by means of indirect estimations. Antecedent total rainfall, piezometric levels, water discharge in neighboring streams (Jakob and Weatherly, 2003), have been use as proxies of antecedent soil moisture. Noteworthy is one of the first attempt to parameterize antecedent soil moisture (AMC) made by US Soil Conservation

Service (USSCS) in 1965 (Tab. 2). In that work AMC was classed into three groups in relation to rainfall cumulated value of the 5-days antecedent period.

Table 2: US-SCS Antecedent moisture conditions classification from USSCS, (1956)

AMC group	**Total 5-day antecedent rainfall (mm):**	
	Dormant season	Growing season
I	Less than 13	Less than 36
II	13 to 28	36 to 53
III	More than 28	More than 53

Nowadays the understanding of hydrologic conditions leading to debris-flow initiation has been greatly improved as a result of the direct and/or instrumental assessment of the soil moisture and of the pore pressure. Tensiometers with electronic pressure transducers and soil moisture probes for example are common instrumentation to be set in experimental catchments nowadays (Coe et al., 2008).

The traditional explanation of pore-pressure generation of hillslope holds that for a uniform slope a saturated zone first develops at the base of the slope and progresses upward with continued rainfall. According to this description failures would be most likely to occur in the lower part of the basin but evidences and common experience show that failures initiate high on hillslopes. In fact near ridge top areas and convex-concave slope transition areas particularly critic regions because of their tendency to become locally saturated. Once saturated, if no cohesive forces (e.g. roots) help in hillslope stabilization these slopes start to fail.

Different geomorphological features terrain variability or human induced modifications, can help causing soil slips or debris flow to initiate.
Typically, in the field, three main conditions for triggering of debris flows can be found (Godt and Coe, 2007, and references therein), in particular debris flows originated by:

- Shallow landslides
- Rilling
- "Firehose effect"

Initiation by shallow landsliding Debris flows can be mobilized from shallow landslides on steep hillslopes. The mechanisms by which rainfall permeation initiates shallow landslides have been exhaustively investigated (e.g., Iverson et al. (1997)). Debris flows generated from shallow landslides are generally coupled with colluvial depressions on steep slopes. Shallow landslides mobilize as debris flows and travel downslope.

Initiation by rilling Debris flows can initiate as single rills or as a system of coalescing rills on unvegetated hillslopes underlaid by noncohesive materials. Often downslope from the system of rills, single channels or gullies can be eroded into the surface.
Gullies are generally deeper and wider than the rills. Rills are typically small and have widths and depths of a few tens of centimeters (Coe et al., 2008). Rill formation is generally attributed to the concentration of overland flow in microchannels. The concentration of overland flow increases the flow depth and thus the component of shear stress acting parallel to the slope mobilizing loose

sediment. Slight variations in hillslope topography play an important role in localizing rill formation and in the subsequent creation of a series of alternating benches and steps, or plunge pools, in the rill channel. The formation of rill channels takes place by erosion and deepening of plunge pools by turbulent flow (Cannon et al., 2001) upslope progression of the headwalls of plunge pools, (Johnson and Rodine, 1984) and bank failures.
Experimental results (Godt and Coe, 2007) showed that erosion and sediment transport by rainfall and overland flow on hillslopes occurred over a continuum of water-solid concentrations ranging from clear-water flow, to concentrated, and hyperconcentrated bed load and suspended flow, to debris-flow. Debris flows temporarily dammed rill channels, creating new rills or plunge pools, and quickly changed to hyperconcentrated flows when mixed with additional water from overland flow. Debris-flow initiation from rilling is common on steep hillslopes where vegetation has been recently burned by wildfire (Johnson and Rodine, 1984; Cannon et al., 2001, 2011).

Initiation by "firehose effect" Debris flows can be also initiated by what Johnson and Rodine (1984) have termed the "firehose effect ". The firehose effect is caused by the mobilization of material by a concentrated flow of water, just as if the material had been washed away by a "firehose "(Johnson and Rodine, 1984; Coe et al., 1997; Gregoretti and Dalla Fontana, 2008). Eyewitness accounts in both the Colorado Rocky Mountains Johnson and Rodine (1984) and the Dolomites of Italy (Simoni, 2005) describe the firehose process as the concentration of surface flow in steep rocky headwaters channels that impact loose debris. Field observations in the Dolomites showed that debris flows were generated by the progressive entrainment of surface water with loose debris from

the channel bed (Simoni, 2005). Material was then transported as a debris-flow, the deposit of which came to rest in the channel, blocking it. The debris dam was breached creating another debris-flow that scoured the channel and entrained moredebris as it flowed.

1.2.1 Rainfall triggering

As stressed above, rainfall is recognized as one of the most important triggering factors for debris flows. Due to complexity, variability in time and space and scale dependency of factors, the distribution of intense precipitations (Norbiato et al., 2007) and their effects in generating soil slips and debris flows is still matter of research.

A common goal of debris-flow research is to improve the ability to forecast the occurrence of the events in space and time. Susceptibility maps and models are used to estimate where debris flows are likely to occur (Borga et al., 2002; Guzzetti et al., 2005; Baum et al., 2010), while rainfall thresholds are determined to define the meteorological conditions that, when reached or exceeded, are likely to result in debris flows (e.g., Caine, 1980; Wieczorek, 1996; Cannon and Gartner, 2005; Guzzetti et al., 2008; Jakob et al., 2012). Rainfall thresholds can be defined adopting physical (process-based, conceptual) or empirical (historical, statistical) approaches (Aleotti, 2004; Wieczorek and Glade, 2005; Guzzetti et al., 2007, 2008; Schneuwly-Bollschweiler and Stoffel, 2012; and references therein), and most commonly take the form of a simple relationship linking rainfall duration to other measures of rainfall, including rainfall intensity or event-cumulated rainfall (Aleotti, 2004; Guzzetti et al., 2007). Usually, rainfall thresholds for the possible initiation of landslides are minimum thresh-

olds i.e., they correspond to a low level above which the process may take place (Reichenbach et al., 1998). Following the pioneering works of Caine (1980) and Innes (1983), rainfall thresholds for debris-flow occurrence have been determined at the local, regional, and global scales (Guzzetti et al., 2008, and references therein).
In literature (Crosta and Frattini, 2001) different types of rainfall related variables are presented, in particular:

- Cumulative rainfall data
- Maximum rainfall intensity for the duration of the event
- Rainfall intensity at the slope failure moment
- Event mean rainfall intensity or intensity calculated at different time intervals
- Antecedent precipitation for different time intervals before the occurrence of the event
- Rainfall data (cumulative or intensity) normalized with respect to the mean annual precipitation of the area

The normalization phase, especially in local scale study areas, is a fundamental step so as to take into account the orographic effect on precipitation regime especially in mountainous regions. The choice of maximum intensity rather than mean intensity or duration strongly influences the events analysis since, as Crosta and Frattini (2001) stress that: *"Maximum intensity refers to limited time intervals during rainfall events, usually, close to the time of the event. As a consequence they tend to underestimate the total amount of rainfall needed*

to trigger the slope failures. On the other hand, intensity values for the whole event cannot describe the presence of short duration-high intensity sub-intervals or bursts". The typical Intensity-Duration equation form is expressed:

$$I = \alpha D^{-\beta} \tag{1}$$

In which I is rainfall intensity, α and β are parameters and D is the duration of the event. Guzzetti et al. (2008) (Fig. 1.5) collected a worldwide database on the rainfall thresholds for the initiation of landslides and debris flows and proposed updated ID (Intensity-Duration) threshold functions.

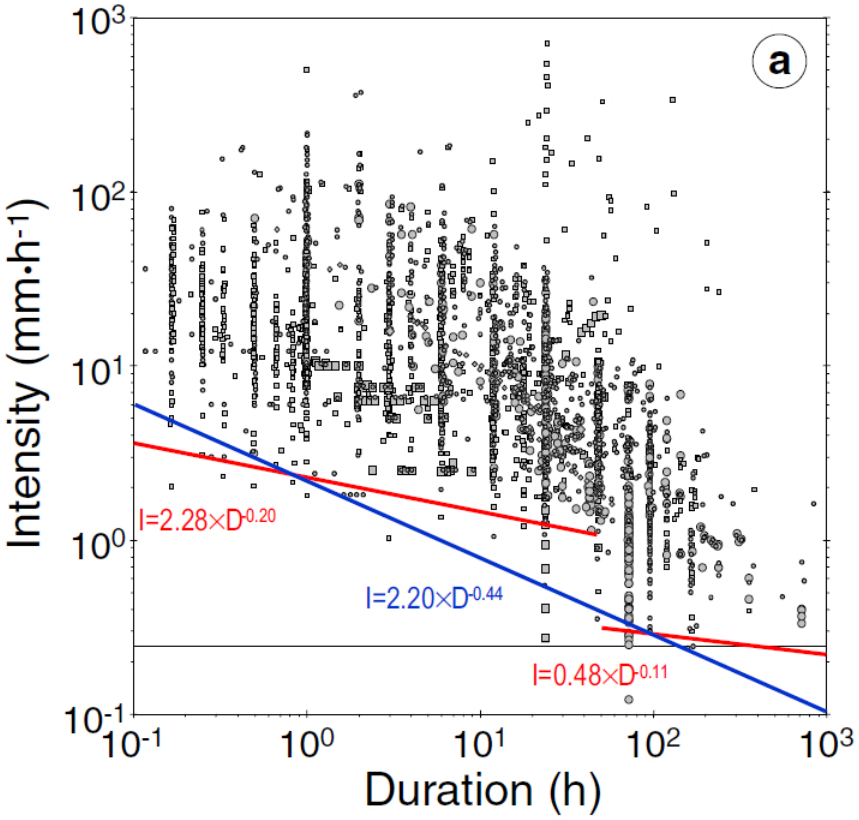

Figure 1.5: Global rainfall ID thresholds for the initiation of shallow landslides and debris flows, from Guzzetti et al. (2008).

With the aim of obtaining climatic differentiated thresholds so as to improve correlations, in the same work Guzzetti et al. (2008) propose also rainfall thresholds for different climatic settings (Fig. 1.6).

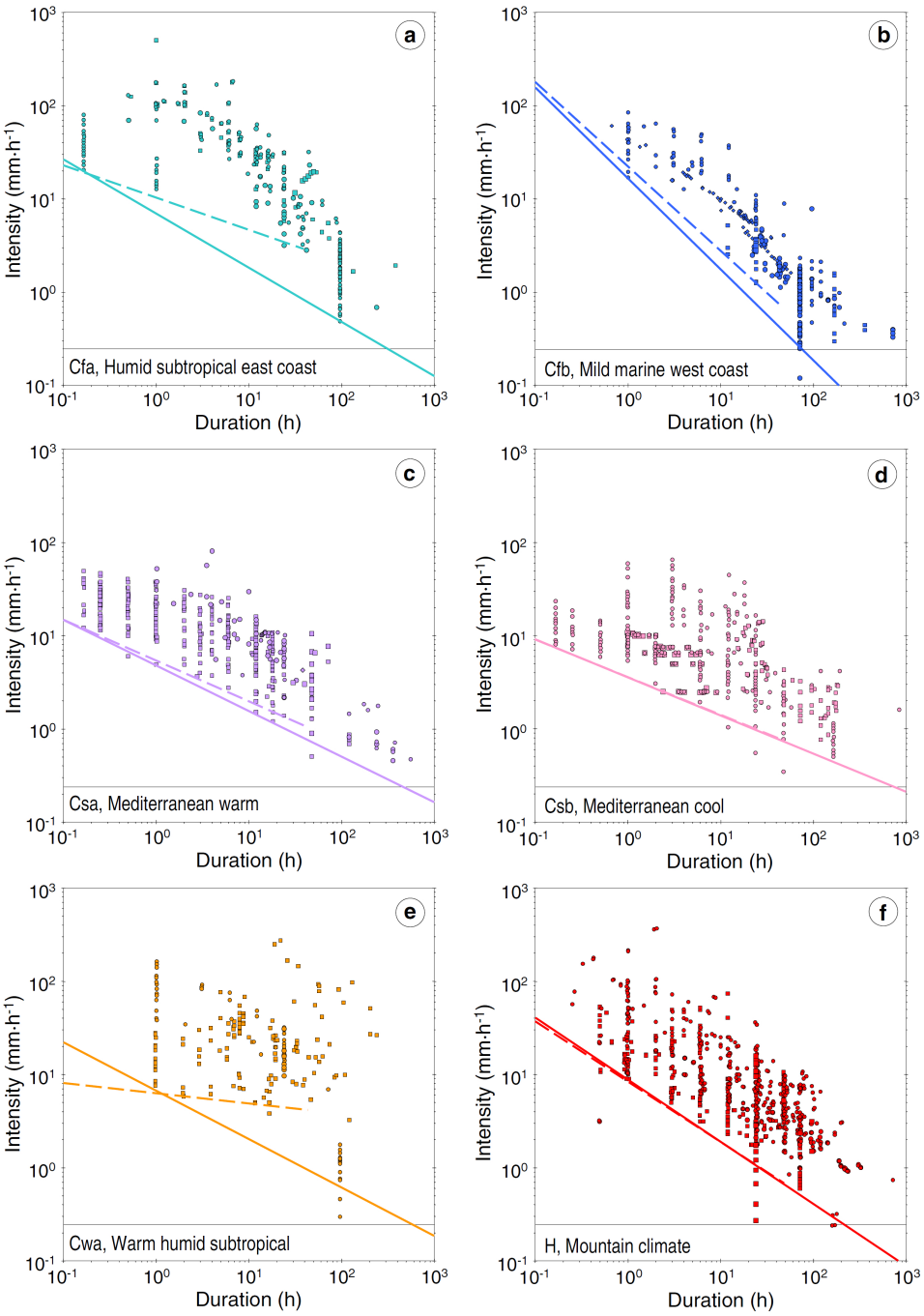

Figure 1.6: Global rainfall ID thresholds for the initiation of shallow landslides and debris flows divided for different climatic areas, from Guzzetti et al. (2008)

The general acceptance of rainfall thresholds for debris-flow forecasting and warning emerges from the considerable literature proposing rainfall thresholds (e.g., Jibson, 1989; Jakob et al., 2012; Aleotti, 2004; Cannon and Gartner, 2005; Guzzetti et al., 2007, 2008; Jakob et al., 2012, and references therein). Despite the popularity, the definition and exploitation of rainfall thresholds for forecasting of the possible occurrence of debris flows is hampered by uncertainties, the sources of which remain largely undetermined. A common problem with the operational use of rainfall thresholds for debris flows is the occurrence of false positives (i.e., rainfall conditions that should have resulted in landslides that were not reported) and false negatives (i.e., rainfall conditions that should have not resulted in landslides that were reported) (Staley et al., 2013). A high False Alarm Rate (i.e., the fraction of forecasted events that did not occur) may reduce the public willingness to respond to the warnings (Staley et al., 2013), but it is unavoidable given the large uncertainties inherent in the threshold-based forecasting of debris-flow occurrence. In part, this uncertainty is associated to the fact that rainfall is not the only causative factor for debris-flow initiation. Other factors play a role, including hydrologic, geologic and climatologic conditions, introducing variability in the thresholds. Investigators have recognized the issue, and recent efforts were made to quantify the dependence of rainfall thresholds on hydrologic and geologic factors (Peruccacci et al., 2012; Berti et al., 2012).

A recognized component of the uncertainty associated with the estimation and use of rainfall thresholds for debris-flow forecasting is related to the large spatial and temporal variability of the precipitation. Surprisingly, although rainfall estimation uncertainty was long recognized as an important factor in definition of the thresholds (Caine, 1980), no studies so far have explicitly investigated

its effect on the estimation of the thresholds. The rainfall that triggers single or multiple debris flows is generally unknown, due to the lack of raingauges at the exact location where the slope failures occur. The amount of rainfall resulting in debris flows is most often estimated based on data from the neighboring raingauges. Recently and with an increasing trend, weather radar and satellite-based rainfall estimates are being used in threshold model estimation (Rossi et al., 2012). The raingauge-based estimates may be affected by significant uncertainties (including biases), especially when the spatial variability of the rainfall is large. This is a particularly severe problem in orographically complex regions. Accounting for the large variability of rainfall in mountainous areas is challenging even for modern raingauge networks. In the Alps, where dense networks of raingauges are available, the typical spacing between the single gauging stations and the debris-flow locations is typically between 4 and 15 km. However, in these areas the distribution of the triggering rainfall varies considerably at length scale smaller than 5 km (e.g. Panziera et al., 2011). The estimation problem is especially severe for the location of the debris flows, with raingauges that are commonly located at low elevation (e.g., in the valley floors) and debris flows that originate at high elevations, in the head part of the mountain catchments (Stoffel et al., 2011).

The literature on rainfall thresholds reports little information on the rainfall observations and rainfall estimation procedures used to derive the thresholds. A rainfall estimation procedure that was often used for the purpose of rainfall threshold identification is the one based on the nearest raingauge. In this procedure, the rainfall measured at the nearest raingauge is used to estimate the rainfall that has resulted in debris flows (Jakob and Weatherly, 2003; Jakob et al., 2012; Brunetti et al., 2010). A number of works have proposed proce-

dures to filter the effects of rainfall estimation uncertainty on the estimation of a threshold (Jakob and Weatherly, 2003; Guzzetti et al., 2007; Jakob et al., 2012). These procedures include the use of rainfall duration thresholds (short rainfall events are not used in the threshold estimation) and of a maximal distance between debris-flow location and the nearest raingauge. The rationale for filtering out very short rainfall events is that these events are also very localized; hence they are characterized by larger uncertainties in rainfall estimation with respect to longer events (Berne and Krajewski, 2013).

1.3 Instrumented basins

Experimental basins deserve particular mention due to the importance they have for the collection of detailed data on debris-flow initiation. Thanks to experimental basins, models can be better calibrated and the debris-flow triggering dynamics better analyzed. Some researchers have dedicated a considerable amount of their activity to debris-flow monitoring in instrumented basins, producing an important literature background in the fields of rainfall threshold analysis, soil moisture and other hydrologic conditions leading to debris-flow initiation. Four instrumented catchments selected amongst many available in literature are herein reported, for the closeness of context and/or for some particular approach they brought to the research in particular:

- Acquabona catchment (Italy)
- Chalk Cliffs catchment (U.S.A.)
- Moscardo catchment (Italy)
- Illgraben catchment (Switzerland)

- Gadria catchment (Italy)

The Acquabona Creek (Tecca et al., 2003) is located on the left side of the Boite River Valley, near Cortina d'Ampezzo, in the Eastern Dolomites, Italy. The monitoring system is equipped with sensors and instruments for measuring: (i) rainfall and pore pressures in the talus at the initiation zone, in order to investigate the hydrological conditions leading to debris flow initiation; (ii) flow depth and total normal stress both in the lower channel and in the retention basin, in order to estimate the instantaneous solid discharge and the unit weight; (iii) ground vibrations induced by debris flow, to estimate the debris flow front velocity. One important achievement of the aforementioned work is the relation of cumulative rainfall and pore pressure with debris-flow triggering (Fig. 1.7).

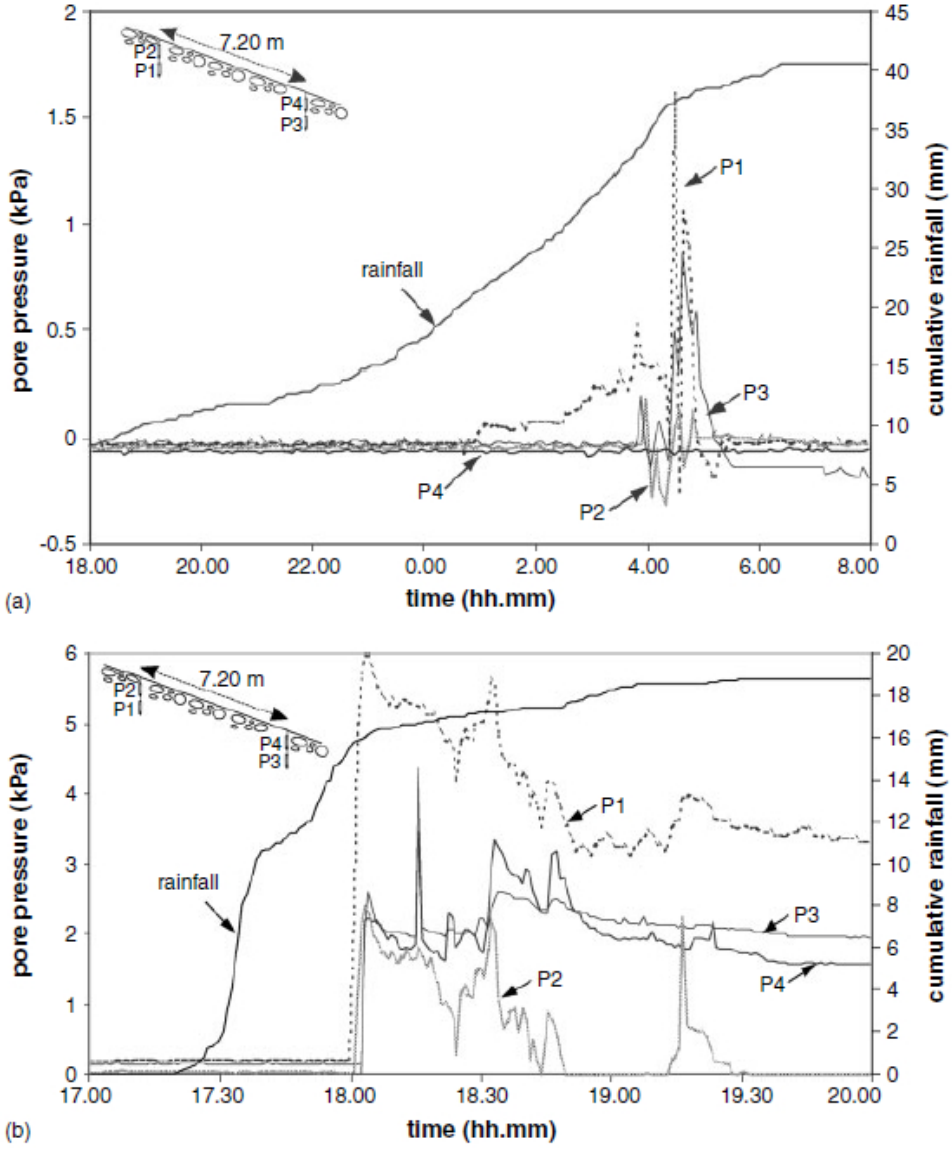

Figure 1.7: Pore pressure response to rainfall in case of: a) no debris-flow triggering, b) debris-flow mobilization, from Tecca et al. (2003)

The role of soil moisture, in particular of soil water content in relation to the triggering of soil slips and debris flows, has been and is still being widely analyzed; significant results have been obtained in recent years, in the U.S. (Coe

et al., 2008). The Chalk Cliffs catchment is located in the Sawatch mountain range in Colorado adjacent to a normal fault which forms the eastern boundary of the range. In particular, the work done by Coe et al. (2008) stresses the role of the soil water content during debris-flow events (Fig. 1.8). Noteworthy is the relation of moisture detected by different sensors in the thalweg of the channel and in the levee, to determine debris-flow triggering time.

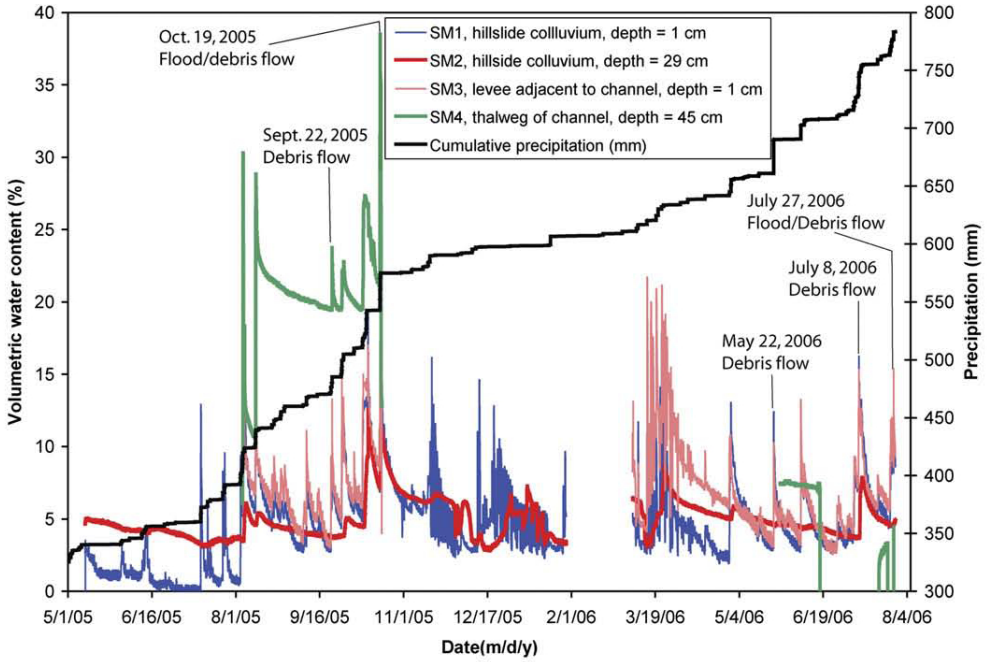

Figure 1.8: Volumetric water content trend and response to debris-flow events, from Coe et al. (2008).

Bearing in mind specifically the role of rainfall, remarkable achievements have been obtained in the Moscardo basin. The Moscardo Torrent is a small stream in the Carnic Alps (Italy), with a drainage area of 4.1 km^2, ranging in elevation from 890 to 2043 m and a mean annual precipitation of 1660 mm. The work done by Deganutti et al. (2000) stresses the importance and the need of a

statistical analysis in approaching different rainfall-related variables in relation to the triggering of debris flows. (Tab. 3).

Hydrological parameters and debris-flow triggering rainfalls have been analyzed also at the Illgraben catchment (Swiss Alps), with the aim of configuring a reliable warning system (Badoux et al., 2009). The Illgraben catchment presents a drainage area of 9.5 km^2, ranging from 850 to 2716 m with a mean channel slope (upstream of the fan) of 16%.
Both high-intensity short-duration and low-intensity long-duration rainfall events have been proved to be related with the triggering of debris flows even though high-intensity short-duration rainfall bursts are more likely to mobilize debris deposits.

Table 3: Descriptive table underlying the different role of rainfall-related variables, in particular the total rainfall and the 60 minutes max intensity have been found strongly influencing the triggering of debris flows, from Deganutti et al. (2000)

	Mean	**Std Dev.**	**p t-test**	**p U-test**
Total storm rainfall (mm)			<.01	<.01
No debris flows	29.2	19.1		
Debris flows	55	33		
Storm Duration (h)			0.12	0.13
No debris flows	7.8	9.4		
Debris flows	14.3	14.6		
Avg. storm intensity (mmh^{-1})			0.33	0.61
No debris flows	7	5.4		
Debris flows	9.7	9.9		
60' max intensity (mmh^{-1})			<.01	<.01
No debris flows	17.1	7.9		
Debris flows	27.9	8.3		
Antec. 24 h rainfall (mm)			0.55	0.14
No debris flows	4	8.3		
Debris flows	5.8	10.4		
Antec. 5 days rainfall (mm)			0.83	0.9
No debris flows	30.4	31.7		
Debris flows	28.7	24.2		
Antec. 10 days rainfall (mm)			0.81	0.72
No debris flows	60	49		
Debris flows	56.6	48.2		
Antec. 15 days rainfall (mm)			0.76	0.64
No debris flows	96.8	64.3		
Debris flows	91.1	63.7		

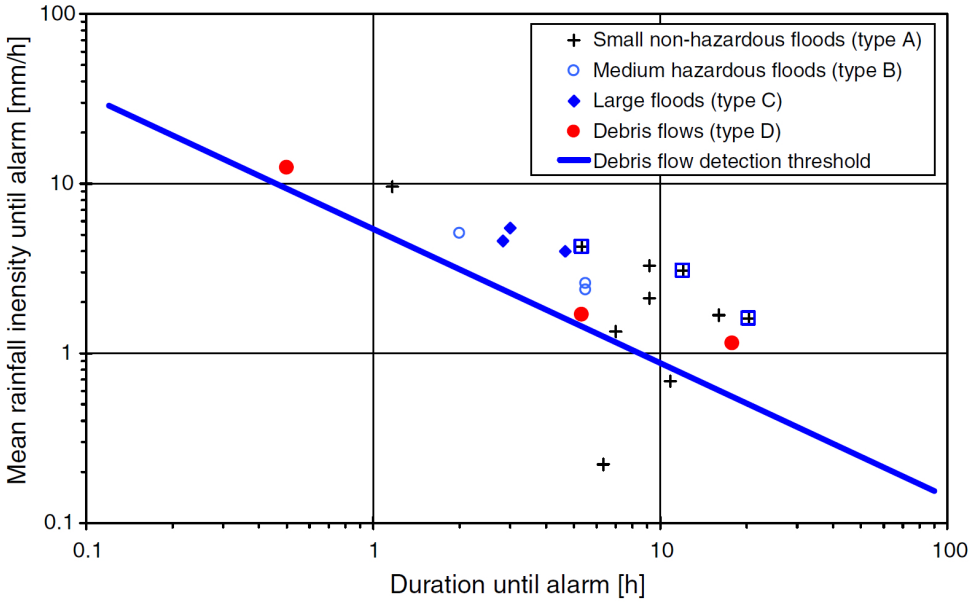

Figure 1.9: Relationship between rainfall duration and average intensity for the Illgraben catchment and location of data from the 2007 debris-flow and flood events, from Badoux et al. (2009).

From debris-flow activity observation and in combination with the analysis of raingauge data, a rainfall intensity-duration threshold was established and comparison with other hazardous events (floods and debris flows), confirmed the validity of the threshold (Fig. 1.9). Due to the short time extent of the observations, there is the need of more years of data in order to consider the threshold curve a reliable predictive tool (Badoux et al., 2009), considering also the large variability of the phenomena.

A novel installation for debris-flow monitoring has been set up in the Gadria catchment (Eastern Alps, Northern Italy). The Gadria basin has been chosen mainly because of the relatively high frequency of debris flows (on average 1-2

per year). The Gadria catchment has a drainage area of 6.3 km^2 and ranges in elevation from 1394 m to 2945 m. An important bedload tributary (Strimm, drainage area 8.5 km^2, minimum elevation 1394 m, maximum elevation 3197 m) joins the Gadria channel close to a filter check dam located near the alluvial fan apex, which has been set as the outlet of both basins. Sensors have been installed both in the Gadria and in the Strimm basins. The monitoring equipment consists of raingauges, radar sensors for flow depth, geophones for ground vibrations, and video-cameras with spotlights (Comiti et al., 2014).
A small magnitude event occurred in August, 2011 (Comiti et al., 2014) and a more severe event occurred in July, 2013; data are still under analysis but the first outcomes suggest important achievements regarding rainfall variability, triggering mechanisms and volume and velocity derivation.

1.4 Precipitation measurement

In order to better understand the hydrologic forcing on debris-flow occurrence, the way rainfall is measured becomes a key issue.
The most common rainfall estimations are made by means of:

- Raingauges
- Radar
- Satellite

Other type of instruments are nowadays available (disdrometers, other optic sensors) but usually they have a non-extensive application.
The above mentioned instruments have obviously different scales of applica-

tion and they are all characterized by several pros and cons that are herein summarized.

Raingauges In respect to more sophisticated technologies, raingauges still remain extremely useful as they are the most widespread sensors for precipitation measurement; moreover they provide the ground truth to compare and calibrate remote measuring systems such as radar and satellite. They provide usually reliable data but they can suffer from undersampling problems and lack of spatial representativeness (due to their "*spotty distribution*") when precipitation is heavily influenced by other effect such as orographic enhancement (Zangl, 2007).
Some of the typical sources of error that are related to this type of instrument involve:

- wind interference
- evaporative losses
- outsplashes

Depending on the local climatic conditions (winds, orographic shield effects etc...) rainfall can be eventually severely underestimated, this leads to stress the importance of the calibration procedure and to the eventual use of specific measures (e.g.: wind shields) in order to provide the most accurate rainfall estimation values.

Radar From the 1940s radar has undergone a rapid development also for meteorological purposes. Radar (Fig. 1.10) can provide definitely good rainfall estimation measures, but it still relies on in situ data to be calibrated and,

especially in complex mountain areas, radar technology will remain for long in need of a ground-truth value.

The wavelengths used are generally 3 cm (X band or 10 GHz), 5 cm (C band or 6 GHz) and 10 cm (S band or 3 GHz), these wavelengths being scattered mostly by targets the size of precipitation particles (Strangeways, 2006).

The principle of operation is connects the radar reflectivity (Z) to the rainfall rate per hour (mm) using an empirical equation of the form:

$$Z = aR^b \tag{2}$$

where a and b are empirical parameters and in particular a is related to the type of precipitation (drizzle, frontal rain, convective showers) (Strangeways, 2006).

Figure 1.10: C-band Doppler weather radar (modified from: *www.meteotrentino.it*). This radar serves the autonomous provinces of Trento and Bolzano, in the north eastern part of Italy, and it has been used foe event-scale analysis in the present work.

Weather radars are in need of different corrections and can also be affected by some major errors (Marra, 2013) herein reported:

- attenuation of the signal at long distances or for intense events

- occlusion, especially in complex mountain regions
- bright band correction in order not to overestimate the precipitation
- wet radome correction to deal with a highly attenuated signal

Radar remains a key instrument for a lot of application, especially devoted to short range forecasts and civil protection issues that make the radar itself an important and reliable source of information notwithstanding the high maintenance cost due mainly to its great energy consumption.

Satellite Satellite measures are nowadays fundamental at different scale and for various purposes. They can be extremely useful for instance to monitor global-scale climatic trends or to follow the development of major systems (frontal events, tornadoes etc...).
The resolution obtained with satellites in the case of the Tropical Rainfall Measuring Mission (TRMM) gives a real-time 3 hours rainfall analysis. Rainfall is usually estimated using infrared wavelengths and active or passive microwaves (Li and Shao, 2010) whose response is related to the depth and the temperature of water they pass.
Several hydrological model have been applied using satellite rainfall estimates and giving usually unsatisfactory results regarding the typical hydrological analysis scale of interest. The typical coarse spatial and temporal satellite resolution ($\sim$5 km gridded data and around 1 day temporal resolution for multi-satellite recognitions) make satellite use unsuitable for watershed or regional-scale analysis, while they still represent the best source of information to monitor and model the global climatic dynamic.
Recent integration between satellite estimations and gauges or other calibrated

information are under development and there seem to be promising result (Li and Shao, 2010) in the improvement of areal rainfall estimates.

1.5 Aim of the study

The purpose of the present work is to analyze the influence of rainfall on debris-flow occurrence in an alpine region, taking into account also issues related to uncertainties in rainfall data. The research involves an analysis carried out at regional scale, which includes the morphometric characterization of debris-flow initiation sites and the estimation of rainfall thresholds for debris-flow occurrence. For selected cases, also the relations between water peak discharge, runoff volume and debris-flow volumes and density have been analyzed. The work is structured as follows:

- **Chapter 2** describes the study area and data collection.
- **Chapter 3** describes methods for the analysis of debris flows at regional scale.
- **Chapter 4** reports the main outcomes of the analysis carried out at regional-scale.
- **Chapter 5** describes the methods for the analysis of selected flood events for which detailed data on debris-flow occurrence and radar calibrated rainfall maps were available.
- **Chapter 6** reports the results of the analysis for the selected flood events.
- **Chapter 7** draws the main conclusions of the research, stresses the important findings of the present work.

2 Study area and available data

2.1 Study area and rainfall data

The study area corresponds to the territory of the Autonomous Province of Bolzano which includes the upper Adige River basin and a small area draining into the Drava River basin. The area is a mountainous region in Northern Italy (Fig. 2.1) covering approximately 7400 km^2. This region has been selected based on three motivations. First, Salvati et al. (2010) have recognized that this area was characterized by a significant societal landslide risk in the period 1950-2008. Second, a database listing 514 debris flows in the period 2000-2010 is available. Third, the area is equipped both with a weather radar and a dense network of raingauges, which enable a sound analysis of the meteorological forcing on debris-flow occurrence.

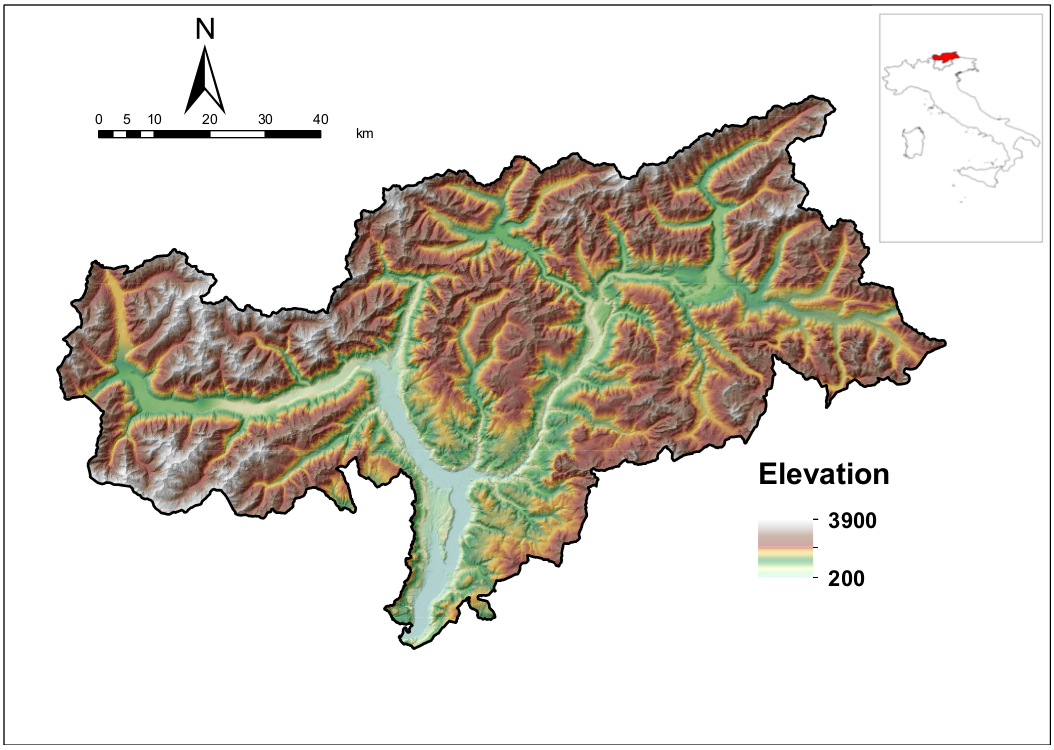

Figure 2.1: The study area

Elevation in the study area ranges between 200 and 3900 m a.s.l, with mean elevation around 1800 m a.s.l.

The geology is characterized mostly by metamorphic rocks: orthogneiss, paragneiss, phyllites and micaschists (Fig. 2.2). Igneous rocks (porphiry) along with sandstones and marls are also present. These rock types are generally characterized by low to very low permeability. A minor, though important, area is covered by carbonate rocks, mainly dolomite, and is characterized, on average by a greater permeability in respect to metamorphic and igneous rocks.

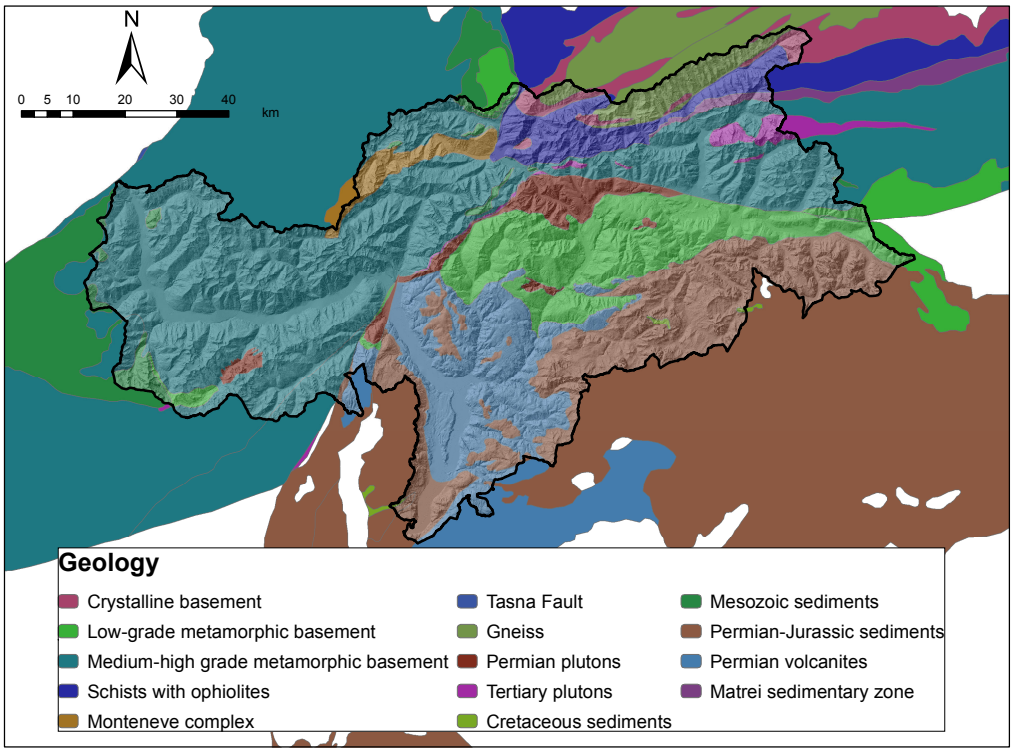

Figure 2.2: Simplified geology for the study area

Moraines, scree and debris accumulated in the bed of headwater channels represent the main source of sediment for debris flows.

The precipitation regime is influenced by western Atlantic airflows and southern circulation patterns. The dominant climate pattern in the region is continental, with the distribution of the monthly precipitation showing two maxima, in August and October. Precipitation in cold months (from October to April) mostly occurs as snowfall. Between May and September, the precipitation is brought by mesoscale convective systems and localized thunderstorms (Norbiato et al., 2009). Part of the western portion of the study area belongs to the dry internal alpine region, with a mean annual precipitation (MAP) ranging between

400 mm and 700 mm, the result of sheltering of the mountain range to southerly and northerly winds. The MAP increases to 1300 mm in the Northern portion of the region, where the rainfall regime is conditioned by the "*stau*" effect i.e., the intensification of rainfall when warm and moist air from the Mediterranean Sea is lifted over the Alps, leading to the *"foehn"* effect on the leeward side. The dry-to-moderate rainfall regime is reflected also in the climatology of the rainfall extremes. Rainfall quantiles corresponding to a 100-year return period rarely exceed 50 mm at 1-hour duration, and 150 mm at 24-hour duration.
Vegetation and land use distribution is typical of inner alpine environments and is divided into elevation bands. On valley floors we encounter the main cities, agriculture settlements and riparian vegetation, before the mountain area (800-1000 m) there is the presence of coppices (deciduous trees) along with beech, Scots pine and silver fir woods. The greater part of woodlands is however included in the so called mountain to subalpine belt (900-2000 m). Here we can find wide spruce and larch forests along with some high-altitude pine species. The woodlands superior limit is around 2200-2300 m, above this belt we find a shrub band that in many case is hosting high altitude pastures and meadows as an important part of the local rural economy. Above 2500 m high-altitude herbaceous vegetation dominates the environment and above 2600 m we find mainly bare soil, exposed rocks and rocky outcrops (Del Favero, 2004).

Raingauges A dense network of raingauges measures the precipitation in the study area (Fig. 2.3), including 95 raingauges located inside the basin area (60 raingauges with data available for at least 90% of the time over the study period 2000-2010). This corresponds to a density of about one raingauge every 100 km^2. The horizontal distance between two neighboring raingauges ranges from

0.44 km to 15.3 km, with an average of 5.8 km. The altitude of the raingauges ranges from 200 m a.s.l. to 2800 m a.s.l., with an average of 1200 m a.s.l. The temporal resolution of the original data is ten minutes.

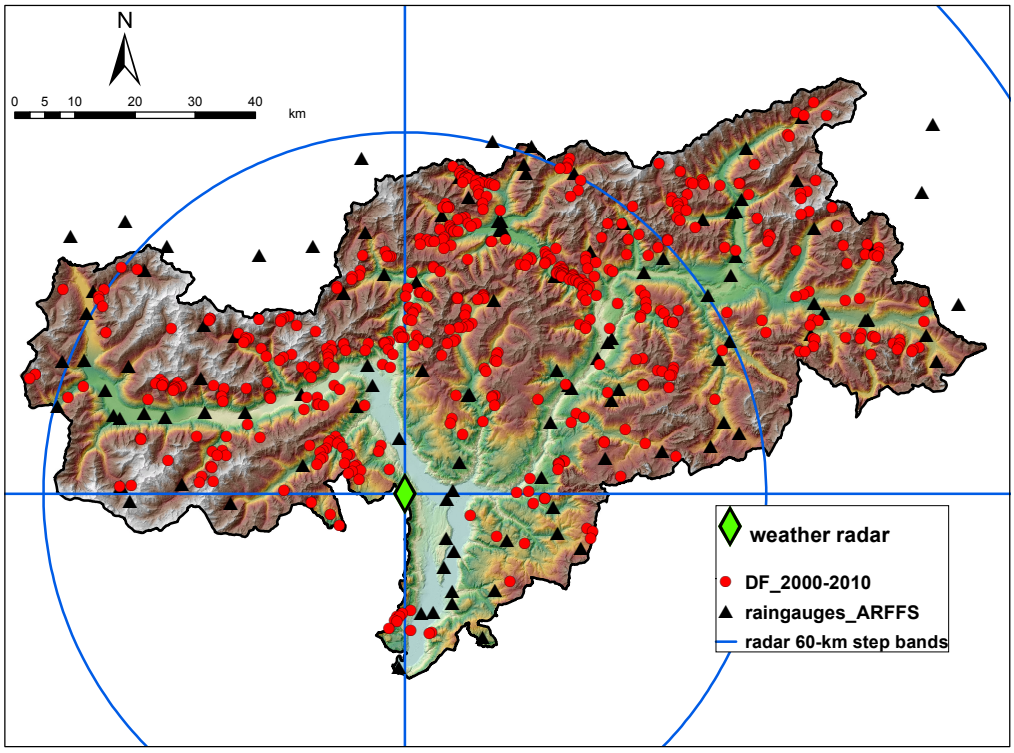

Figure 2.3: Debris flows, raingauges network and radar location/scan radius for the study area

Weather radar A C-band weather radar is also available for the study area, covering almost the whole province (Marra et al., 2013); selected events have been analyzed in detail using radar-calibrated rainfall maps.

The potential scan radius of radar (120 km) in such mountain areas is seriously limited by various factors (attenuation, occlusion ...); these limitations lead to the following consideration: the more the target area is far from the radar and

not in line of sight, the more we need to rely on gauges-interpolated values.

2.2 Scales of analysis

The analysis has been split in two parts: the first part of the analysis has been carried out at a regional and decadal scale to improve our knowledge of the local rainfall thresholds for debris-flow occurrences, the uncertainty related to this estimations and the main morphometric characterization of the debris-flow initiation sites; in the second part, the focus was on the analysis of the hydrologic response of some watersheds for a selection of events with the help of detailed input information, both topographic and hydrological;

2.2.1 Analysis of debris flows at regional-scale: overview of the debris-flow database

The ED30 database (Event Documentation of the 30th Division of the Autonomous Province of Bolzano, in charge of designing and maintaining hydraulic structures) (Macconi and Sperling, 2008) has been collected and analyzed.

Regarding debris-flow occurrences, several information were available (e.g. location of the event, date, magnitude, traveled path of the flow, damage and other attributes). This information has been managed in a GIS environment by means of geodatabase tools. Another fundamental phase of the study included the creation of a unique Digital Terrain Model (DTM) for the entire area of Bolzano Province. This step was conducted recovering all needed layers from the provincial GIS Web-service. A 2.5-meters resolution DTM for all the area was built up; from this high-resolution DTM, a 5-meters DTM was created. The 5-meters DTM was used in the morphometric analysis as it combines high

spatial resolution with acceptable computation time. The two main sources of information (DTM and ED30) were then joined together to obtain basic geomorphological features for the points of interest. The hydrologic correction of the DTM was then performed by filling the local depressions (pits).

All cases with too high uncertainty in the date of debris-flow occurrence (time span greater than two days) have been removed from the database. Each point has been checked and more precisely located; the slope along flow direction and the upslope contributing area to that point have been computed for each debris-flow initiation point. Several points have been discarded from the dataset due to uncertainties in the location or because they do not correspond to debris-flow initiation points (e.g.: valley bottom with upstream areas $> 50\ km^2$), probably located there because of important damage caused by the event to anthropic structures).

The resulting dataset was made of 514 points for which some descriptive parameters and relations have been calculated and reported (Figs. 2.4 - 2.8).

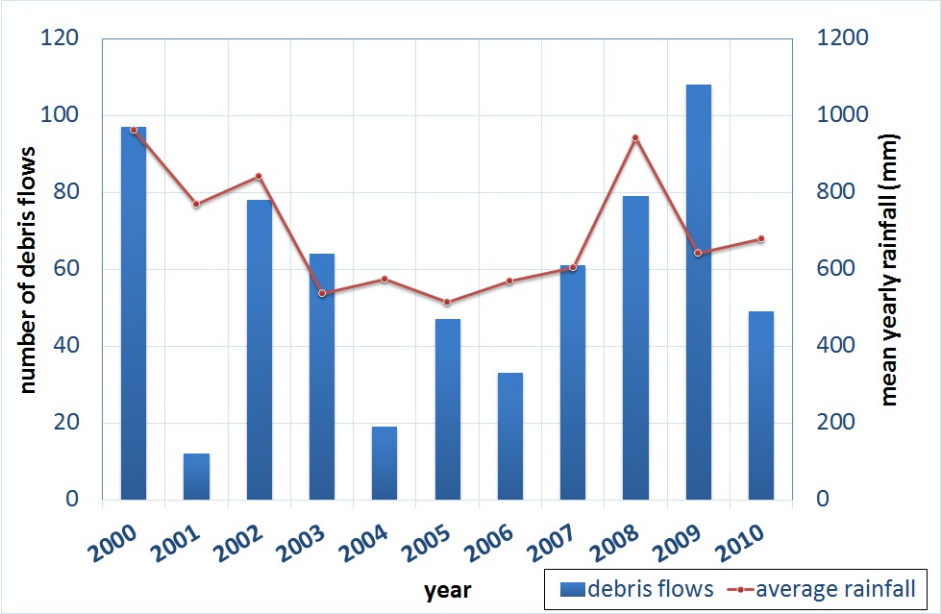

Figure 2.4: Yearly distribution of debris flows in relation to mean precipitation.

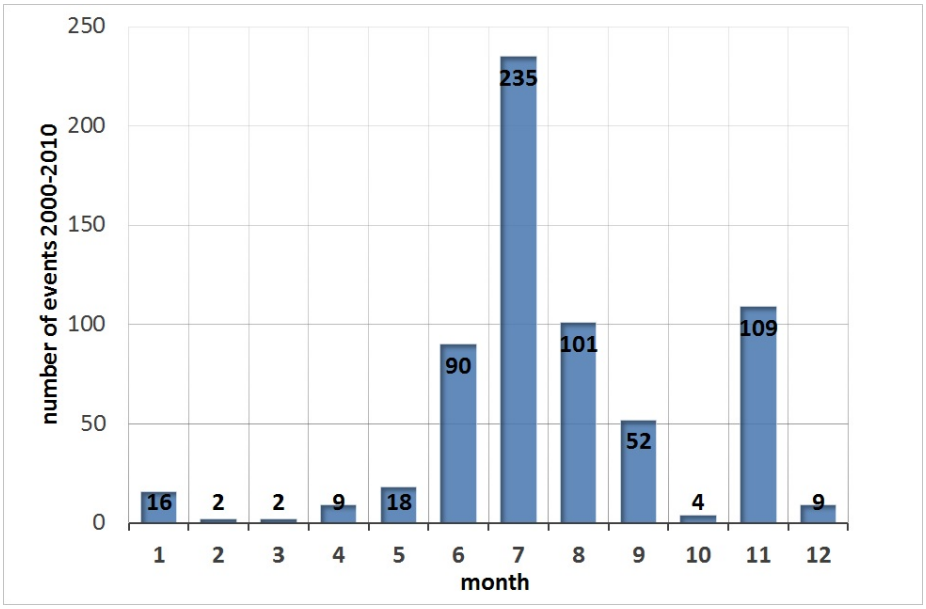

Figure 2.5: Monthly distribution of debris flows for the entire available dataset.

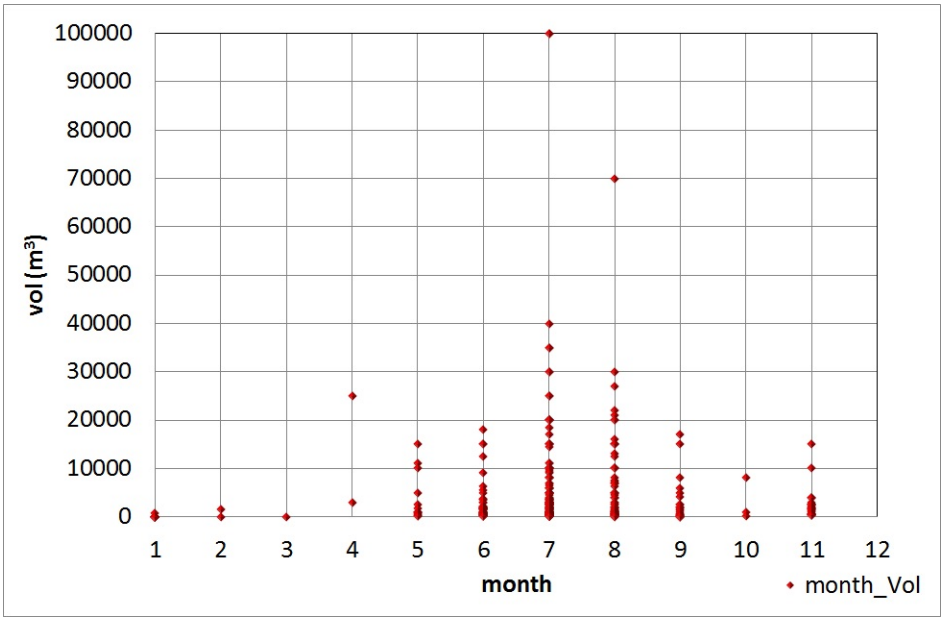

Figure 2.6: Debris flows magnitude monthly distribution

It is possible to observe (Fig. 2.5) the typical summer concentration of the events with a peak in July, usually related to intense precipitation events, and a general relation between the mean annual precipitation and the number of debris-flow events can be also gathered from Fig. 2.4.
Debris flows in November are ascribed to frontal rainfall; some instability phenomena, mostly located at low elevations, occur also during winter.

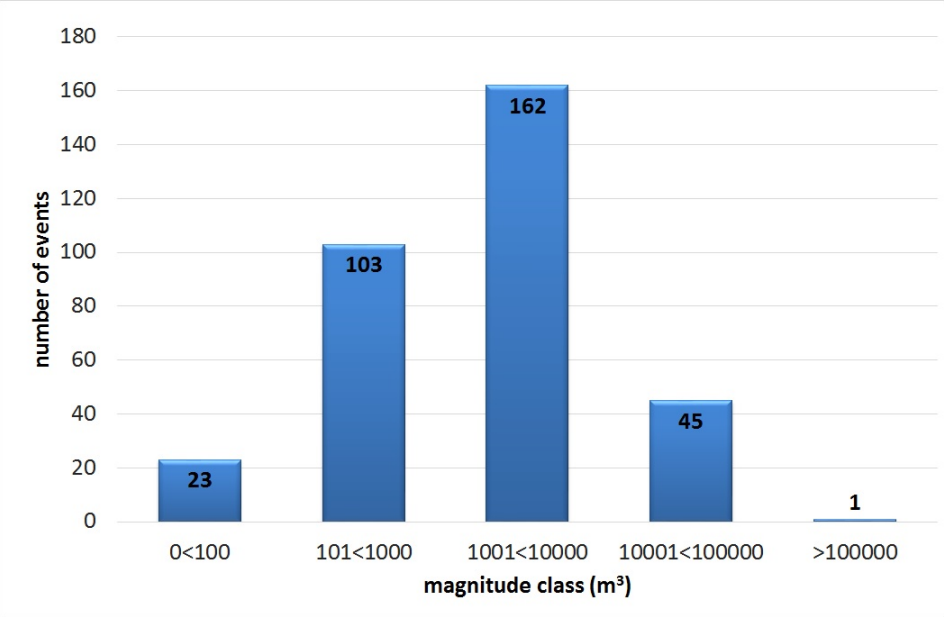

Figure 2.7: Debris-flow magnitude distribution

Data on debris-flow magnitude were available for 363 cases (70% of the dataset). The most frequent debris-flow event class is the 1000<10000 m^3 one (Fig. 2.7), this statistic may be due to different reasons, in particular to the fact that minor events are not always recorded or noticed, as they do not pose great danger to the community.

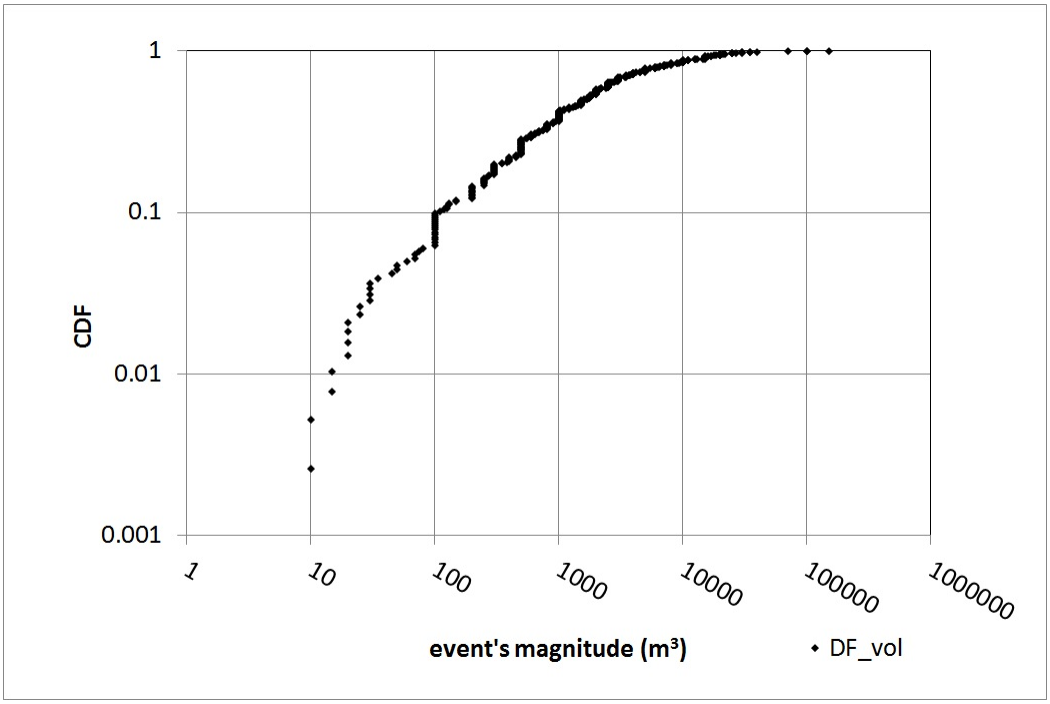

Figure 2.8: Cumulative Distribution Function of debris-flows magnitude, a clear logarithmic trend is shown by the data distribution.

Fig. 2.9 provides an overview of the debris-flow dataset distribution with emphasis on the magnitude attribute.

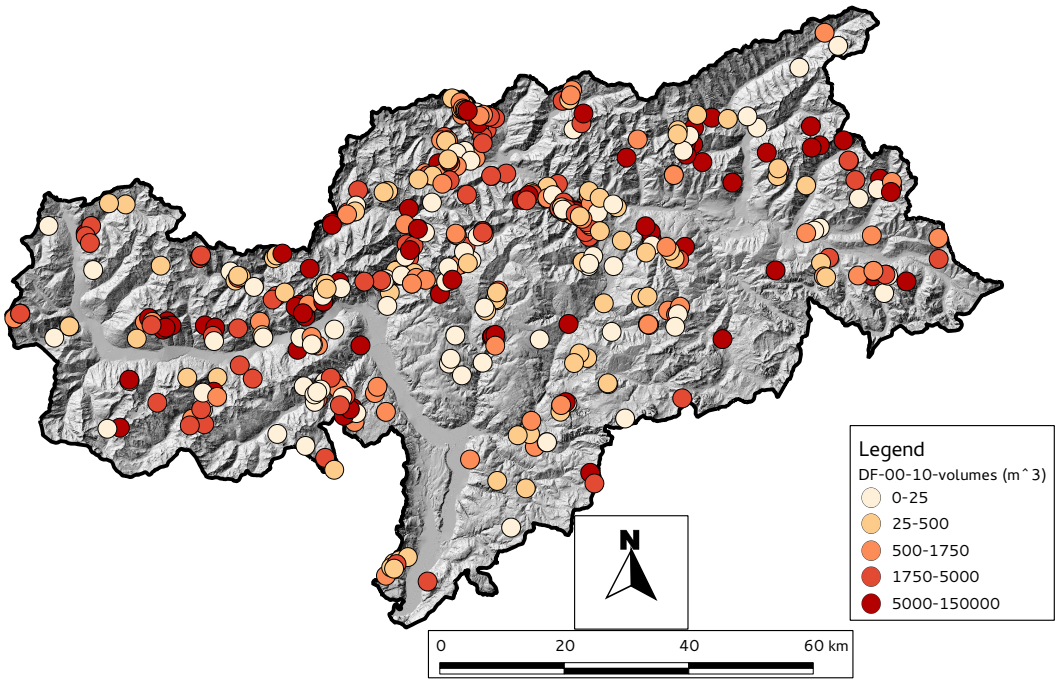

Figure 2.9: Debris flows presented in relation to their magnitude (cubic meters of deposited volumes)

2.2.2 Selected events: studied basins

Three storm systems which occurred on October 3-4, 2006, June 20-21 2007 and September 3-4, 2009 and resulted in different catchment responses, were studied in detail.

The choice of these events was supported by the availability of detailed data, including radar-derived rainfall, and by the characteristics of the events. Analyzing debris-flow occurrences in the period 2000-2010 we noticed that June 2007 and September 2009 events counted 27 debris flows each, thus represent-

ing the most severe events in terms of single-day debris-flow occurrences. The October 2006 hit the same catchments as the 2007 event but without triggering debris flows.

Fig. 2.10 shows the basins affected by the three events, whose general features are summarized in Tab. 4

Table 4: General features of the analyzed events.

Year	**Date**	**Catchments**	**Description**
2006	Oct, 3^{rd}-4^{th}	Ridanna, valley and Fleres catchment.	Almost dry antecedent conditions, moderate flash flood response, not reported debris flows.
2007	Jun, 20^{nd}-21^{st}	same as 2006 area.	Very wet antecedent conditions, mainly debris flow response, not reported flooding events.
2009	Sep, 4^{th}	SW-NE orientation between Talvera and Aurino catchment.	Regional-scale event, almost wet antecedent conditions, both widespread flash flood and debris flow responses.

The October 2006 event was characterized by a significant input in terms of cumulative rainfall values but not very high values for intensity of the rainfall, and the basins' predominant response was in terms of flash floods events' production. The June 2007 event was instead characterized by very high values of intensity and cumulative rainfall but extremely localized, while the great part of

the storm was moderate both in terms of intensity and cumulative rainfall values. The basins responses have been marked by mainly debris flow production but not important flash flood events have been noticed. The September 2009 event was characterized by a very important regional-scale cumulative rainfall value contribution with not so high intensity values and the response has been marked by both flash flood and debris flow events production.

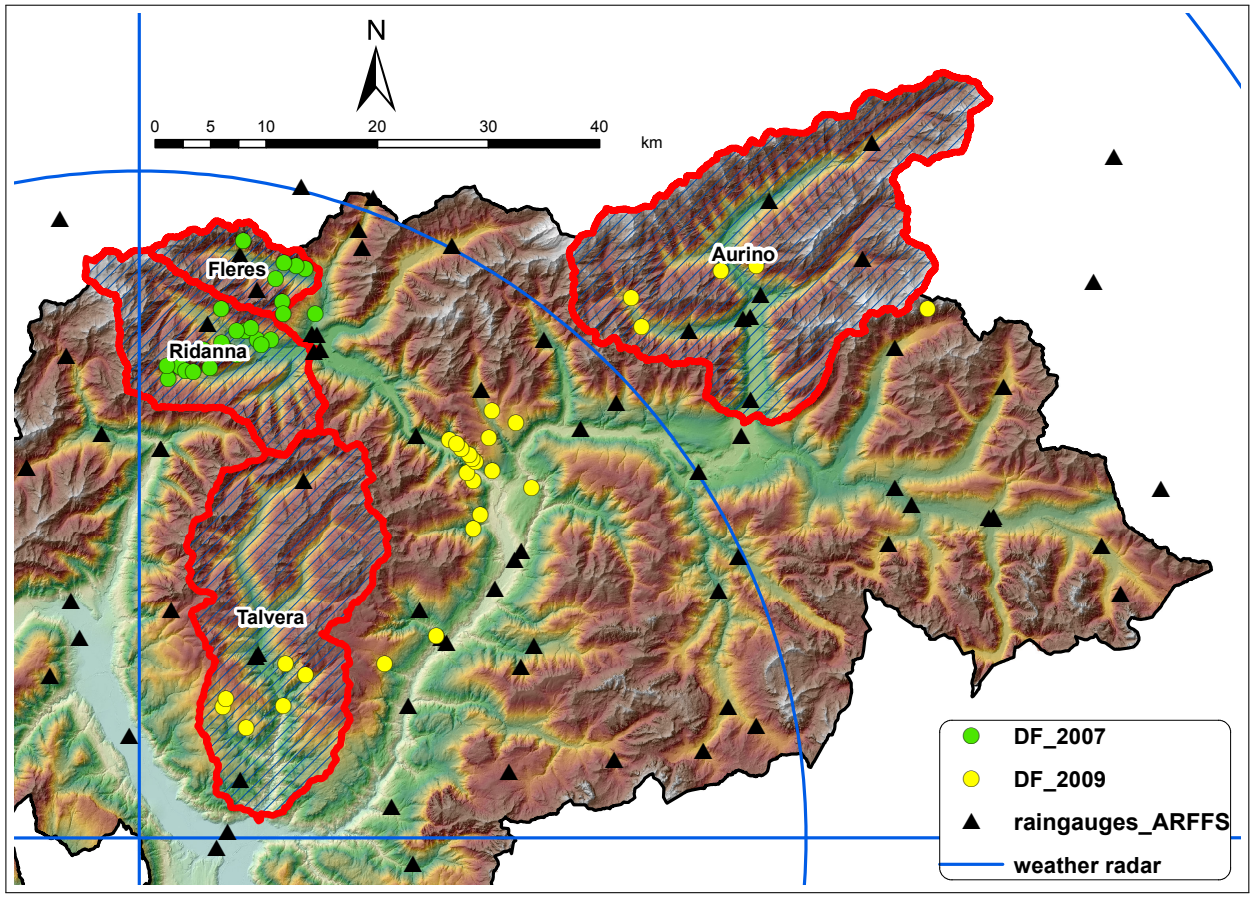

Figure 2.10: Area overview with radar coverage,raingauges locations, major analyzed watersheds and debris flow locations. The radar could monitor in a good way the 2006-2007 events (green dots) but not all the 2009 events (yellow dots) that spanned at regional scale and were affected by other problems (occlusion, attenuation and wet radome)

Tab. 5 reports the main morphological features of the four selected basins for the 2006-2007 events and of the five selected basins for the 2009 event.

Table 5: Main morphological parameters of the analyzed basins.

Basin	**Area (km^2)**	**Elevation (m a.s.l.)**	**Slope (deg)**
Fleres Colle Isarco	74	min: 1068 max: 3236 average: 1962	max: 78 average: 31
Rio Pian	16	min: 2135 max: 3455 average: 2844	max: 67 average: 21
Racines Stanghe	48	min: 960 max: 2793 average: 1809	max: 67 average: 25
Ridanna Vipiteno	207	min: 935 max: 3455 average: 1919	max: 69 average: 27
Aurino Cadipietra	157	min: 1037 max:3470 average: 2157	max: 70 average: 30
Aurino Caminata	418	min: 845 max: 3470 average: 2114	max: 70 average: 29
Riva Caminata	116	min: 862 max: 3420 average: 2280	max: 67 average: 29
Aurino san Giorgio	614	min: 817 max: 3484 average:2032	max: 71 average: 29
Talvera Bolzano	426	min: 277 max: 2770 average: 1669	max: 73 average: 24

3 Analysis of debris-flow occurrence at regional scale

3.1 Morphometric analysis

In order to carry out an analysis on the main morphometric features that characterize debris-flow triggering, local slope (slope over the direction of maximum declivity) and contributing area have been investigated for debris-flow catchments in the upper Adige River basin.

The analysis was conducted using the 5-meters resolution Digital Terrain Model (DTM) and the ED30 database (a detailed geodatabase, managed and updated by the Autonomous Province of Bolzano, reporting triggering locations of debris flows and some other information such as timing and mobilized volumes). The analyzed points correspond to the most probable triggering locations of debris flows.

The original dataset was restricted to 434 debris-flow records in order to have a database consistent with the analysis of rainfall estimation (sections 3.3, 3.2), for these points we obtained also storm related information on triggering rainfall.

The dataset has been explored also considering some subdivisions aimed at discriminating the possible influence of geology, season of debris-flow occurrence and rainstorm duration: (i) debris-flow initiation sites on carbonate settings and other settings have been considered separately, (ii) summer and non-summer locations have been analyzed independently, (iii) slope-area values have also been analyzed considering different storm durations.

3.2 Analysis on Intensity-Duration thresholds

The IDW (Inverse Distance Weighted) interpolated rainfall field covering the 2000-2010 time span over the Autonomous Province of Bolzano was initially considered.

A total number of 434 debris flows out of 442 records (8 cases of no rainfall, or lower to 5 mm of cumulative value for all the event) has been analyzed, in order to evaluate rainfall Intensity-Duration (ID) relations at the debris-flow locations.

These events were retrieved from the ED30 database, considering a maximum uncertainty of two days in the date of occurrence, (more than 90% of the events are within zero or one day of uncertainty).

The general form of the equation linking rainstorm duration D (in hours), to mean rainfall intensity I (in mm/h) is

$$I = \alpha D^{-\beta} \tag{3}$$

where α and β are parameters of the equation. To compare the ID relationships for the upper Adige River basin, two equations derived from literature have been kept as reference:

- equation derived from Guzzetti et al. (2008), retrieved by the analysis of a global dataset for landslide and debris flows

$$I = 2.20D^{-0.44} \tag{4}$$

- equation derived from Brunetti et al. (2010), for Italy and for the 1%

exceedance probability threshold

$$I = 7.74D^{-0.64} \tag{5}$$

Rainstorms have been defined considering a 6 hours hiatus as separator between two following precipitation events and a 5 mm rainfall threshold to define a storm (once 5 mm of rainfall are reached the real starting time of the storm is back-computed).

Debris flows have been divided into summer occurrences (June to September) and other seasons.

Fig. 3.1 reports an ID scatter plot with the above mentioned reference equations.

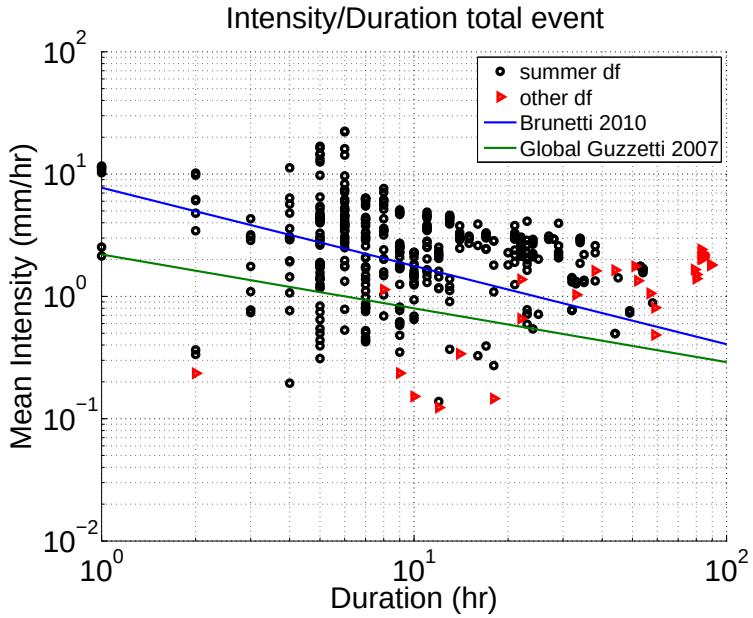

Figure 3.1: ID scatter plot with IDW interpolation as reference, total series are herein considered.

The investigation followed two directions: one is the IDW interpolant itself, the other approach is the nearest gauge, which means that rainfall values at triggering point location are surrogated by the nearest gauge with an available record.

Due to the great variability of the data, some filtering and more detailed analyses have been carried out, in particular, in order to link Intensity/Duration values to the most probable occurrence time of the events, the Intensity trend has been analyzed in its dynamic. In different and more fragile context debris flow timing has been recognized not to be linked to the very first significant part of an important storm event rather than to the overall storm duration or to the max intensity step (Staley et al., 2013).

We have analyzed the ID values:

i) considering the whole duration of the rainstorm,

ii) at the occurrence of the maximum hourly intensity value.

This later point was kept in order to be coherent with the outcomes of some case studies belonging to the ten-year dataset. For some of the analyzed events, timing information was available from local people interview and database records, and with a degree of uncertainty in the range of 2-3 hours. It ws observed that the occurrence time of debris flow was located around the maximum hourly precipitation step.

In order to better discriminate the influence of different parameters on the ID shape, various thresholds have been considered within the analysis. In particular, thresholds on rainfall intensity have been applied along with thresholds on raingauges inter-distances and percentage of contributing gauges used for the interpolation and some thresholds on the search radius (distance between triggering point and gauge) for the case of nearest gauge approach. Further analyses,

to discriminate any peculiarities in the ID dynamic, included the discrimination of triggering location between carbonate settings and other lithologies and the influence of the distance between the triggering point and its relative closest gauge.

Thresholds based on the frequentist approach (Brunetti et al., 2010) have been computed also using the ten-year dataset herein discussed. All the scores and coefficients have been computed for the different above mentioned reference thresholds are hereunder explained.

The score to Guzzetti's global equation, (Guzzetti et al., 2008) is computed as percentage of points above the reference ID curve.

One of the considered parameters to evaluate the performance in respect to the different thresholds is represented by the number of points that are remaining once the various thresholds on intensity, contribution percentage or distance in search radius have been applied, in this case not in relation to the frequentist approach.

Another considered parameter is the score coefficient, which represents a combination of the performances in respect to the reference threshold considering also the number of remaining points compared to the total number of events in the dataset.

It is expressed as follows:

$$(R_p/tot_p) * 0.15 - (100 - S_G) \tag{6}$$

where R_p is the number of remaining points after the threshold application, tot_p is the total number of points, (434 in our case) and S_G is the score to Guzzetti global equation (the ratio between number of points above and below

threshold). The value of 0.15 has been chosen empirically and represents the level of importance given to the percentage of remaining points from the whole dataset.

3.3 Uncertainty on rainfall thresholds

The following section is part of a paper that has been submitted to Geomorphology and at present is under revision (Nikolopoulos et al., 2014).

The analysis is centered on the assessment of the impact of rainfall estimation uncertainty on identification and use of rainfall thresholds for debris-flow occurrence.

3.3.1 The simulation experiment

Rainfall information at the location of a debris flow initiation point is generally unknown, and most commonly estimated based on measurements obtained at the nearby raingauges. The examination of the rainfall sampling impact on the ID threshold model requires the development of a simulation experiment, which exploits the available rainfall information. In the simulation experiment, we divided the raingauge network into two subsets. The first subset included all the raingauges that simulate the location where the debris flows have occurred (labelled DFR), and that provide the triggering rainfall. The second subset included the measurement raingauges used to estimate the rainfall at the location of the simulated debris flows (labelled MR). The rainfall estimation technique used here is based on the nearest raingauge (Brunetti et al., 2010), which implies a one-to-one correspondence between DFR and MR raingauges. Comparison of

rainfall estimates with the data measured at the DFRs allows the evaluation of the uncertainty in the rainfall estimation, and on how the uncertainty propagates to the estimation of the ID relationship.

To investigate the impact of the rainfall sampling problem on the rainfall ID threshold a set of reference power-law ID relationships was assumed for the study area. The ID relationships were used to identify the simulated debris-flow triggering events i.e., the rainfall events that exceeded the assumed ID threshold, at the location of the DFRs. Rainfall estimates obtained at the nearest MR station were used to determine the rainfall duration and the mean rainfall intensity conditions that have resulted in the simulated debris flows, and to estimate an empirical ID relationship for possible debris-flow occurrence. Finally, the performance of the ID threshold models was evaluated.

3.3.2 Selection of DFR and MR locations

An important step in the analysis consisted in the definition of appropriate locations for the raingauges representative of debris flows (DFR), and of the corresponding measurement raingauges (MR). Considering that the rainfall variability between the location of the debris flow and the nearest raingauge depends on the geographical (Euclidean) distance and on the difference in elevation, selection of DFR and MR accounted for the representativeness of these variables. In other words, selected DFR and MR raingauges should maintain, as close as possible, the geometrical relationship (in terms of distance and elevation difference) obtained from the available debris flows and the nearest raingauge record. Thus, selection of DFR and MR (shown in Fig. 3.2) was made so that the resulting distribution of (a) the difference in elevation, and (b) the geographical

(Euclidean) distance between DFR and MR would match the corresponding distribution derived from the individual debris-flow locations in the database, and their nearest raingauges (Fig. 3.3 a,b). A total of 17 pairs of DFR-MR were selected, and used for the analysis. Note that the 17 pairs resulted from a combination of 25 (instead of 34) unique gauge locations because, in order to match better the observed geometrical relationships, some of the gauges were involved in more than one pair and also played both the role of DFR and MR for different pairs (these are represented as superimposed DFR/MR symbols in Fig. 3.2). To match the largest values of the observed differences in elevation between the DFR and the corresponding MR, raingauges at distances larger than the observed distances were selected. A compromise was accepted between the degree of representation of the two distributions (distance and elevation differences) to maintain a realistic representation of the observed geometrical relationships. The final selection of the raingauges was made so that the range of the observed distances was maintained, but the higher-end values of the observed differences in elevation was not represented since to match those elevation differences DFR-MR gauges had to be located at a very high (relative to observed) distance ($>$ 14 km). We acknowledge that this limits the representativeness of the (DFR, MR) sample. However, we stress that the differences in elevation that were not captured correspond to less than 10% of the entire sample.

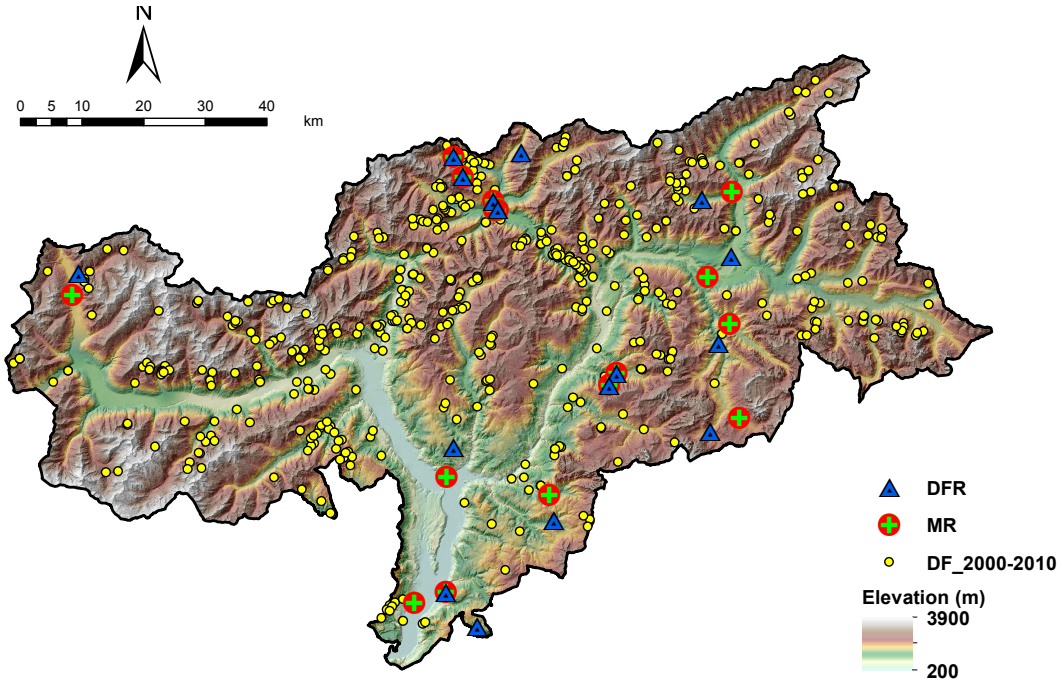

Figure 3.2: The study area with selected DFRs and MRs along with the location of debris flow occurrences for the period 2000-2010

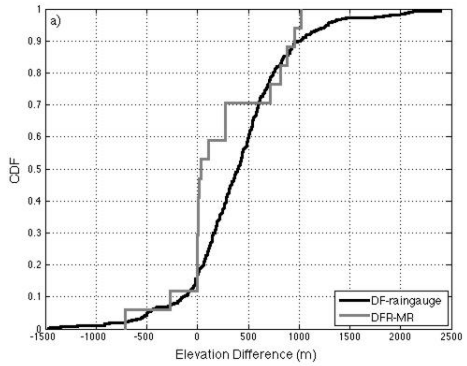

(a)

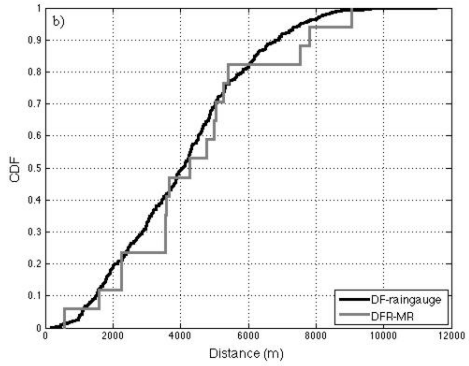

(b)

Figure 3.3: Cumulative distributions (a) for the difference in elevation, and (b) the geographical (Euclidean) distance between the raingauges and the location of the debris flows (black line), and the selected debris flow representative (DFR) and measurement (MR) raingauges (grey line).

3.3.3 Reference set of Intensity-Duration thresholds

The ensemble of the reference ID threshold scenarios is represented by a total of 15 reference ID rainfall thresholds, resulting from the combination of five α coefficients (1, 2, 4, 6, 8) and three β exponents (0.4, 0.5, 0.6) as expressed in eq. 3. The range of values for the α and β model parameters is realistic,

considering the empirical ID relationships proposed for Northern Italy (Guzzetti et al., 2007). Furthermore, the range of the α parameter was selected after inspection of the rainfall conditions in the locations of the DFRs. Specifically, we ensured that the range of the model parameters α and β was representative of the entire range of the rainfall conditions, and that for all ID thresholds examined, a sufficient number of rainfall events (> 100) was available for the analysis.

3.3.4 Estimation of Intensity-Duration thresholds based on reference scenarios

All individual rainfall events were identified from DFR observations using the frequentist approach Brunetti et al. (2010) with 1% exceedance probability, and were compared against the reference ID relationships. For each threshold scenario, the events falling above the reference threshold were identified as rainfall events with debris flows. For events with rainfall duration D $>$ 24 hours, the date for the debris flow was taken to coincide with the day including the center of mass (derived from rainfall time series) of the debris flow event. We then used the identified debris-flow dates and the rainfall observations at MR to estimate the ID relationship. The procedure was adopted to reproduce what is usually done in practice when defining empirical rainfall thresholds from (D, I) measurements (Brunetti et al., 2010). This means that the start time and the end time for the rainfall that has resulted in a debris flow is usually unknown, and the only known time is the day (or period of the day) of the debris-flow occurrence. There has been some example for which the estimated ID relationship was equal to the one derived from actual observations; this fact confirms

that the rainfall sampling uncertainty can lead to a significantly biased ID relationship identification.
We compared then the DFR and the MR rainfall observations to provide a quantitative estimate of the rainfall error magnitude, and to highlight the differences with respect to the debris-flow rainfall events.

Following the methodological approach described in the previous sessions, the model parameters $\hat{\alpha}$ and β of the ID thresholds were estimated using the frequentist approach proposed by Brunetti et al. (2010). The estimated ID threshold relationship has the general form:

$$I = \hat{\alpha} D^{-\hat{\beta}} \tag{7}$$

Comparison between the model coefficient for the reference and the estimated threshold was based on the calculation of biases, defined as the ratios $\alpha_r = \hat{\alpha}/\alpha$ and $\beta_r = \hat{\beta}/\beta$, where α_r and β_r are the estimation bias for the constant α and the exponent β, respectively.
We further examined the differences between the rainfall events (instead of the hourly values), which is more relevant to uncertainty in ID thresholds.

3.3.5 Performance of ID threshold for the prediction of debris-flows occurrence

The performance of a threshold i.e., the ability of the threshold model to identify the rainfall events that have resulted in debris flows, was examined calculating for each scenario standard contingency table statistics, including: (i) the Probability of Detection (POD), (ii) the False Alarm Ratio (FAR), and (iii) the

Critical Success Index (CSI). The POD measures the fraction of rainfall events with debris flows successfully detected by an ID threshold. The range of values for POD goes from 0 to 1, the latter value being desirable. A POD of one means that all occurrences of the event were correctly forecasted. The FAR gives the fraction of the rainfall events above the estimated ID threshold that did not correspond to rainfall events with debris flows (i.e., the false positives). The range of values for FAR goes from 0 to 1, the former value being desirable. A FAR of zero means that no non-occurrences of the event were forecasted to occur. The CSI assesses the skill of the prediction using information on positive and false detections, and on the missed detections. The range of values for CSI goes from 0 to 1, the latter being desirable.

3.3.6 Sensitivity of the selection of exceedance levels on ID model estimation and prediction accuracy

It is important to understand how improvement in ID estimation relates to exceedance level used and furthermore, what is the effect of this on the performance of the estimated ID threshold. We examined the influence of the selection of an exceedance level on the ID selection and prediction accuracy. To investigate these aspects, we applied seven different exceedance levels in the frequentist method (namely 1%, 5%, 10%, 20%, 30%, 40% and 50%) to estimate the ID threshold model based on MR data. The experiment was carried out for a reference ID threshold, characterized by α=4 and β=0.5 that correspond to the central values of the set of reference ID thresholds examined in this work. Estimation of the ID model based on different exceedance levels essentially results in a set of different IDs that have the same exponent but

different multipliers, one for each exceedance level. Therefore, each exceedance level in the frequentist method corresponds to a specific error in the estimation of the parameter α.

3.3.7 Sensitivity of ID estimation to debris flow-gauge distance and rainfall event duration

Considering that rainfall variability increases with distance, and that it depends on rainfall characteristics (e.g., short-duration convective events are associated to higher spatial variability than long-duration widespread rainfall events) we hypothesize that the uncertainty in the ID estimation can be reduced by filtering out the "highly uncertain" cases from the DFR-MR sample. Filtering was carried out based on two different values, including: (i) a value for the maximum distance between DFR and MR, and (ii) a value for the minimum duration of the rainfall event with debris flows. The threshold on the DFR-MR distance was used to examine the hypothesis that using only information from gauges at a close distance (≤ 5 km) can reduce the estimation bias. The threshold on the debris-flow event duration was used to examine the hypothesis that by excluding the short duration (≤ 12 hrs) rainfall events (generally associated with larger spatial variability) the bias in the ID estimation is reduced. We repeated the analysis presented in the previous sections (3.3.4, uncertainty and performances), for three different scenarios, summarized in Table 6.

Table 6: Different scenarios examined for thresholds at i) DFR-MR distance and ii) rainfall duration.

	Threshold on max distance between DFR and MR	Threshold on min duration of rainfall events
Scenario 1	None	12 hrs
Scenario 2	5 km	None
Scenario 3	5 km	12 hrs

3.4 Statistics on different interpolation techniques compared do DFR-MR

In order to improve rainfall estimation at debris-flow location, different interpolation techniques have been analyzed to evaluate their performance in comparison to the nearest gauge approach.

Five MRs (measurement gauges) have been selected to be used for the interpolation over the DFR (debris-flow raingauge), with the following criteria:

i) the very nearest has been kept the same as in the nearest gauge analysis;

ii) the other 4 has been selected applying a 20-km search radius (euclidean distance) and they have been ordered in a decreasing data-continuity sense (the second gauge presents less gaps in the data than the third and so on).

Gauges located in between the selected nearest one and the DFR, if any, have been discarded to keep the analysis consistent.

The 20-km search radius criterion combined with the data continuity one, on average has probably led to the selection of "*far*" gauges, somehow "*forced*" to have a low weight for all the chosen interpolation techniques.

Only summer events (June to September included) have been analyzed and only the case for which we have the availability of at least 4 records (4 stations with a valid record) have been taken into account. Furthermore, we imposed the condition that the eventual missing station/value should never be the selected nearest one (which means the same of the approach described in the previous session), so, in the case it coincides with it the record was treated as *"Not a Number"*.

Several Interpolation algorithms have been considered:

- Inverse Distance Weighted (Shepard, 1968), using euclidean distances
- Inverse Distance Weighted using surface distances
- Ordinary Multiquadratic (polynomial interpolation)
- Ordinary Kriging (Matheron, 1963), with a 20-km range
- Ordinary Kriging with a 5-km range
- Equal-Weights (average)

  For this approach equal weights have been assigned to the different gauges applying an average operator. In the case there were only 4 gauges available a weight of 0.25 was assign to each gauge; in the case we had all the 5 gauges available a weight of 0.20 was assigned to each gauge. For this analysis distances were not taken in consideration in order to determine the improvements given by the interpolation effort in respect to a simple average of the available records, not taking into account the spatial data variability.

The following statistics have been computed for all the analyzed interpolations:

- bias for different total rainfall intervals
- correlation coefficients
- Nash-Sutcliffe efficiency coefficient expressed as follows:

$$E = 1 - \frac{\sum_{t=1}^{T}(Q_0^t - Q_m^t)^2}{\sum_{t=1}^{T}(Q_0^t - \overline{Q_0})^2} \tag{8}$$

  where Q_m represents the modeled value and Q_0 the observed one, at time t.

- the ratio of estimated to theoretical α and β
- POD, FAR, CSI (as described in section 3.3.5).

4 Analysis of debris-flow occurrence at regional scale: results

4.1 Morphometric analysis

Fig. 4.1 shows the analyzed drainage basins of the debris flows surveyed in the years 2000-2010 by the Autonomous Province of Bolzano.

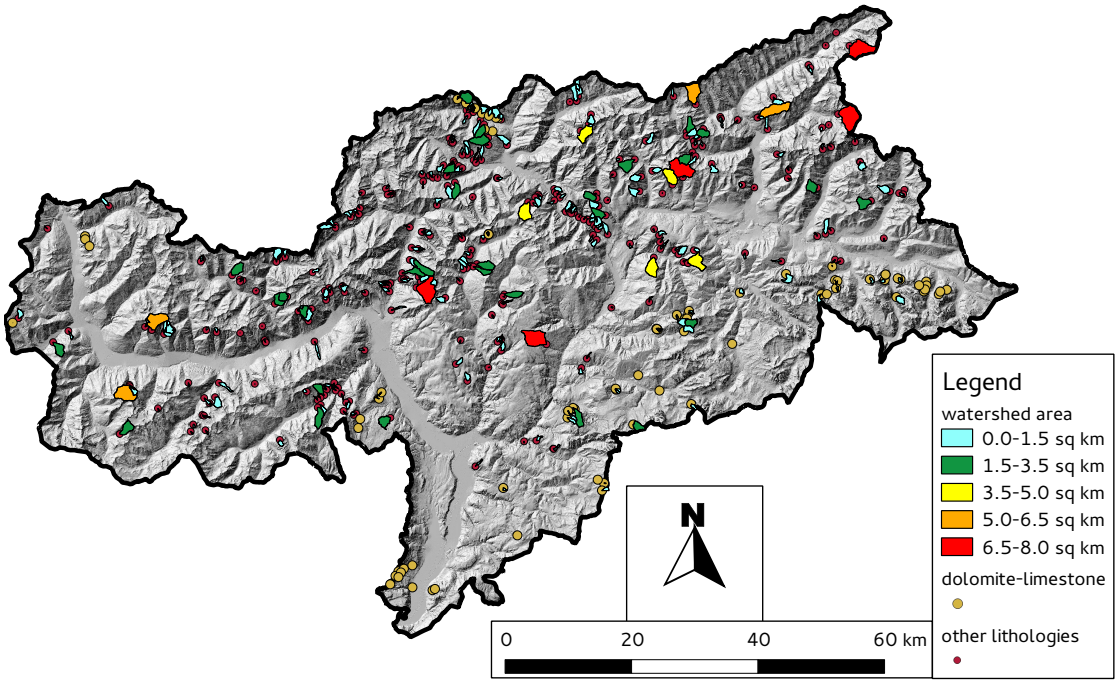

Figure 4.1: Regional DF watersheds distribution, for slope and area analysis

Scatter plots of local slope versus upslope area are presented undifferentiated (Fig. 4.2), with seasonal subdivision (Fig. 4.3), subdivided according to geologic condition (Fig. 4.4) and in relation to storm durations (Figs. 4.5, 4.6). From a first analysis none of the applied criteria seems to influence specific slope-area combinations.

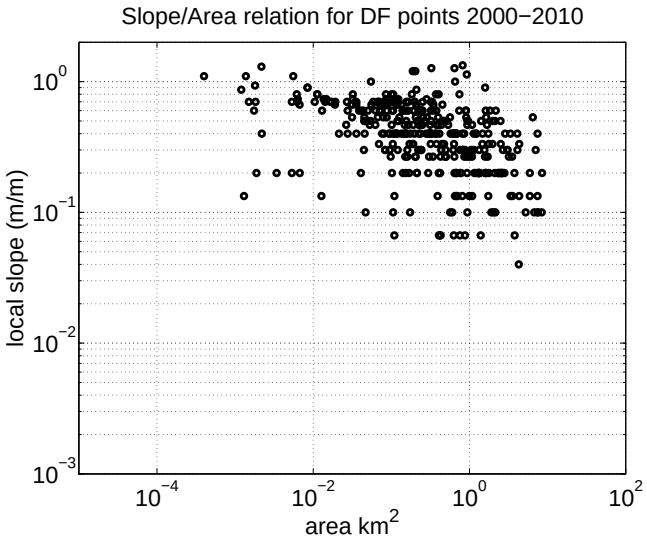

Figure 4.2: Slope-area relation for the 10 years point locations: raw data

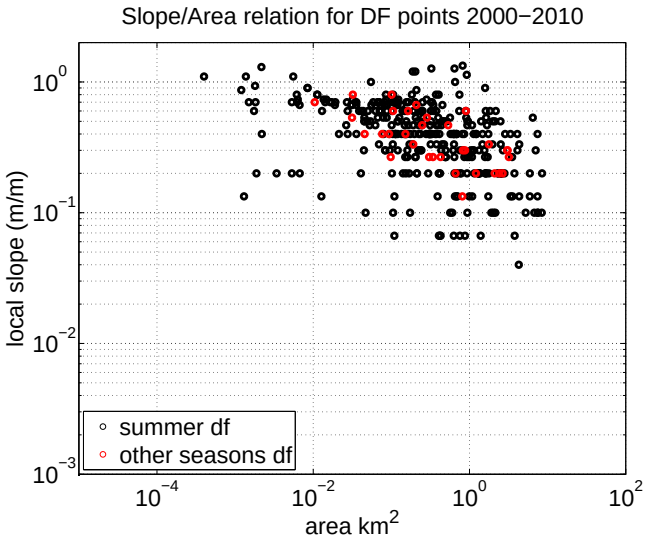

Figure 4.3: Slope-area relation for the 10 years point locations: data divided between summer occurrences and other seasons

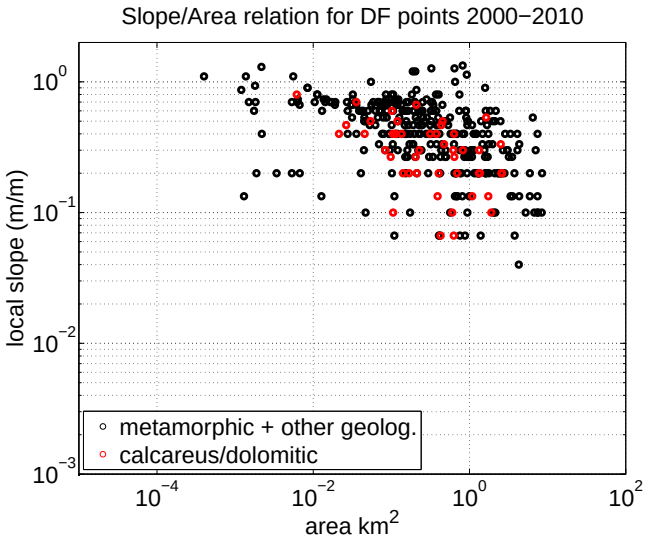

Figure 4.4: Slope-area relation for the 10 years point locations: data divided between occurrences over calcareous/dolomitic matrix and over other geologic contexts (mainly igneous and metamorphic)

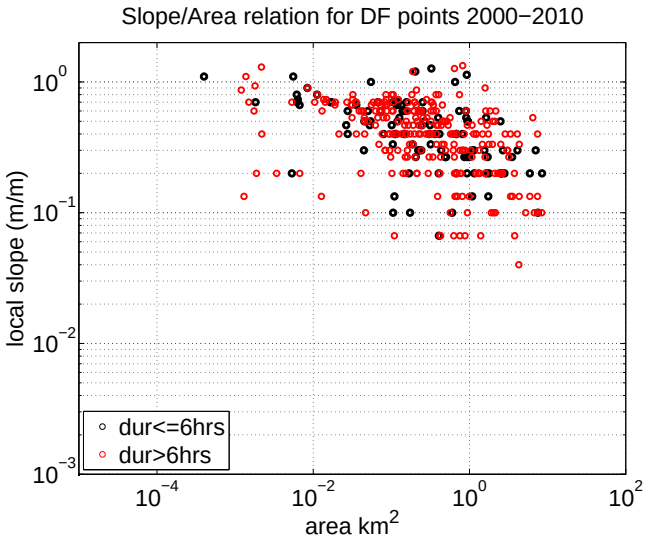

Figure 4.5: Slope-area relation for the 10 years point locations: data divided between events that registered storms lower or greater than 6 hours, from regional rainfall interpolation analysis

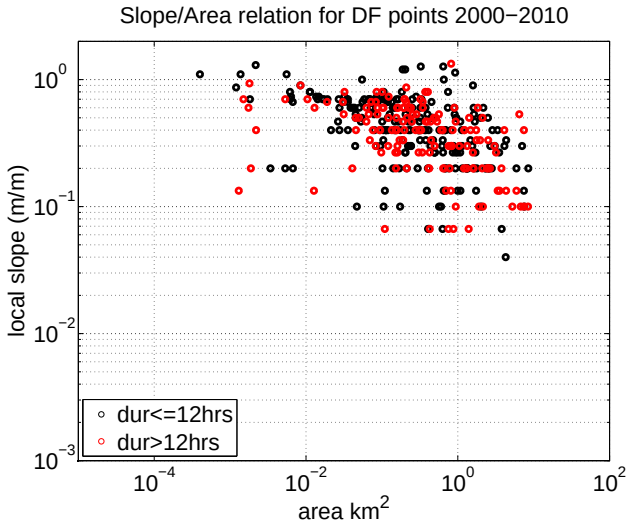

Figure 4.6: Slope-area relation for the 10 years point locations: data divided between events that registered storms lower or greater than 12 hours, from regional rainfall interpolation analysis

In general data appear to be in line with what we find in literature (Montgomery and Foufoula-Georgiou, 1993; Montgomery, 2001; Tarolli and Dalla Fontana, 2009).

Some slope-area combinations are located at low slope values and/or large upstream areas; these points have been checked on orthophotos and usually the correspond to glacial valleys context (where the glaciers or permanent snow are playing an important role in terms of runoff routing and melting contribution), or to localized channels conveying runoff from a higher elevation plateau followed by a steep slope, thus increasing the contributing area to the point. For some cases they actually appear to be at almost flat conditions, these situations are heavily influenced by upstream coming flow rather than local morphology.

Data have also been analyzed considering storm durations of 1, 2 and 3 hours, in relation to the maximum intensity rainfall step registered by the event with 5 and 10 and 20 mm as reference, and in relation to the total rainfall registered by the event with 25, 50 and 100 mm as reference, but, almost like in the other filtered cases no significant trends have appeared.

Empirical Cumulative distributions of contributing area and local slope are herein presented (Figs. 4.7, 4.8), along with some examples points located at low slope conditions or high contributing area ones (Fig. 4.13, 4.14) with some considerations on the peculiarities of these examples.

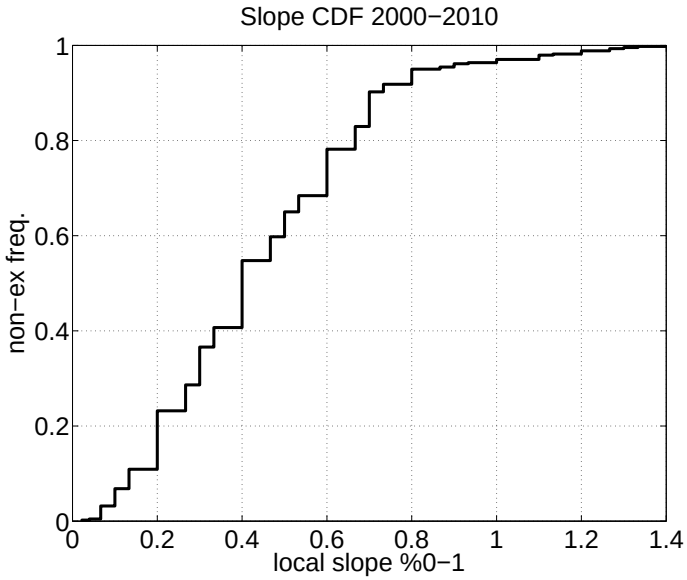

Figure 4.7: Empirical cumulative distributions of the local slope values

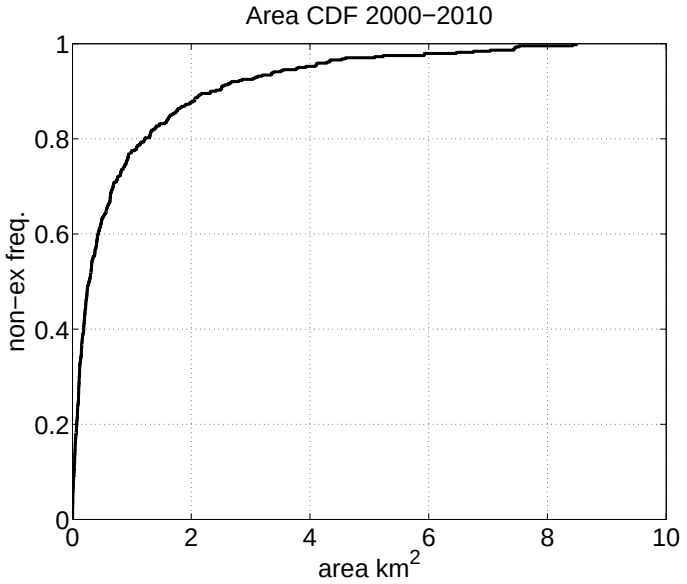

Figure 4.8: Empirical cumulative distributions of the areal values

Slope-area distributions have been analyzed also differentiating points located over dolomitic-limestone context from other lithologies (igneous and metamorphic mainly), detecting some distribution differences in the contributing areas especially for small size watersheds (Fig. 4.11); in calcareous and dolomitic setting it appears that a larger minimum area is needed for the debris flow to occur. This could be ascribed to the higher permeability of carbonate rocks which needs larger areas to produce runoff required for debris-flow initiation. On the other side of the distribution (Fig. 4.11) larger basins are found over igneous and metamorphic lithologies, probably resulting from the much larger sample size. Regarding the local slope the two distributions differ (Fig. 4.12) and it seems that triggering points are located at steeper conditions over igneous and metamorphic lithologies. This could be ascribed to the frequent occurrence of debris flows in steep channelized upper part of the catchments over metamorphic lithologies (Fig. 4.9) while lower slope values for dolomitic and limestone lithologies could be influenced by the usual presence of a strong slope discontinuity between the rocky headwaters and the scree slopes; at this interface there is usually a sudden change in slope and many debris flows are triggered due to flow conveyance from the upper rocky headwaters (Fig. 4.10).

Fig. 4.15 presents slope-area values averaged per increasing areal classes (with a log step) as in Montgomery (2001), with values coherent with what we find in literature.

Figure 4.9: Example of a debris-flow initiation site over metamorphic lithology

Figure 4.10: Example of a debris-flow initiation site over dolomitic lithology

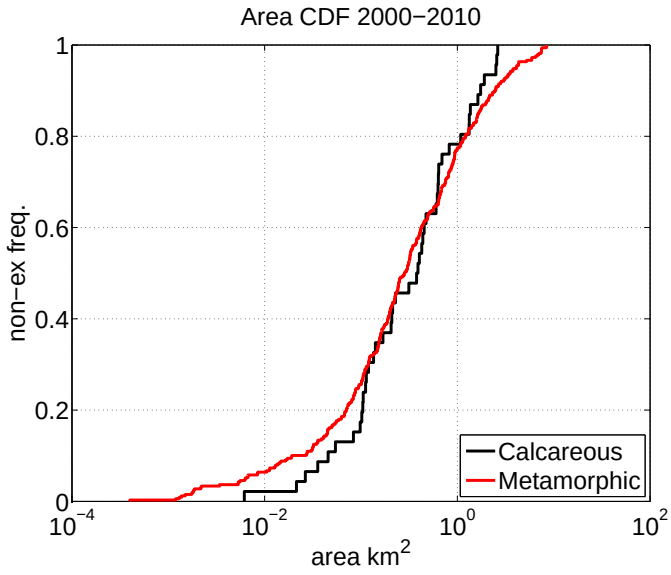

Figure 4.11: Empirical cumulative distributions of the areal values for the analyzed locations divided into calcareous and metamorphic lithology

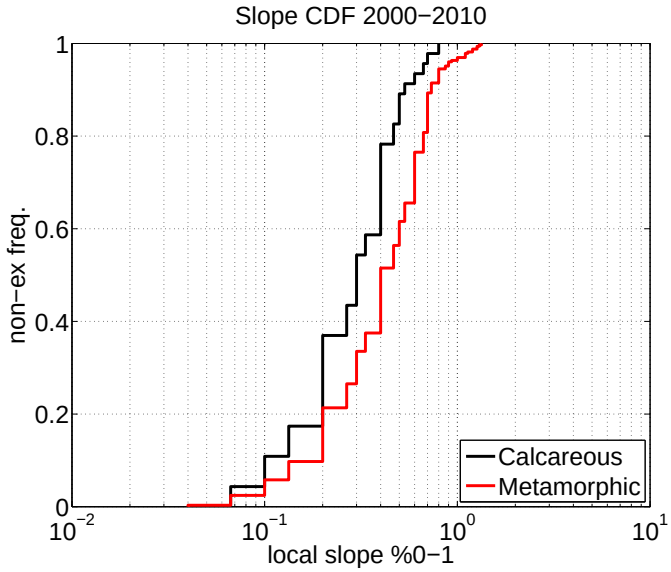

Figure 4.12: Empirical cumulative distributions of the slope values for the analyzed locations divided into calcareous and metamorphic lithology

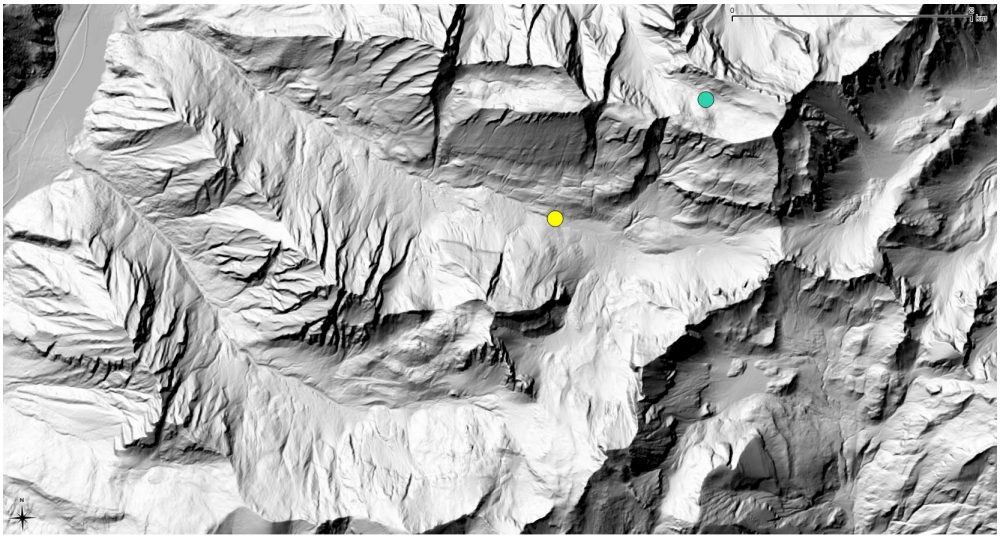

Figure 4.13: Example of low slope DF triggering point (yellow dot): potential contribution from lateral channels conveying water probably with important discharges/velocities are visible

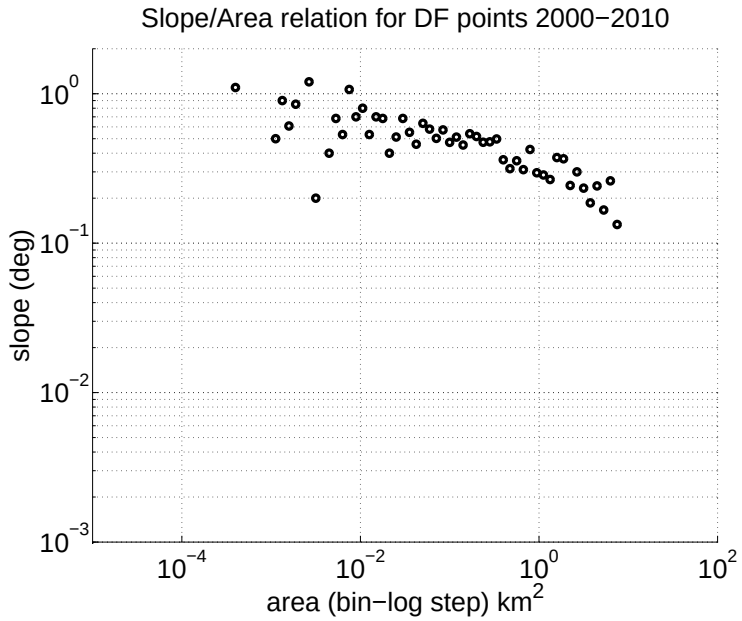

Figure 4.15: slope-area relation average values for increasing classes with a log step

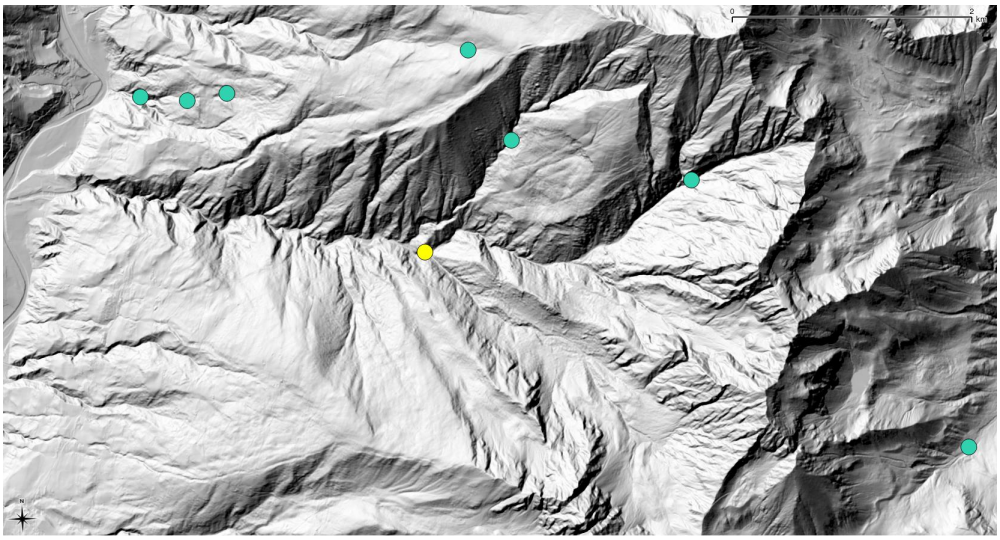

Figure 4.14: Example of high contributing area-located triggering point (yellow dot): the area is at the confluence of three DF active channels, (the process is more evident after the confluence) potentially DF could start upstream of this point but eventually DF can start also at this location, in the case for example of something similar to the well known firehose effect, but at large scale (the location can receive sediment-rich flows, enhancing the kinematic energy on the point)

In conclusion, this morphometric analysis showed that the topographic features that characterize the analyzed triggering locations are comparable with literature findings for studies carried out in similar contexts (Tarolli and Dalla Fontana, 2009). Regretfully, the effort carried out to discriminate potential relation of the morphometric features with other variables such as lithology or storm duration/intensity has not led to clear relations or distinctions. These results suggest that, in order to be able to assess influencing conditions for the triggering of debris flows, a deeper analysis is needed and also a field mapping activity is many times imperative to point the variability of the analyzed phenomena (Brardinoni et al., 2012), especially when dealing with local lithological variability.

4.2 Intensity-Duration thresholds

The results of the Intensity Duration (ID) analysis are reported from Fig. 4.16 to Fig. 4.22. The complete series and the series stopped at maximum hourly value both for the IDW interpolation and the nearest gauge approach are shown along with a distance weight (Fig. 4.21) plot, a discrimination between carbonate and other lithologies (Fig. 4.20) and a 5-mm threshold (per single step) filtered series (Fig. 4.22) are finally considered.

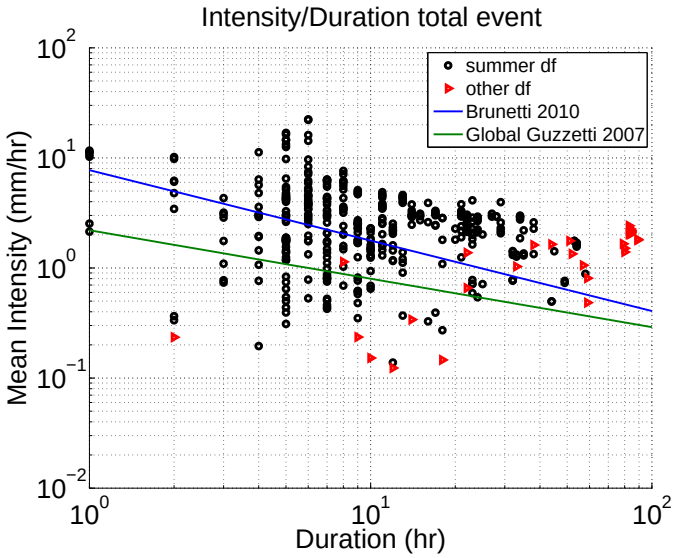

Figure 4.16: ID scatter plot with IDW interpolation as reference, total series are herein considered.

As a general comment on this analysis, the discrimination between carbonate (calcareous and dolomitic) and other lithologies seems not to differentiate particular conditions; similarly, greater "triggering point to gauge" distances seem to be located in higher percentage below the reference thresholds but a

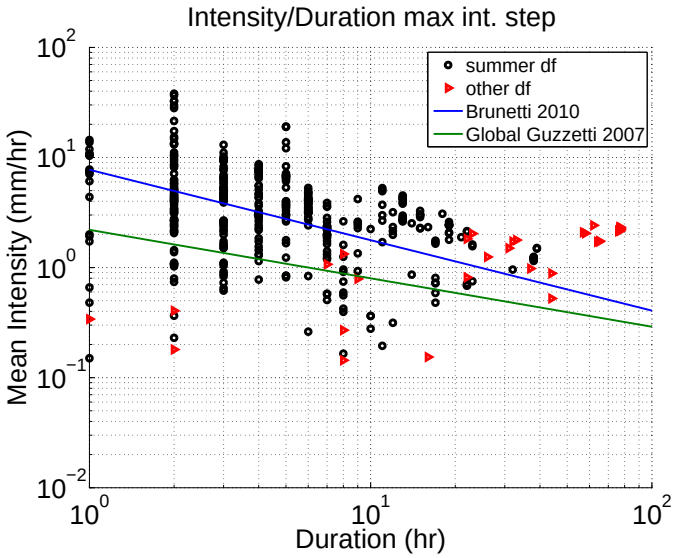

Figure 4.17: ID scatter plot with IDW interpolation as reference, series refer to the maximum hourly value.

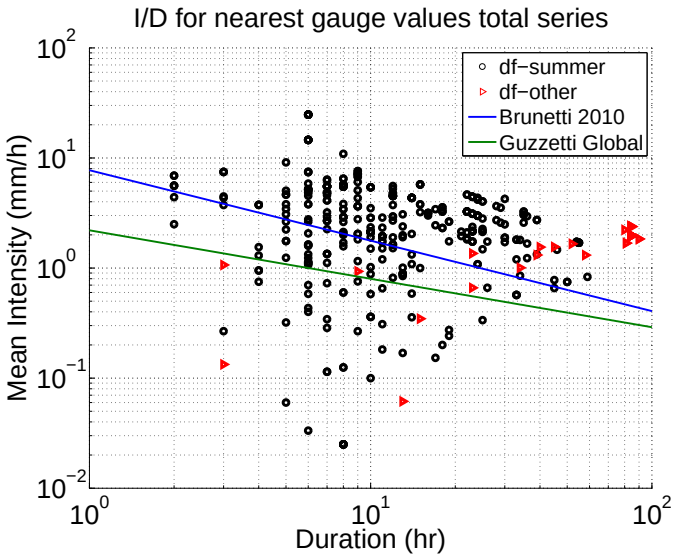

Figure 4.18: ID scatter plot with IDW interpolation as reference, total series are herein considered.

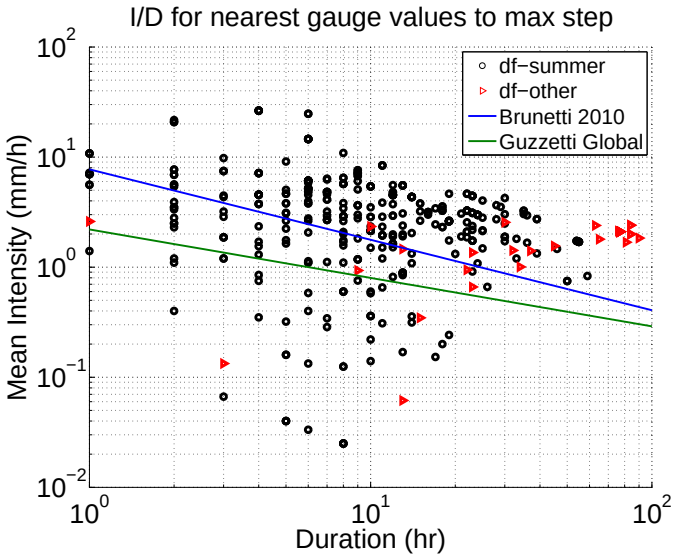

Figure 4.19: ID scatter plot with nearest gauge as reference, series refer to the maximum hourly value

clear trend is not visible.

Stopping the series at maximum hourly values is from one side coherent with the already mentioned studied events, and on the other side performs better in respect to the reference thresholds.

For all the non thresholded cases (Tab. 7), part of the sample (12-18%), is located below the reference global threshold (Tab. 7). This could be partially ascribed to the strong climatic regional variability. Part of the western portion of the study area belongs in fact, to the dry inner alpine region, with a mean annual precipitation (MAP) ranging between 400 mm and 700 mm, the result of sheltering of the mountain range to southerly and northerly winds. The MAP increases to 1300 mm in the Northern portion of the region, where the rainfall regime is conditioned by the intensification of rainfall when warm and moist air from the Mediterranean Sea is lifted over the Alps. The dry-to-moderate rain-

fall regime is reflected also in the climatology of the rainfall extremes. Rainfall quantiles corresponding to a 100-year return period rarely exceed 50 mm at 1-hour duration, and 150 mm at 24-hour duration.

Strong precipitation orographic gradients along with an intense short range (2-5 km) rainfall directional variability are also well known issues for the area (Marchi et al., 2014; Marra et al., 2013).

If we combine the above mentioned considerations with the average density of the raingauges network (1 every 70 km^2) the potential undersampling of gauges-derived threshold in such a complex environment becomes evident. Looking at Fig. 3.3 we can observe that for more of the 20% of the cases the nearest gauge is located at a distance >6 km, thus probably not detecting the real storm dynamic over the triggering location.

Thresholds based on the frequentist approach (Brunetti et al., 2010) have been computed also using the ten-year dataset herein discussed and the results are summarized in Table 7.

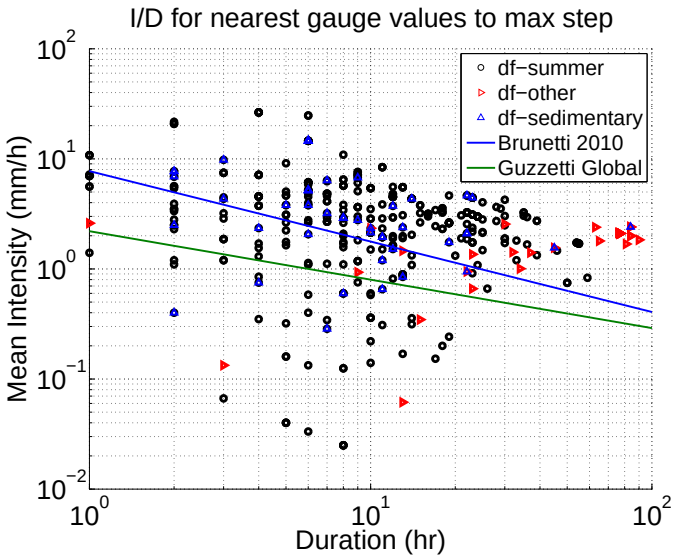

Figure 4.20: ID scatter plot with nearest gauge as reference, series refer to the maximum hourly value, carbonate context points are herein highlighted.

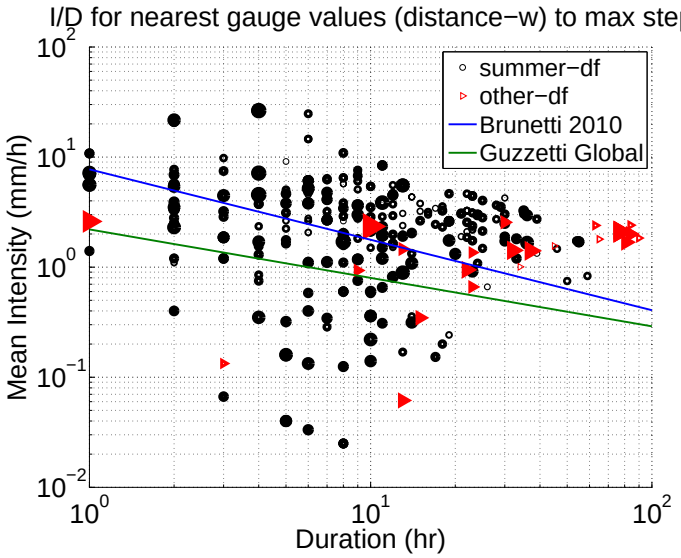

Figure 4.21: ID scatter plot with nearest gauge as reference, series refer to the total series, marker dimension is a function of the distance to the df triggering location.

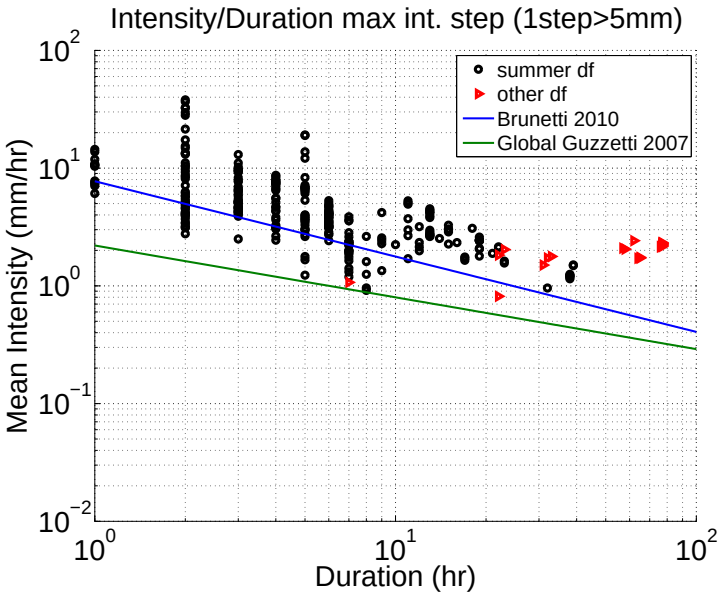

Figure 4.22: ID scatter plot with IDW interpolation as reference, series refer to the maximum hourly value and a threshold of 5-mm (to be registered at least in one case) on the intensity value is chosen.

Table 7: Intensity-Duration equation parameters (derived with a frequentist approach as described in Brunetti et al., 2010), and threshold comparison to the reference global equation (Guzzetti et al., 2008) for values derived from a regional IDW interpolation and from the nearest available raingauge

Dataset	**Threshold**	**coeff_1%**	**exp_1%**	**coeff_5%**	**exp_5%**	**zeros**	**# of events**	**score to ref(%)**	**# pts / total %**	**score coeff. %**
Interpolation to max										
all data (442 records) 8 NaN	-	0.8323	-0.3313	1.3172	-0.3313	-	434	87.09	100.00	2.09
	2.5 mm one step	1.909	-0.4309	2.8003	-0.4309	-	381	97.63	87.79	10.80
	5 mm one step	3.2725	-0.4654	4.4751	-0.4654	-	317	100	73.04	**10.96**
	120 km inter distance	1.3914	-0.3823	1.9937	-0.3823	-	322	92.23	74.19	3.36
	5% contributing gauges	0.9207	-0.3442	1.4273	-0.3442	-	416	88.46	95.85	2.84
	50% contributing gauges	1.6531	-0.3828	2.3114	-0.3828	-	198	95.45	45.62	2.29
	100% contributing gauges	3.7975	-0.4885	4.5696	-0.4885	-	25	100	5.76	0.86
Interpolation complete										
all data (442 records) 8 NaN	-	0.6555	-0.2059	1.0195	-0.2059	-	434	88.24	100.00	3.24
	5 mm one step	2.9207	-0.3691	3.8516	-0.3691	-	317	99.68	73.04	**10.64**
	120 km inter distance	1.3115	-0.303	1.8325	-0.303	-	322	94.09	74.19	5.22
	50% contributing gauges	1.4506	-0.2758	1.9473	-0.2758	-	198	96.97	45.62	3.81
Nearest gauge to max										
all data (442 records) 8 NaN	-	0.9122	-0.3837	1.4489	-0.3837	25	434	82.25	100.00	-2.75
	2.5 mm one step	2.2878	-0.4524	3.4225	-0.4524	0	362	96.96	83.41	9.47
	5 mm one step	3.2978	-0.4762	4.7424	-0.4762	0	332	99.39	76.50	**10.86**
	2.5 km search radius	4.569	-0.6627	6.46	-0.6627	3	80	91.25	18.43	-5.99
	5 km search radius	2.454	-0.5845	3.6374	-0.5845	5	220	90	50.69	-2.40
	10 km search radius	0.9071	-0.3934	1.4385	-0.3934	15	412	83.73	94.93	-2.03
Nearest gauge complete										
all data (442 records) 8 NaN	-	0.3981	-0.1281	0.6546	-0.1281	25	434	82.94	100.00	-2.06
	5mm one step	2.3673	-0.3592	3.3445	-0.3592	0	332	99.00	76.00	**10.90**
	5 km search radius	1.2641	-0.2774	1.8611	-0.2774	5	220	90.2	50.50	-2.32

All the scores and coefficients as described in the previous sections are reported for the different analyzed thresholds, in Tab. 7.

In conclusion, considering the above mentioned set of analyses it appears that the rainfall needed for debris flow initiation in the upper Adige River basin is in general low, if compared to other alpine areas; this is coherent with the climatic features that characterize the area as a dry inner alpine region. Furthermore it appears that the most efficient combination of thresholds and filtering in the datasets, in order to have both a good score to the reference equation and to preserve a good dataset size is the 5-mm threshold on rainfall intensity for the single step. This fact may be due to the selection of storms with, at least, one step presenting a sufficient threshold on intensity to consider the occurrence of a debris flow more probable taking into account also the kinetic energy that characterizes more intense rainfall bursts.

Thresholds on rainfall intensity are also the most weighty in modifying the ID equation if compared to thresholds on raingauges percentage contribution and threshold on inter distances or search radius.

4.3 Uncertainty on rainfall thresholds

In order to assess the influence of rainfall estimation on the thresholds for debris-flow initiation, the experiment described in the section 3.3.1 has been carried out.

We recall here that two sets of raingauges have been selected, one assumed to represent debris-flow initiation point (DFR), the second representing the closest rainfall measurement point (MR).

4.3.1 Comparison between DFR and MR observations

We compared the DFR and the MR rainfall observations to provide a quantitative estimate of the rainfall error magnitude, and to highlight the differences with respect to the debris-flow rainfall events. Fig. 4.23 compares the values of the hourly rainfall intensity for the period from June to September, between 2000 and 2010. The average bias (expressed as the ratio MR/DFR) decreases nonlinearly with increasing rainfall intensity. The ratio starts from a 60% overestimation (at MR) for low intensity rainfall events (< 2 mm/hr), decreases rapidly to underestimation for high intensity rainfall events, and reaches almost 40% underestimation for rainfall intensities larger than 10 mm/hr. This confirms that low rainfall values are usually overestimated, whereas large rainfall values are underestimated.

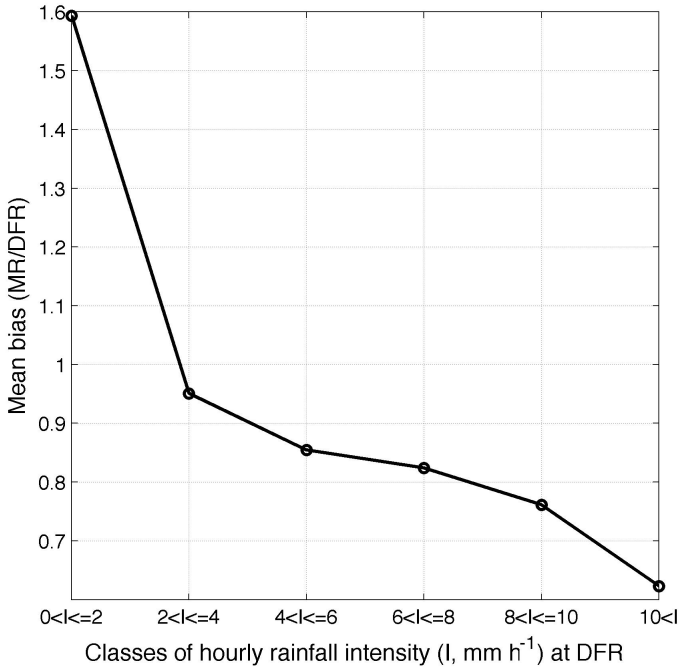

Figure 4.23: Mean bias (as ratio of MR to DFR) of hourly rainfall intensity versus different classes of rainfall intensity measured at DFR.

We further examined the differences between the rainfall events (identified with a 2 days hiatus between two following events and using a threshold on cumulative rainfall (5 mm) to set the beginning of an event), which is more relevant to uncertainty in ID thresholds. Fig. 4.24 shows quantile-quantile plots for the debris-flow triggering rainfall cumulative depths (E) measured at MR and DFR raingauges for various rainfall durations (D). Results are shown for the reference ID $I = 4.15D^{-0.68}$ and four different rainfall duration ranges are considered: D<=6 hours; 6 hours $< D <=$ 12 hours; 12 hours $< D <=$ 24 hours; and D>24 hours. The quantile-quantile plots permit a comparison of the corresponding distribution of rainfall depths between the MR and the DFR

raingauges. Comparison of the various quantiles, and more specifically of the lower quantiles for debris-flow triggering rainfall events, is quite intuitive regarding the general effect of rainfall uncertainty and ID threshold. Inspection of Fig. 4.24 shows clearly that the lower quantiles (first and second lowest points correspond to 1% and 5% exceedance, respectively) are systematically underestimated by MR, for all durations. This is particularly interesting because the higher quantiles exhibit a different pattern, with slight overestimation for durations less than 12 hours, and no apparent bias for durations longer than 12 hours. This provides additional evidence showing that indeed uncertainty in rainfall estimation is particularly important for the estimation of lower thresholds. Thus showing that the rational discussed above regarding underestimated ID thresholds due to uncertainty in rainfall estimation is valid.

4.3.2 Impact of rainfall estimation uncertainty on ID thresholds

Comparison between the model coefficient for the reference and the estimated threshold was based on the calculation of biases, defined as the ratios $\alpha_r = \hat{\alpha}/\alpha$ and $\beta_r = \beta/\beta$, where and are the estimation bias for the constant α and the exponent β, respectively.

Fig. 4.25 summarizes the results. The bias for the constant α (Fig. 4.25a) is in the range 0.25 - 0.5, suggesting a significant underestimation of the estimated rainfall thresholds due to uncertainty in the rainfall estimation. Overall, there is a slight decrease in the bias (i.e., a larger underestimation) for increasing α, which is more apparent for the case of $\beta = 0.4$. For the other two exponents examined (0.5, 0.6) the bias converges to ~ 0.32 for values of α greater than

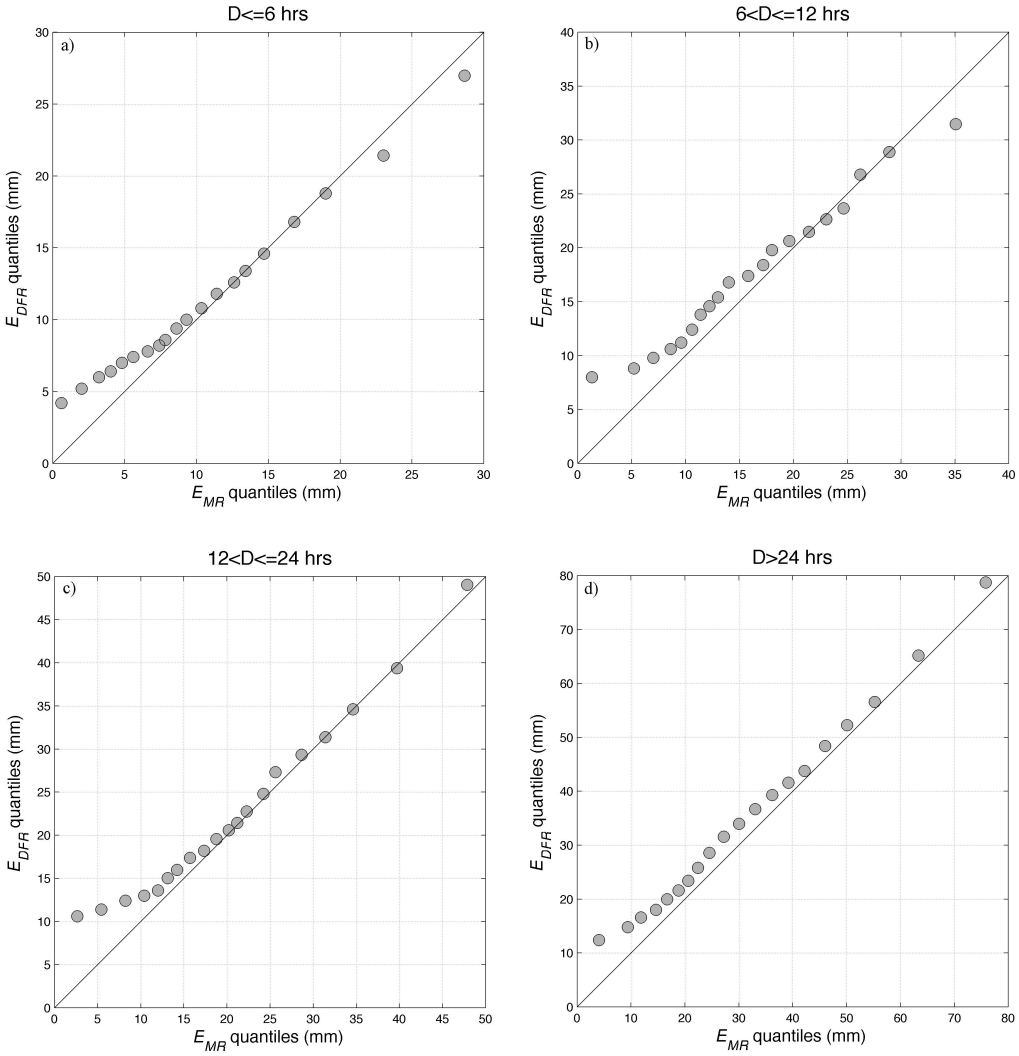

Figure 4.24: Quantile-quantile plots for the debris flow triggering rainfall depths measured at MR and DFR raingauges. Four different rainfall duration ranges are considered: a) $D <= 6$ hours; b) 6 hours $< D <= 12$ hours; c) 12 hours $< D <= 24$ hours; d) $D > 24$ hours. Results are shown for the reference ID $I = 4.15D^{-0.68}$.

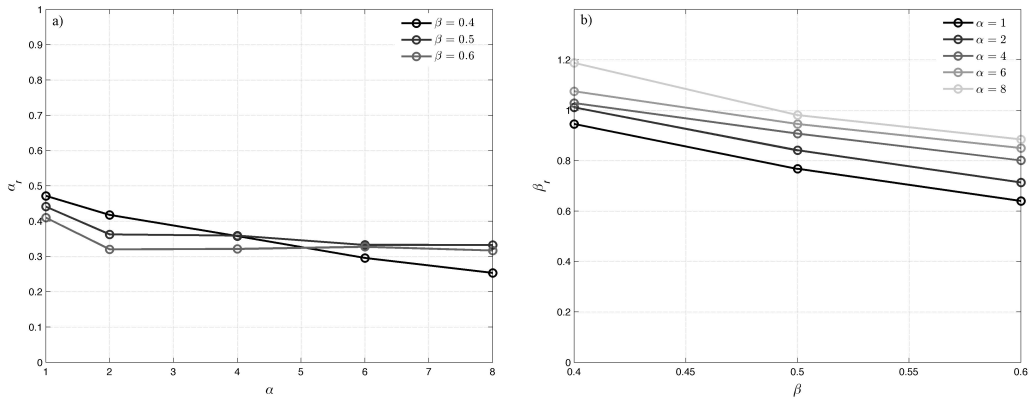

Figure 4.25: Ratio of estimated to theoretical a) multiplier and b) exponent for the various theoretical ID relationships examined.

4. The bias for the exponent β (Fig. 4.25b) is smaller than the bias for the constant α, and ranges between 0.62 and 1.2. With the exception of $\beta = 0.4$, for which the bias changes from underestimation (0.9) to overestimation (1.2), the exponent β is underestimated for all the examined scenarios. The underestimation of the exponent increases with increasing β and decreasing α. We conclude that for values of $\beta > 0.5$ and for thresholds located at the higher end of the rainfall spectrum ($\alpha > 4$), the estimation of the exponent β of the ID threshold relationship are more accurate than for the thresholds located in the lower end of the possible rainfall regime. Overall, the bias in the exponent reflects differences in the spatial structure of short duration and long duration rainfall events; more specifically, it shows the well known effect of increasing variability of rainfall with reducing the duration of the event. Variation of the bias with the severity of the threshold is likely to depend on the percentage of short duration rainfall events in the over-the-threshold rainfall events.

4.3.3 Performance of ID threshold for the prediction of debris-flows occurrence

The performance of a threshold i.e., the ability of the threshold model to identify the rainfall events that have resulted in debris flows, was examined calculating for each scenario standard contingency table statistics, including: (i) the Probability of Detection (POD), (ii) the False Alarm Ratio (FAR), and (iii) the Critical Success Index (CSI). The POD measures the fraction of rainfall events with debris flows successfully detected by an ID threshold. The range of values for POD goes from 0 to 1, the latter value being desirable. POD = 1 means that all occurrences of the event were correctly forecasted. The FAR gives the fraction of the rainfall events above the estimated ID threshold that did not correspond to rainfall events with debris flows (i.e., the false positives). The range of values for FAR goes from 0 to 1, the former value being desirable. A FAR of zero means that no non-occurrences of the event were forecasted to occur. The CSI assesses the skill of the prediction using information on positive and false detections, and on the missed detections. The range of values for CSI goes from 0 to 1, the latter being desirable. Results for all scenarios are summarized in Fig. 4.26. Considering the CSI values, the performance is decreasing nonlinearly with increasing rainfall thresholds α and with decreasing the value of the exponent β. This means that the higher the rainfall quantile corresponding to debris-flow triggering events, the lower the performance of the threshold. Overall, for the lower thresholds ($\alpha <= 2$) the performance is from good to excellent (0.7 - 0.95 CSI), but it drops to a poor performance (< 0.5) for $\alpha >= 4$. It is worth to note that while POD values remain above 92% for all the examined cases, the high ratio of false detection is responsible for low-

ering the overall performance of the system. Note that the dependence of FAR and CSI with ID is similar (but inverse). This means that the main problem with the exploitation of an estimated ID threshold is false detection, especially for high rainfall thresholds. In terms of rainfall distribution between DFR and MR, it means that the high precipitation events (i.e., corresponding to a higher quantile) over DFR are associated with less extreme (i.e., corresponding to a lower quantile) than for the MR. Physically, this can be ascribed to high precipitation events concentrated over DFR but with lower rainfall values where the MR are located.

4.3.4 Influence of the selection of exceedance levels on ID model estimation and prediction accuracy

Results from previous sections have shown that estimated ID at 1% exceedance level are underestimated relative to the reference thresholds. This suggests that application of a higher exceedance level in the ID estimation procedure would reduce underestimation. However, it is important to understand (i) how improvement in ID estimation relates to exceedance level used and, furthermore, (ii) what is the effect of this on the performance of the estimated ID threshold. In this section we examine the influence exerted by the selection of a certain exceedance level on the ID selection and prediction accuracy. To investigate these aspects, we applied seven different exceedance levels in the frequentist method (namely 1%, 5%, 10%, 20%, 30%, 40% and 50%) to estimate the ID threshold model based on MR data. The experiment was carried out for a reference ID threshold, characterized by $\alpha = 4$ and $\beta = 0.5$ that correspond to the central

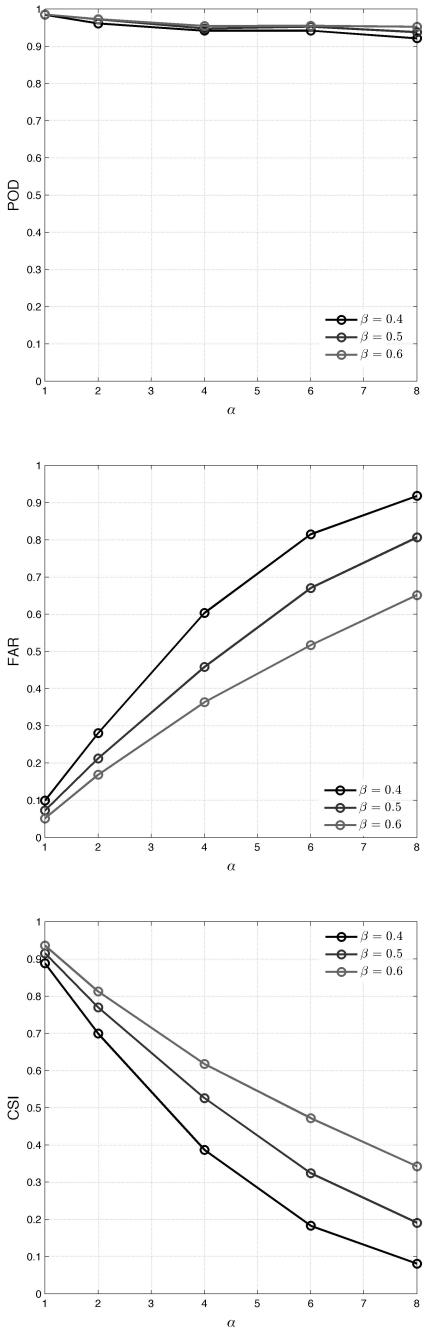

Figure 4.26: Probability of detection (POD) (top), false alarm ratio (FAR) (middle), and critical success index (CSI) (bottom), as a function of the various theoretical ID relationships examined.

values of the set of reference ID thresholds examined in this work. Estimation of the ID model based on different exceedance levels essentially results in a set of different IDs that have the same exponent but different multipliers, one for each exceedance level. Therefore, each exceedance level in the frequentist method corresponds to a specific error in the estimation of the parameter α. Fig. 4.27a reports the relationship between the used exceedance level and the bias in the identification of the ID model, showing that the relative error in parameter α ranges from -64% for an exceedance level of 1% to + 10% for an exceedance level of 50% (note that minus in relative error denotes underestimation with respect to reference ID). One should note here that there is no theoretical need for a model identified by using an exceedance level of 50% to be unbiased.

The analysis of the results illustrated in Fig. 4.27a may shed light on the relationship between bias of the ID model multiplicative parameter α and the performances of the estimated threshold, hence assisting in the understanding of the findings previously reported. Fig. 4.27b shows the frequency of debris-flows events (relative to overall events exceeding the estimated ID) as a function of the relative error in the estimation of the α parameter with the frequentist method. Fig. 4.27c reports the corresponding statistics POD, FAR and CSI relative to error in α parameter. Inspection of Fig. 4.27b shows that the frequency of debris-flow triggering rainfall increases with increasing the exceedance level and moving from ID underestimation to overestimation, as expected. This means essentially that the higher the estimated threshold is, the more likely is that a point above the threshold will be a debris-flow event. This has a direct impact to FAR, suggesting that the higher the threshold the lower the false alarm ratio as shown in Fig. 4.27c. However, the higher the threshold means also that the more debris-flows events will be located lower than the threshold

and this affects POD. The interplay of POD and FAR for different levels of error results in an overall performance (shown by CSI) that varies only by 15% over the range of errors examined. It is worth noting from these results that the optimal value of CSI is not achieved for the unbiased case but for relative error close to 20% underestimation of ID, which corresponds to an exceedance level approximately to 25% (Fig. 4.27a). One should note also that a 60% underestimation in the estimation of the α parameter has an equal CSI value with the case of 10% overestimation.

In summary, examination of the influence of exceedance level selection revealed that a) the use of different exceedance levels results in a relatively small variation of model threshold performance, as measured by CSI; b) the relationship between threshold model performances and bias in ID estimation is not monotonic (i.e. similar performances can be achieved with significantly different biases in ID estimation) and c) an unbiased ID estimate does not imply optimal performance.

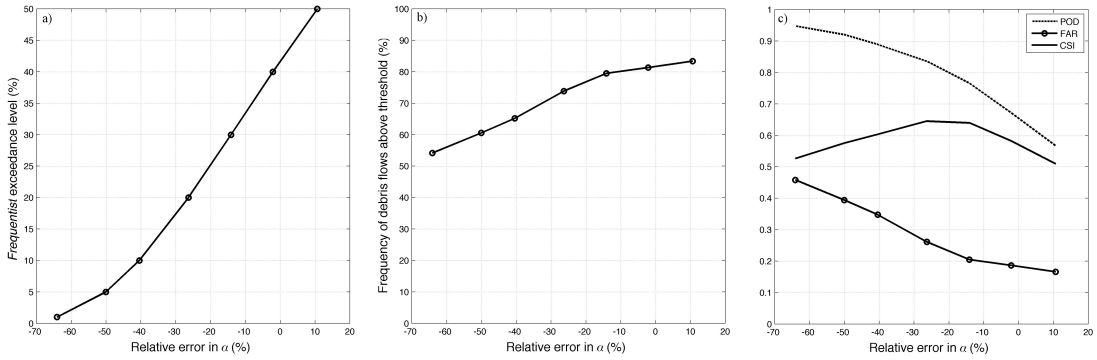

Figure 4.27: Ratio of estimated to theoretical a) multiplier and b) exponent for the various theoretical ID relationships examined.

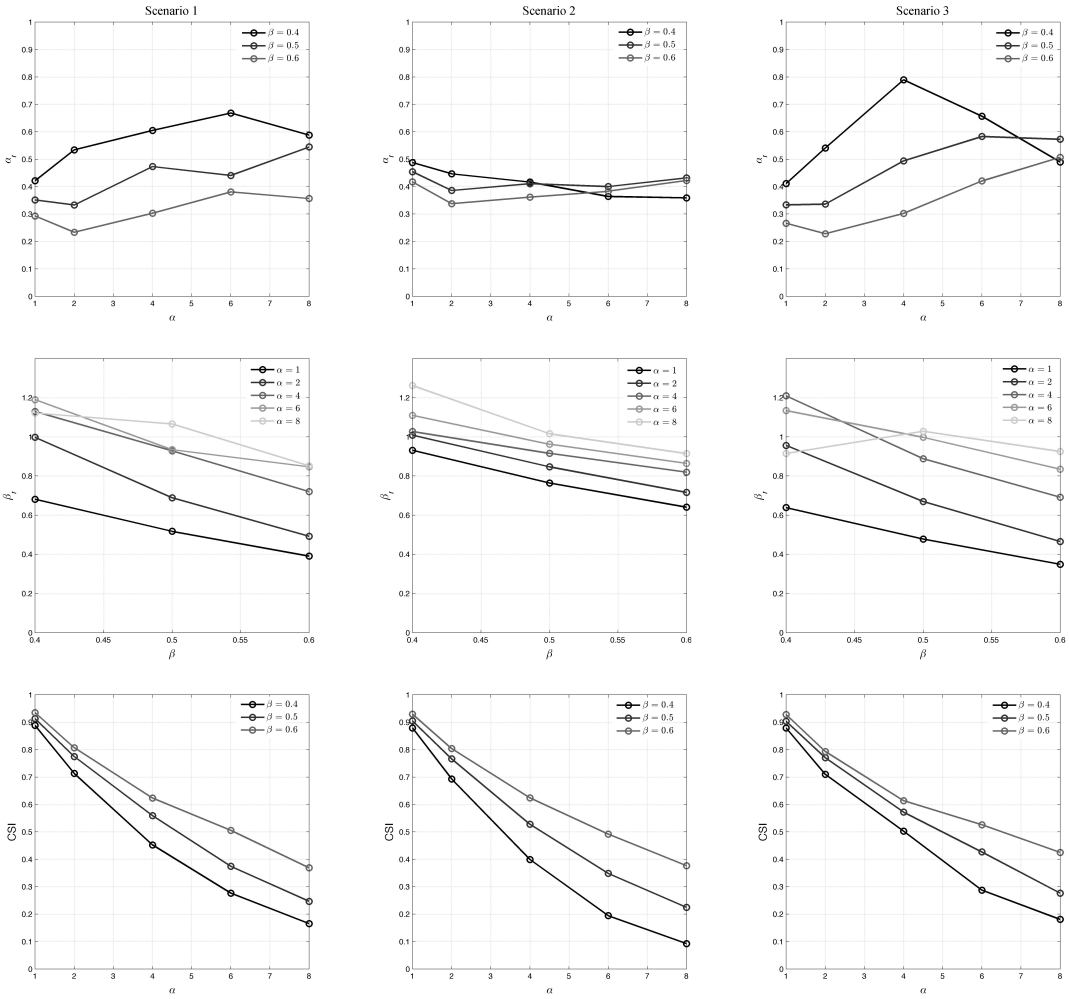

Figure 4.28: Bias in constant α (top), bias in exponent β (middle) and CSI (bottom) for different threshold scenarios reported in Table .

4.3.5 Sensitivity of ID estimation to debris flow-gauge distance and rainfall event duration

Fig. 4.28 shows the results for the estimation bias of parameters α and β. The performances in the prediction of debris-flows occurrence are also reported in terms of CSI statistics. Comparison of the results shown in Fig. 4.28 with the results for the unconditional (i.e., no distance- and rainfall duration- threshold applied) case shown in Fig. 4.25 and in Fig. 4.26 (considered as the reference case) is used to understand the importance of the factors examined in the ID estimation bias and performance. The application of the duration threshold (Scenario 1) leads to improvement in the estimation of parameter α only for cases with high values of α ($\alpha > 4$). This suggests that the application of such threshold works favorably for high ID relationships. The finding is reinforced by the fact that underestimation of exponent β, for the same scenario, is larger (relative to reference case) for $\alpha < 4$. The application of the distance threshold (Scenario 2), shows no significant changes with respect to the reference case. This suggests that the degree of uncertainty in rainfall estimation for raingauges up to 5 km distance is equivalent with that of raingauges up to 12 km distance (the max distance involved in our sample). Results for the third Scenario, which involved application of both thresholds, follow generally the pattern of Scenario 1 with the exception of bias in constant α for the case of $\alpha = 4$ and $\beta = 0.4$ which exhibited a significant improvement when compared to Scenario 1.

4.4 Statistics on different interpolation techniques compared do DFR-MR

This section presents an extension of the analysis of uncertainty on rainfall thresholds: different interpolation techniques have been applied to assess their performance in comparison to the nearest gauge approach.

4.4.1 Complete series analysis

Initially the bias for the different interpolation approaches was calculated following the approach described in 4.3.1, in order to assess the general overestimation/underestimation issue. Correlation coefficient and Nash-Sutcliffe coefficients were than computed, in particular Nash-Sutcliffe coefficient was preferred when evaluating the performance of an interpolation, due to the fact that this coefficient takes also bias in account.
For the main interpolation techniques also the ratio of estimated to theoretical α and β along with the POD, FAR and CSI have been calculated.
As a general comment, looking at the correlation coefficients (Tab. 8) for the whole dataset, the different interpolation techniques seem to have good correlation values, except for the kriging with a 5-km range and the equal-weights approach; the latter has been chosen indeed to evaluate the performance increase brought by the interpolation and its general performance was expected to be low.

Regarding the mean bias estimation (Figs. 4.29, 4.30), the trend reveals an expected overestimation/underestimation of low/high intensity events, but it is interesting to notice the important change in the bias related to the MR. Figs.

Table 8: Summary of the applied statistics to the whole dataset scale.

	MR	**IDW**	**KG_20**	**KG_5**	**MQ**	**SURF**	**EQUAL**
Corr. coeff.	0.663	0.711	0.714	0.684	0.714	0.711	0.645
RMSE	1.838	1.631	1.625	1.676	1.625	1.632	1.759
Nash-Sutcliffe	0.292	0.265	0.279	-0.031	0.285	0.265	-0.210
Bias_paper_approach	1.026	1.078	1.087	1.127	1.091	1.076	1.167
Bias_sum_differences	-0.216	-0.223	-0.215	-0.295	-0.210	-0.224	-0.314

4.29, 4.30 depict indeed two different conditions: the first takes into account values > 0 at both DFR and MR or the interpolant value, while the second considers values > 0 at DFR and values ≥ 0 at MR or the interpolant value. Interesting is the reduced bias in the latter situation (more stable and with a lower range), condition that leads to think to a potential increased performance, due to a better representation of moderate rainfall events. These events were not included in Fig. 4.29 due to the consideration of values strictly > 0, while in the second case (Fig. 4.30) a supposed very low event at DFR is somehow detected even by no rainfall at MR (or interpolant). The difference between a small event at DFR and zero rainfall at MR in the all dataset reveals lower in respect to intense events at DFR which were characterized by moderate rainfall at MR, these latter intense and localized events are indeed the ones increasing the bias.

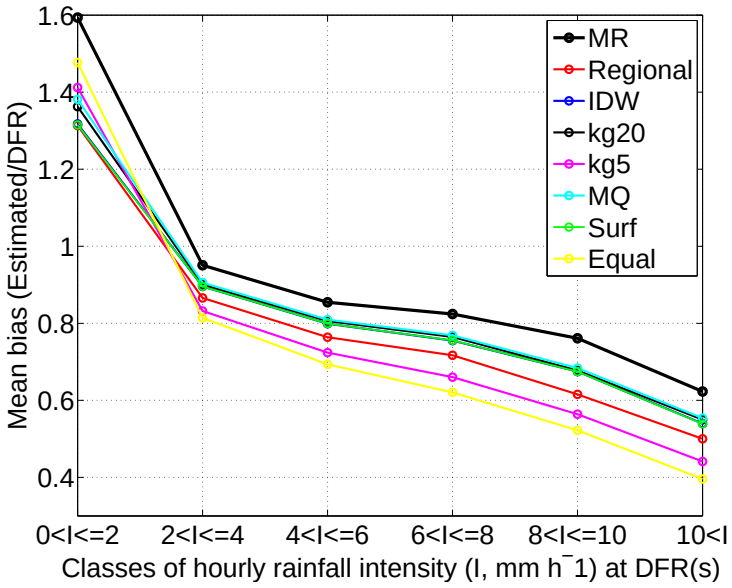

Figure 4.29: Mean bias (ratio estimated to DFR) of hourly rainfall intensity vs different classes of rainfall intensity, (rainfall > 0 both in DFR records and in MR or interpolation).

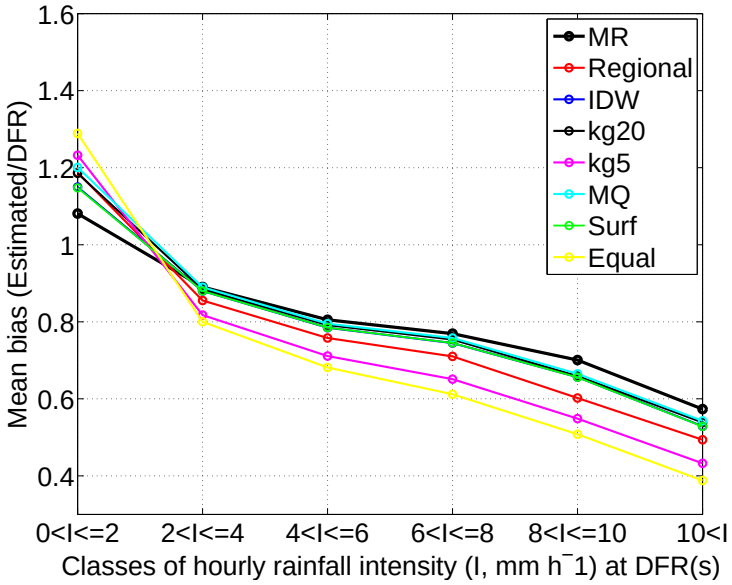

Figure 4.30: Mean bias (ratio estimated to DFR) of hourly rainfall intensity vs different classes of rainfall intensity, (rainfall > 0 at DFR and ≥ 0 at MR or interpolations).

We recall here the considered interpolation algorithms:

- Inverse Distance Weighted (IDW) using euclidean distances (Figs. 4.31, 4.32)
- Inverse Distance Weighted (IDW) using surface distances (Fig. 4.33)
- Ordinary Multiquadratic (Fig. 4.34)
- Ordinary Kriging with a 20-km range (Fig. 4.35)
- Ordinary Kriging with a 5-km range (Fig. 4.36)
- Equal-Weights approach (Fig. 4.37)

4.4.2 Gauges-related analysis

In the following paragraphs the outcomes of correlation analysis for the different interpolations as described in section 3.4 (considering separately all the 17 DFR) are reported; correlation is expressed in respect to the rainfall data and in respect to the distance from the selected DFR, along with correlation Nash-Sutcliffe efficiency coefficient is graphically reported.
Ratio of estimated to theoretical α and β, POD, FAR and CSI outcomes (Fig. 4.31) have been reported only for the case of IDW interpolation because the general trends were very similar for the analyzed interpolations except for the equal weights approach and the kriging with 5-km range that showed a lower performance, as expected.

IDW-euclidean distances

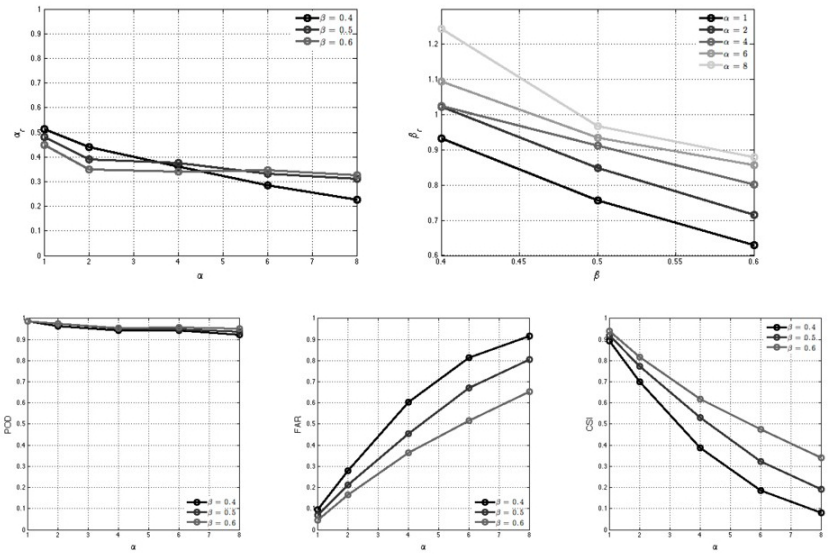

Figure 4.31: Ratio of estimated to theoretical α and β, POD, FAR and CSI calculation for IDW interpolation (euclidean distances).

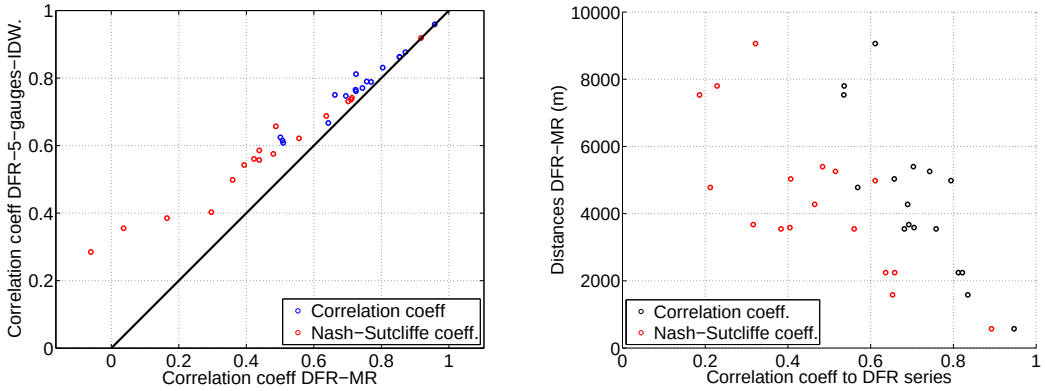

(a) (b)

Figure 4.32: Correlation and Nash-Sutcliffe coefficients for IDW (euclidean distances) interpolation compared to the nearest gauge approach (a); relation of these coefficients with distance (b).

IDW-surface distances

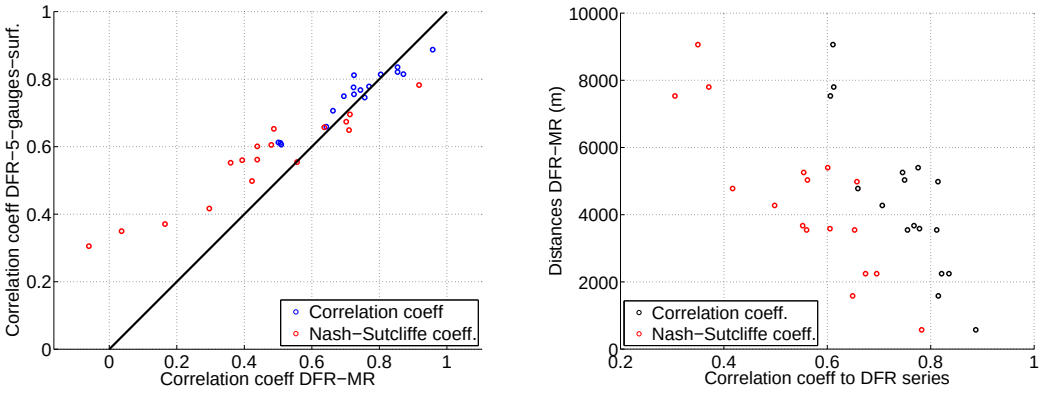

(a) (b)

Figure 4.33: Correlation and Nash-Sutcliffe coefficients for IDW (surface distances) interpolation compared to the nearest gauge approach (a); relation of these coefficients with distance (b).

Ordinary Multiquadratic

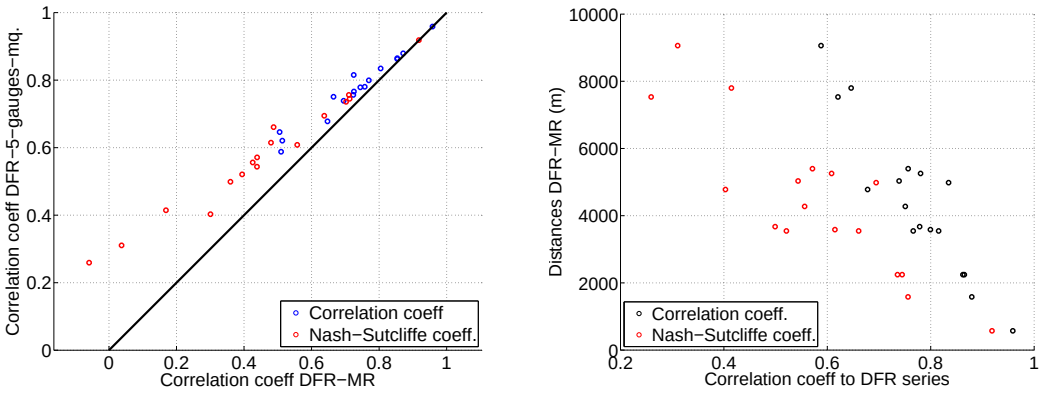

(a) (b)

Figure 4.34: Correlation and Nash-Sutcliffe coefficients for Ordinary Multiquadratic interpolation compared to the nearest gauge approach (a); relation of these coefficients with distance (b).

Ordinary Kriging 20-km range

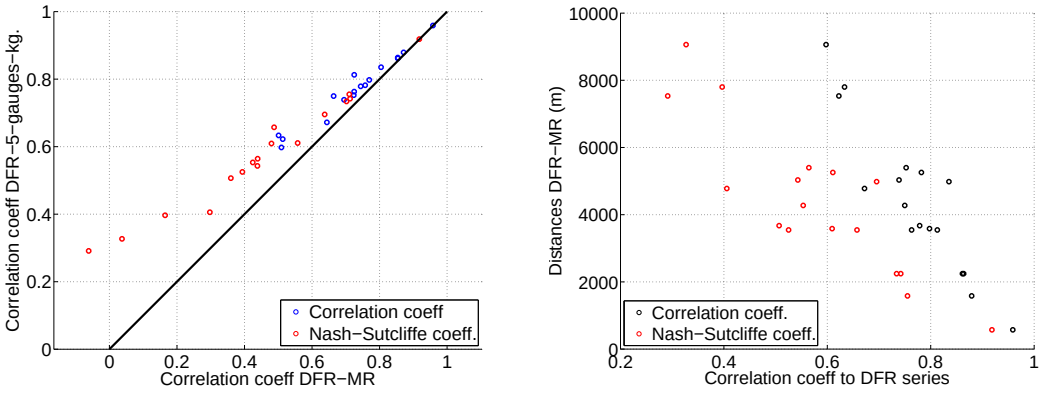

(a) (b)

Figure 4.35: Correlation and Nash-Sutcliffe coefficients for 20-km range Ordinary kriging interpolation compared to the nearest gauge approach (a); relation of these coefficients with distance (b).

Ordinary Kriging 5-km range

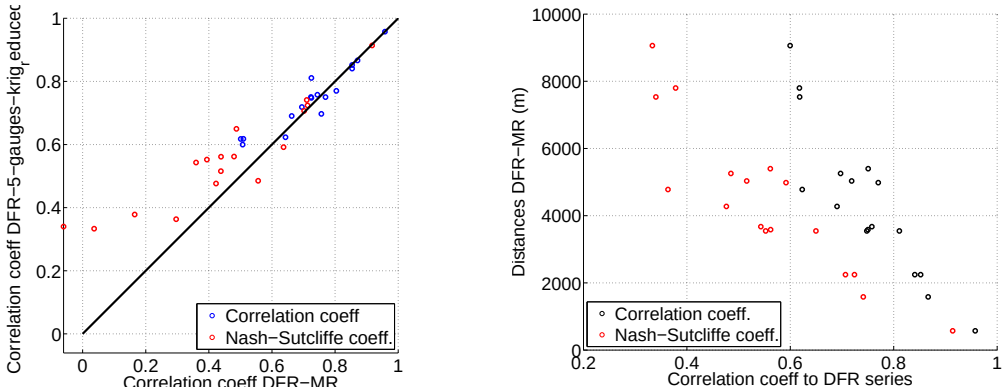

(a) (b)

Figure 4.36: Correlation and Nash-Sutcliffe coefficients for 5-km range Ordinary kriging interpolation compared to the nearest gauge approach (a); relation of these coefficients with distance (b).

Equal-Weights approach We recall here that this approach is an average operator thus not considering different weights deriving from the spatial vari-

ability. It has been used as a comparison to evaluate the performance increase given by the different interpolations.

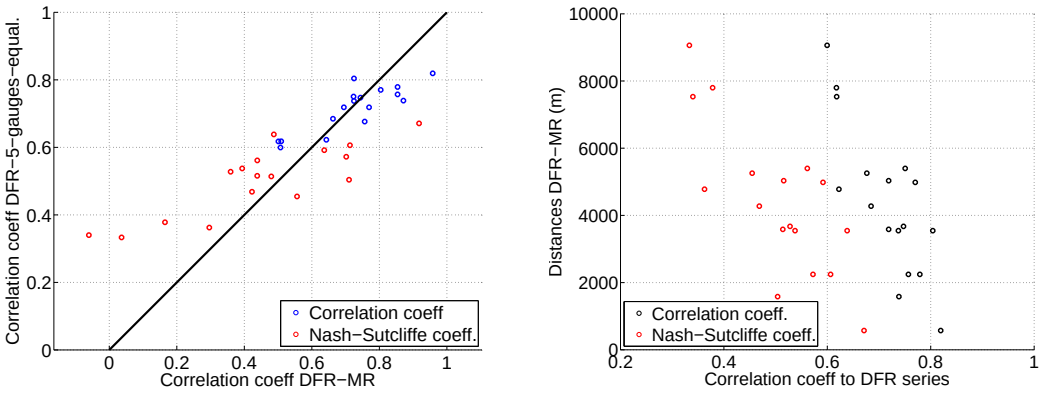

(a) (b)

Figure 4.37: Correlation and Nash-Sutcliffe coefficients for Equal-Weights interpolation compared to the nearest gauge approach (a); relation of these coefficients with distance (b).

4.4.3 Main outcomes

Presenting the main outcomes of the analysis carried out in this section, we can say that the main forcing affecting this type of analysis is related to the distances of the gauges. The correlation coefficients are in fact usually well related to the distance from the gauges.

IDW, kriging (with a 20-km range) and multiquadratic interpolation led to correlation coefficients (and Nash-Sutcliffe too) always greater or equal to the ones of the nearest gauge approach, thus bringing to a better (though not dramatically improved) estimation. The other interpolation techniques (Kriging with a 5-km range, Equal Weights approach) in some cases have shown a worse correlation if compared to MR approach.

Introducing surface distance into IDW interpolation has led not to significant

changes in the estimates thus indicating that surface distance is related to the euclidean one.

Reducing the range of the kriging from 20 to 5 km has revealed to be not a good choice with the present dataset; in particular these interpolation led to a worse performance if compared to the IDW-euclidean-distances and kriging-20-km-range for example, this way suggesting that the nearest gauges within a 5-km range may suffer especially from heavy undersampling of intense events.

Interpolations however have shown correlation improvement, though limited to the case of bad correlation between DFR and MR, thus being important source of information when MR estimation is poor. The experiment of the Equal-weights approach has led to the worst average correlation if compared to the other interpolation techniques but still it is showing a correlation that is on average comparable with the nearest gauge approach, thus confirming that the choice of the 5 nearest gauges is suffering from a bias probably linked to the distance values.

Also the relation to distances is intentionally tho poorest for this type of interpolation, but it is still holding thus emphasizing the explanatory role of distance even when not included as a weight in the interpolation itself. This approach in fact isolates and stresses the distance dependence of the overall analysis, that is related to the underestimation of localized intense events and overestimation of wide long lasting ones.

The influence on the POD, FAR and CSI and the ratio of estimated/theoretical α and β has been almost negligible thus leading to the general conclusion of a small improvement given by the interpolation technique, but still significant especially in the case of poor DFR-MR correlation.

4.5 Conclusions for the regional-scale analyses

The goal of this analysis was to characterize the morphology of debris-flow triggering sites, to derive and analyze a set of rainfall thresholds for debris-flow initiation and to investigate the associated uncertainty in these estimations. Regarding the morphometric characterization of triggering locations, the main outcomes have resulted in:

- Local slope and contributing areas distributions were found comparable with literature findings for similar contexts works.
- The assessment of the local variables (both lithological and hydrological) influence on the triggering process suffers from the scale of the approach. In order to detect the spatial variability of the processes influencing the triggering debris flows sometimes there is the need of a very detailed field analysis, especially when dealing with lithological variability.

Regarding the Assessment of rainfall thresholds for debris-flow initiation the main outcomes are herein presented:

- The analysis of rainfall thresholds manifested in general low amount of rainfall sufficient for the triggering process; this is coherent with the climatic features that characterize the area as a moderate dry inner alpine region. It appears than, that the most efficient way of filtering the datasets, in order to have a good performance of the threshold is to impose a minimum intensity to be achieved at least once in the rain series. This fact may be due to the selection of storms with, at least, one step presenting a sufficient threshold on intensity to consider the occurrence of a debris

flow more probable taking into account also the kinetic energy that characterizes more intense rainfall bursts.

- The rainfall characteristics of the events that have resulted in debris flows can be significantly different from that measured at nearby raingauges. Comparison between DFR and MR showed that lower rainfall accumulation quantiles of rainfall events above a reference ID threshold (i.e., assumed to be debris-flow triggering events) was systematically underestimated. This has consequences on the definition of the rainfall thresholds for possible debris-flow occurrence, and for the application of the thresholds in operational landslide warning systems.

- The differences in the rainfall characteristics of the events that have resulted in debris flows estimated at the locations of the debris flows (DFR), and measured at the nearby raingauges (MR), bias the constant α and the exponent β that control the power law ID threshold model. The bias in the constant α remains nearly constant for a large range of rainfall conditions, whereas the bias in the scaling exponent β increases for lower thresholds. The finding has consequences for the operational use of the thresholds.

- The performance of the ID thresholds, measured by the Critical Success Index (CSI), depends on the threshold, and decreases for higher (more severe) thresholds. The Probability of Detection (POD) was found only slightly affected by the level (severity) of the threshold, whereas the False Alarm Ratio (FAR) increases significantly with increasing thresholds. This outlines the problem of an inconsistent ranking of rainfall

conditions estimated at the locations of the debris flows, and measured by raingauges located in the vicinity of the debris flows, but not at the exact same location.

- The choice of exceedance level applied in frequentist method affects the error in ID estimation and the performance in debris-flow prediction. However, it was shown that optimum performance is not achieved for unbiased ID and moreover similar performance can be achieved for different levels of error in ID estimation.

- Estimation of ID thresholds based only on long duration (> 12 hrs) events can improve bias and performance of estimated ID but only for high ($\alpha > 4$) rainfall thresholds (effect is opposite for low rainfall thresholds). The distance between debris-flow location and nearest gauge did not affect significantly ID estimation for the range of distances examined (up to 12 km).

- The integrations with interpolations from a set of nearby gauges has shown correlation improvement, though limited to the case of bad correlation between DFR and MR, thus being important source of information when MR estimation is poor. The choice of the 5 nearest gauges was anyway suffering from a bias linked to the strong relation with the distance from DFR site.

As previously stated, in this analysis only the natural variability of rainfall was considered as source of uncertainty. Measurement error can be an addi-

tional source of uncertainty not accounted herein. In addition, the uncertainty introduced by the method adopted to determine the threshold model is not considered from the empirical rainfall data (in this case, the frequentist method of Brunetti et al. (2010). Peruccacci et al. (2012), working in Central Italy, have shown that the uncertainty associated to the constant α and exponent β that control the threshold model can be significant, and depend on the number and distribution of the empirical (D, I) data points.

Finally, in the analysis, only rainfall thresholds based on mean rainfall intensity-rainfall duration (ID) type were herein considered. However, the conclusions of this analysis are applicable to different types of thresholds, including cumulative event rainfall-rainfall duration (ED) thresholds Guzzetti et al. (2007), and other thresholds that consider the antecedent rainfall conditions to forecast the possible occurrence of debris flows and other shallow landslides.

5 Analysis of selected events

The hydrometeorological and hydrological controls on the triggering of debris flows are examined through the analysis of three storm systems occurred on October 3-4, 2006, June 20-21 2007 and September 3-4, 2009. The purpose of the analysis is to relate the variability of the hydrological responses of the catchments to the different features that characterized the storm systems. The relations among runoff response, debris-flow magnitude and solid concentration in debris flows are also examined.

5.1 Rainfall data overview

Concerning the rainfall data analysis, I was provided by Dr. Francesco Marra (LEAF Dept., University of Padova) calibrated radar maps for the studied events. The radar is a C-band weather radar located at Monte Macaion and serving both the autonomous provinces of Trento and Bolzano. For the 2006 and 2007 floods the radar was already calibrated and an effort was made in order to optimize also the 2009 rainfall radar map. The 2009 event, differently from the local-scale 2006 and 2007 events, was characterized by a regional scale extent. The big extent carried with it a series of problems related to the occlusion and to the attenuation of the signal. Furthermore during the 2009 event, it was raining also at the radar location. In these terms a calibration was done by Francesco Marra and a unique calibrated rainfall map for the 2009 event was provided combining and interpolating raingauges and radar data (raingauges interpolation where the radar signal was not available). Another important step consisted in the selection of the proper *"radar target areas"* within the overall radar rainfall maps. The term *"radar target area"* is to be intended as a

"well calibrate single-event radar rainfall map". The selected radar target areas are shown in Fig. 5.1, the areas have been manually selected considering the involved basins and the overall dynamic of the storm.

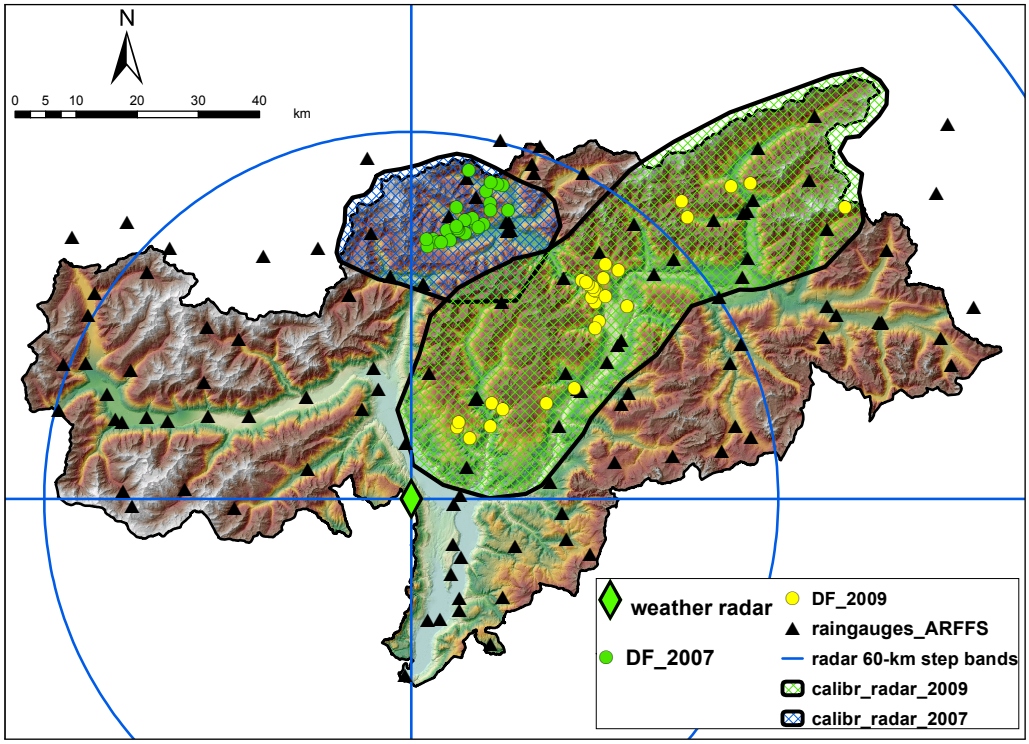

Figure 5.1: Calibrated radar target areas for 2006, 2007 and 2009 events. For 2006-2007 events 615 km^2, for 2009 event 2200 km^2. The radar range and the radar location are reported in the figure along with the raingauges network distribution and the location of debris flows for the 2007 and 2009 events. The radar first reported radius covers a distance of 60 km.

5.2 Hydrologic model

A distributed hydrological model (Cazorzi, 2002; Zoccatelli et al., 2010; Zanon et al., 2010) named KLEM, (Kinematic Local Excess Model) has been applied in order to validate in terms of rainfall runoff calibration rainfall input maps so

as to say that the rainfall is coherent with the measured discharges considering the average parameters and rainfall-runoff balance for this alpine area. The model has been used also for deriving hydrological parameters for the analysis of debris-flow volumes at debris-flow catchment scale.
The model is developed at LEAF Dept. (University of Padova) mainly by Dr. Davide Zoccatelli. The model had to be modified in order to better catch the second-rainfall-peaks behavior. The model tended to over magnify runoff produced by the showers occurring after the main rain burst that caused the flood peak; in order to improve the performance some modifications have been introduced, in particular in relation to the distributed baseflow propagation and to different exponential ways to empty the model reservoir.

Concerning the structure of the model, this hydrological model operates over a regular grid mesh of cells, which are not connected. Rainfall is obtained from either radar or raingauges. The runoff from each cell is then calculated using a modified SCS-CN (Curve Number) runoff model, accounting for rainfall intermittency and subsurface runoff. Each cell produces runoff, which is routed to the outlet using a Lag model. The lag is computed based on the time taken to propagate the runoff to the outlet based on hillslope and channel paths and corresponding celerities. The complete hydrograph of the flood at the outlet is obtained by addition of the routed runoff.

The runoff model is here below explained.
The runoff *ie(t)* at a given time t derives from the SCS instantaneous formulation:

$$ie(t) = i(t)\left[\frac{P(t) - Ia}{P(t) + S - Ia}\right]\left[2 - \frac{P(t) - Ia}{P(t) + S - Ia}\right] \tag{9}$$

where *i(t)* denotes the precipitation intensity at the time t, *P(t)* the amount of rainfall since the beginning of the event, and S the water deficit computed based on CN. Please note that the runoff coefficient at a given time t

$$Runoff\_coeff. = \left[\frac{P(t) - Ia}{P(t) + S - Ia}\right]\left[2 - \frac{P(t) - Ia}{P(t) + S - Ia}\right] \tag{10}$$

only depends on both S (which does not change during the whole event) and the cumulated rainfall *P(t)* since the beginning of the event. *P(t)* can be considered as the state of the cumulated rainfall reservoir, whose capacity is infinite. In order to account for the fact that the potential runoff coefficient can decrease during periods when no rain occurs (rain hiatus), the cumulated rainfall reservoir is drained by a discharge which depends linearly on the level in the reservoir. Thus the state *P(t)* in the cumulated rainfall reservoir is actually calculated by

$$\frac{dP}{dt} = i(t) - K_1 P(t) \tag{11}$$

where the discharge coefficient *K1*[T^{-1}] is assumed to be constant for a given catchment. This allows that the runoff coefficient decreases during periods with no rain, because of near surface evaporation or deep drainage of the soils for example. The state of the reservoir at the beginning of each event is *P(0)=0*. In order to account for slow discharge of soils or aquifers, an additional runoff is considered, as a part of the cumulated infiltration since the beginning of the event. The runoff coefficient partitions the rainfall in runoff and infiltration. The infiltration then fills a "cumulated infiltration reservoir", whose finite

capacity equals *S*. The state *SS(t)* of this reservoir is computed by :

$$\frac{dSS(t)}{dt} = i(t) - ie(t) - K_2 SS(t) \tag{12}$$

where *K2*, is the coefficient of discharge of the reservoir, due to losses by evaporation, percolation to the deep aquifer and lateral flow. Both "cumulated infiltration reservoir"and "cumulated rainfall reservoir"should have the same coefficient of discharge because the two reservoirs must be empty at the same time. The additional delayed runoff *id(t)* is finally expressed as a proportion, *min(1,W)* of the discharge from the "cumulated infiltration reservoir":

$$id(t) = min(1, W) K_2 SS(t) \tag{13}$$

The runoff generated at time t from the given cell is

$$it(t) = ie(t) + id(t) \tag{14}$$

which is then propagated to the outlet by means of the Lag model.

Finally, in order than to separate the baseflow contribution and to calculate proper runoff coefficients, a simple geometric baseflow separation has been adopted. The procedure is derived by the combination of the constant discharge method and the constant slope method as shown in Fig. 5.2.

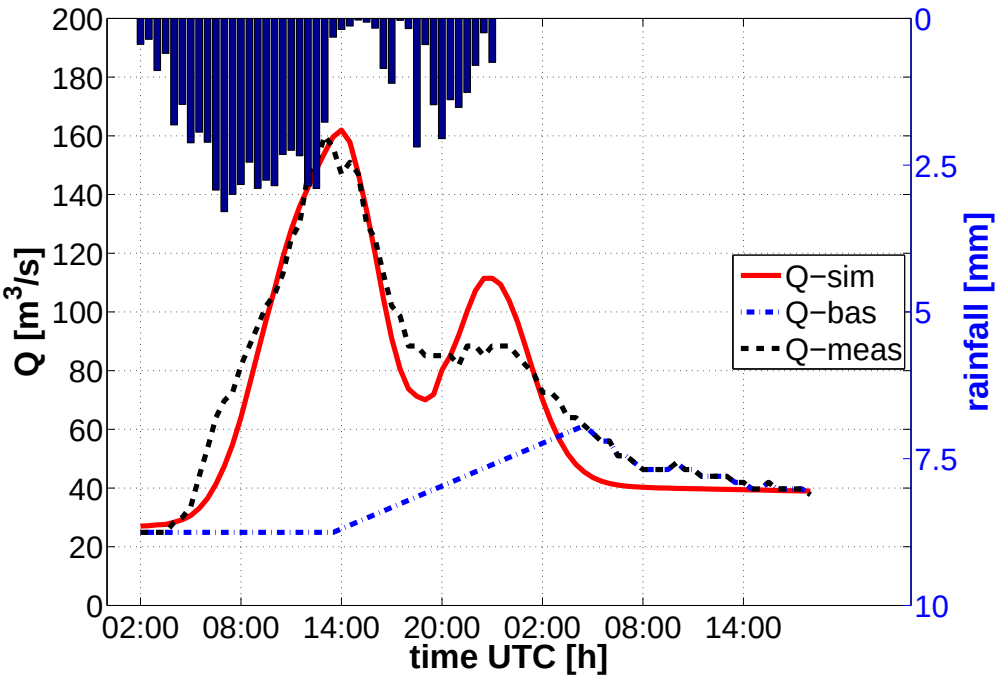

Figure 5.2: Example of KLEM results, showing rainfall input, simulated discharge, measured discharge and baseflow separation.

5.3 Graphical tools for rainfall events analysis

5.3.1 Area over rainfall threshold

At each time step the rainfall intensity is calculated and the area of all the pixel over a chosen rainfall threshold is related to the overall basin area thus expressing a percent value, following the equation:

$$\left(\frac{\sum p > thr * A(p)}{A(b)}\right) * 100 \tag{15}$$

being *thr* the considered threshold, p the number of radar pixel, $A(p)$ the unit area of the radar pixels and $A(b)$ the total basin area.

The outputs of this analysis permit to combine considerations on the time pattern of the rainfall intensity (e.g., if it was concentrated in few time steps or if it manifested high values for prolonged time), with information on the spatial extent of the rainstorm.

5.3.2 Rainfall-surface distributions

A way of describing the impact of a storm on a basin is to relate the cumulative rainfall values as a threshold to the corresponding total area above threshold. At each increasing cumulative rainfall value step the surface value will be calculated as follows:

$$\sum_{i=1}^{n} A(P_{step} > thr) \tag{16}$$

being n the number of pixel greater than the threshold and A the sum of the all the areas of the pixels with a cumulative rainfall until the considered step P_{step}, greater than the threshold thr, considering the overall duration of the event.
This type of analysis gives space for an immediate understanding of different dynamics of the event. Such graphs detect the lowest threshold that occurred in all the basin, than they can be useful also in explaining whether high or moderately high rainfall contributions have been characterized by a widespread discussion over the basin or whether they have been localized just in small part of the basin, thus destabilizing those specific locations much more than the basin in general.
The shape of the curve helps understanding some hydrological features: a convex curve is typical of widespread high amount of rainfall, and a concave and sharp curve is usually related to a rainstorm characterized by severe but very localized conditions within the basin.

In the case that different events occurred over the same basins such analysis can be even more helpful detecting, in a synoptic view the different impact of the storms over the basins and thus helping in the explanation of the possible different hydrologic responses.

5.3.3 Cumulative rainfall and intensity values

One very first analysis conducted in order to explain the dynamic and the responses causes by the three different events has been the relation between cumulative rainfall values and maximum intensity values. The relation is a scatter plot that considers, for each grid cell (pixel) of the radar datum, the following variables:

- the cumulative rainfall value for each pixel at the end of the event

$$\sum_{i=1}^{n} R(i) \tag{17}$$

  being R the grid cell rainfall value and n the number of rainfall images at step time t, in our case the interval time between two images was 1/2 hour.

- the maximum intensity registered over the grid cell

$$\max_{i=1}^{n} R(i) \tag{18}$$

In order to homogenize the results the intensity values have always been converted to hourly rainfall intensity.

The information related to the position of debris-flow initiation sites was used to locate the debris-flow points on the radar map and to monitor the hydrologic variables behavior over these locations.

5.3.4 Timing of the events

For the 2007 and the 2009 events there was also information on the time of debris-flow occurrence with an accuracy of around 2-3 hours. The timing information has been derived from provincial workers involved in the event area and from local people interview. This information has been included in a specific type of analysis. In order to better understand the hydrologic conditions at the debris-flow locations, an analysis on the local dynamic of the cumulative rainfall and intensity variables has been conducted. Within the radar map, the grid cells including the debris flows have been selected both for 2007 and 2009 events and, for these points two graphs reporting the trend of the cumulative rainfall and the intensity variables, have been analyzed. The trend of the selected variables spans across the overall duration of the storm and the most probable timing point is marked for each debris flow trend curve.

5.3.5 Analysis with elevation

As an extension of the cumulative rainfall-intensity correlation, elevation has also been included in the analysis.
Including elevation adds an important explanatory variable to the interpretation of the events. This permits following the trend of cumulative rainfall in respect

to elevation so as to determine at which elevation belt the storm has been more intense, or whether it has been insisting on a particular elevation range or not. An elevation value had to be assigned to each radar rainfall pixel, but here a problem arose: which values of elevation is to be assigned to a 1 km cell size pixel? As a first attempt it has been chosen the elevation value projecting directly upon the geometric center of the pixel.

The cumulative rainfall-elevation trend and the intensity-elevation trend can be analyzed separately, thus fully monitoring the variable behavior at different elevations.

Having both the elevation values for the pixel and the real elevation value at debris flow location can help also in the comparison between these two elevation values and, on average, the central pixel elevation has proved to be lower than the actual debris flow location, thus suggesting that maybe another type of elevation attribute such as a weighted average could better detect the actual real elevation distribution of the rainfall variables.

In order to complete the analysis an average operator has been applied to the elevation distribution values for the different pixel of the radar rainfall map. For both the cumulative rainfall and intensity values it has been computed a mobile average in order to try to follow the mean value (at each step) of the analyzed variable and to determine whether, for example, extreme conditions happened in the debris-flow most suitable elevation belt or not. This simple operator helps within a scatter plot, to better detect the trend of the average elevation for both the two rainfall variables following an averaged line, and thus explaining where each class of cumulative rainfall values, has had it centroid in terms of elevation range within the basin.

5.3.6 Frequency distributions

The cumulative rainfall-frequency analysis and intensity-frequency analysis represent a quick overview of the dynamic of the two variables over the basins. In detail, the cumulative rainfall-frequency analysis represents the same concept expressed in the cumulative rainfall-surface graphs, already provided. The advantage of presenting the graphs in frequency terms is the possibility to compare different events over a unique graph, thus allowing the immediate interpretation of the different impacts and dynamics of the different storms. It is in fact possible to determine whether the intensity or the cumulative rainfall values played a major role, whether the extreme values are isolated or widespread and to determine the main differences among different storm events within a synoptic view.

In the results section these schematic view of the rainfall-related variables frequency distributions is presented as one of the few analyses really capable to put together and to explain the different events' dynamic within a framework .

5.4 Downscaling at debris-flow watershed-scale

The hydrological parameters obtained after the model calibration, were used to run the same model on ungauges debris-flow watersheds. The purpose is to check the viability of such a downscaling approach in terms of volume ratios between solid and liquid phase.

For a number of debris flows, estimations of deposited debris-flow volumes were available from post-event surveys and have been used and cross-checked with the hydrologic model outputs to determine whether the solid-liquid ratios were consistent with literature findings.

Once the consistency was checked some other relation were explored in order to find any significant correlation between hydrological parameters and debris-flow magnitude.

6 Analysis of selected events: results

6.1 Events

6.1.1 Basins and rainfall

Figs. 6.1, 6.2 and 6.3 report a brief overview of the cumulative rainfall trend over the basin for the 2006, 2007 and 2009 event.

Concerning the 2006 storm, no debris flows have been reported in the minor tributaries, but a flash flood occurred in the main stream. It can be noticed that the storm event presents its most severe conditions (cumulative values ∼125 mm/18 h) mainly on the upper part of the basins, characterized by thin soils mixed to rocky outcrops. No important rainfall has been registered in the lower part of the basins and a dry antecedent period emerged from the rainfall records analysis.

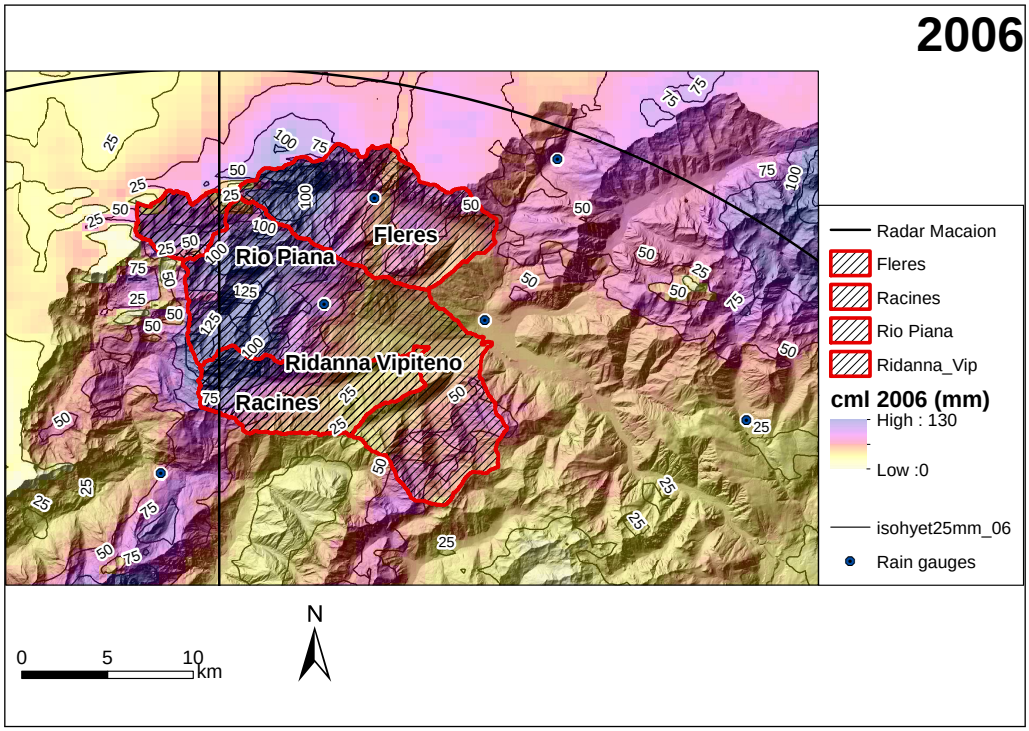

Figure 6.1: 2006 event, basins and isohyets.

Concerning the 2007 storm instead, it can be noticed that, within the same catchments, the most abundant rainfall occurred in the central and lower part of the basins with narrow areas receiving great amount of rainfall ∼150 mm in 23 hours. These areas received the great part of the rainfall within two peaks of few hours around the beginning and the end of the event. The raingauges rainfall record analysis for this event suggests very wet antecedent conditions due to rainfall in the days before and to the snowmelt contribution.

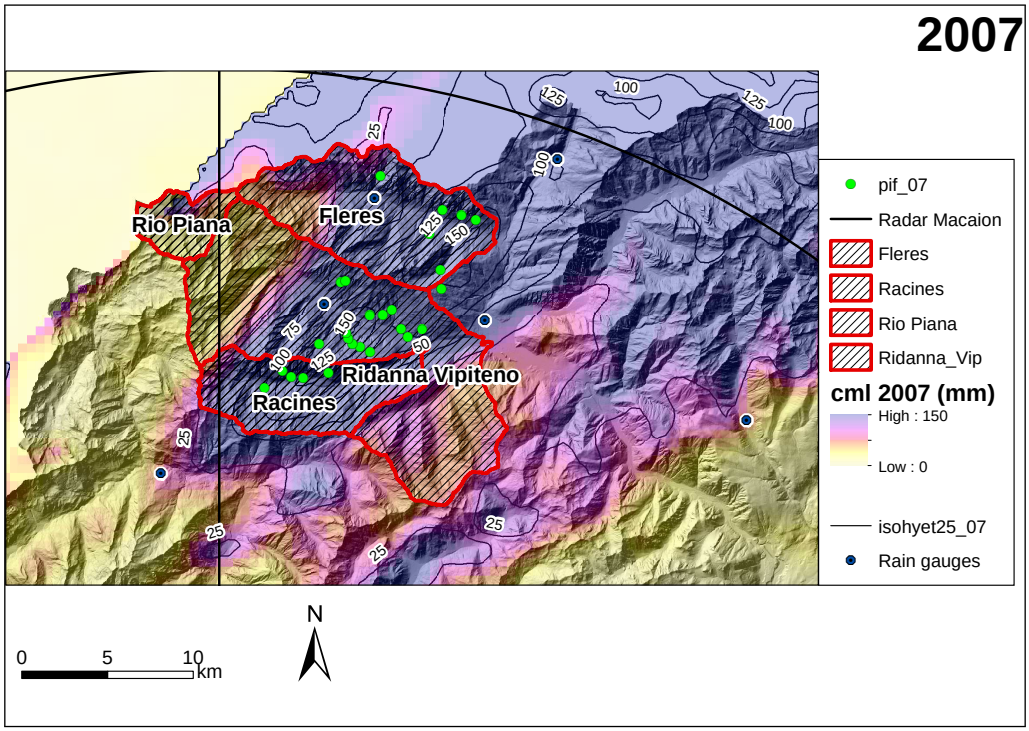

Figure 6.2: 2007 event, basins, isohyets and debris flow locations.

Concerning the 2009 event, the main characteristics are related to the regional scale of the event with a central cluster of debris flows that were hit twice by the passage of two precipitation sub-events with a SW-NE and a NW-NW orientation, while the general direction of the event kept a SW-NE orientation at regional scale. Antecedent saturation conditions close to average (but with a smaller event 2 days before the considered one) have been detected analyzing raingauges rainfall records; both flash flood and sparse debris flow responses have been registered. Differently from the 2007 event, high cumulative rainfall values (>120 mm in 22 hours) are widespread and not limited to small areas.

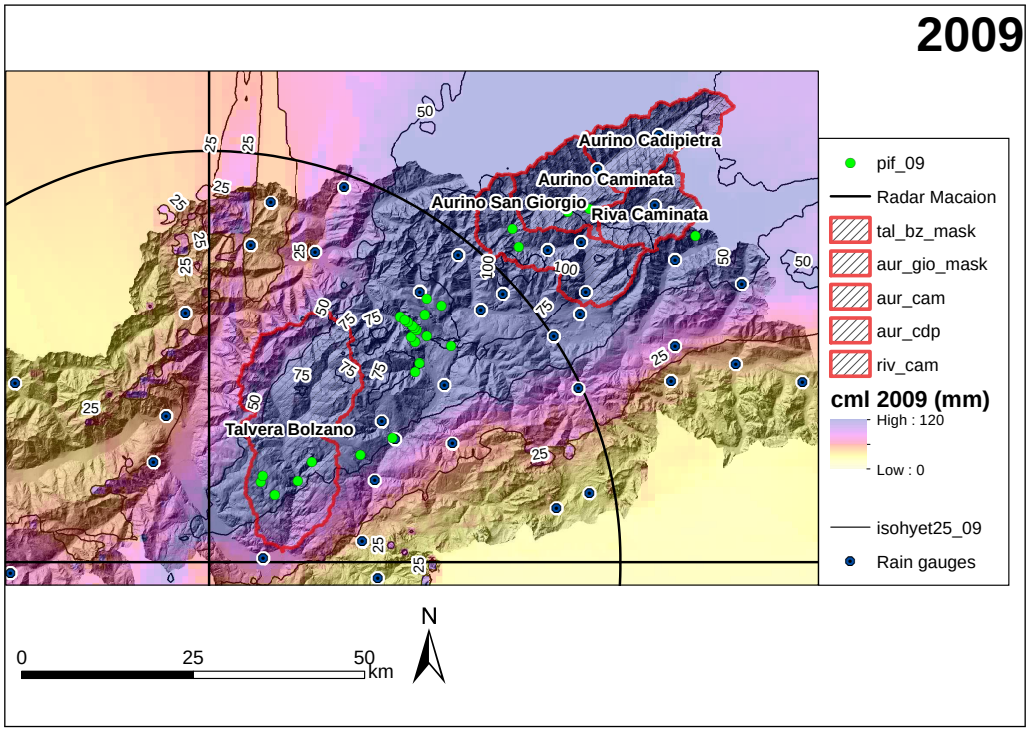

Figure 6.3: 2009 event, basins, isohyets and debris flow locations.

Another interesting feature that made the authors consider both the 2006 and the 2007 event came from the analysis of the maximum discharge series for the main selected watershed (Ridanna basin) and its relation with the number of registered debris flows.

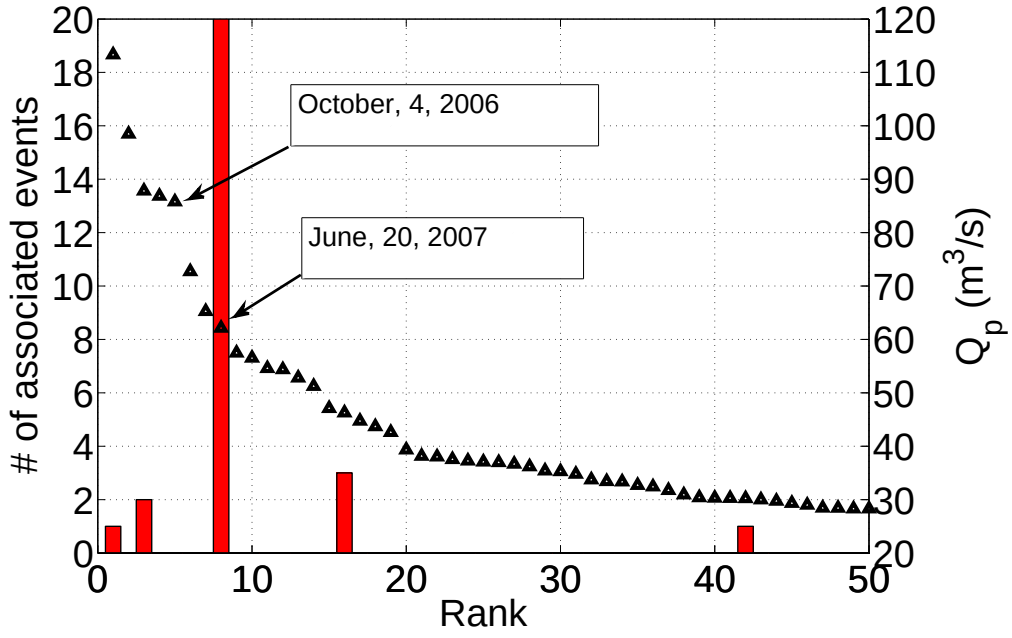

Figure 6.4: Ranking of peak discharge in relation to number of debris flows from 2001 to 2010 in the Ridanna catchment

It is indeed interesting to notice (Fig. 6.4) that the 2006 registered discharge was much higher than the 2007 one, and it is one of the highest in the last years, despite these facts in 2007 a number of debris flows (27) were triggered while none were registered in 2006.

6.1.2 Comparison of raingauges data and radar-derived rainfall estimation

The influence of rainfall data source on the values of cumulative rainfall and maximum 30-minutes intensity associated to debris-flow initiation has been analyzed by comparing radar-derived rainfall with rainfall fields obtained by means of inverse distance weighted interpolation of raingauge data (Fig. 6.5). For the June 2007 rainstorm, characterized by highly convective rainfall affecting

spatially-limited areas and featuring strong spatial gradients, large differences arise between the interpolation of raingauge data and radar-derived rainfall fields, the latter showing, in most cases, higher values. In the September 2009 event, which covered a much larger area with lower rainfall intensities, the differences between raingauges interpolation and radar-estimated rainfall are usually much smaller, especially as to maximum 30-intensity. It is also possible to note that, for several debris-flow initiation points, raingauge data show higher values than radar-derived rainfall. It was then decided to keep the calibrated and distributed radar derived maps as the source of information thus preserving the spatial and temporal variability of the events. The consistency of radar rainfall was anyway checked by means of application of an hydrological model whose results will be described in sec. 6.4.

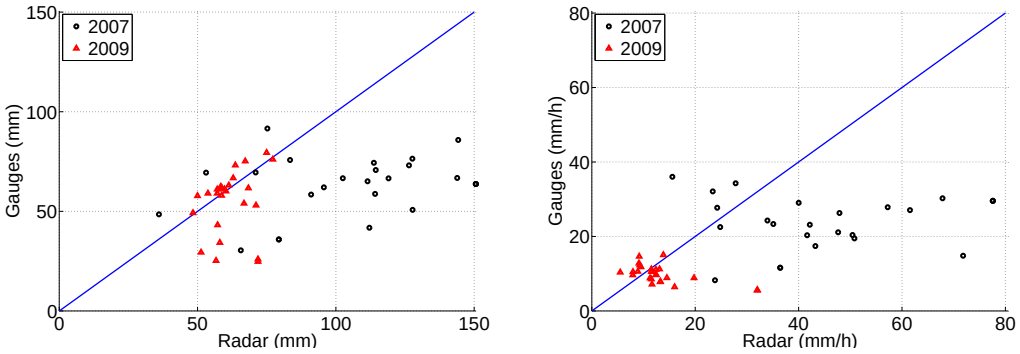

(a) (b)

Figure 6.5: Scatter plot of cumulative rainfall (a) and rainfall intensity (b), from the interpolation of rainfall data and radar observations for debris-flow initiation points.

6.1.3 Antecedent rainfall and saturation conditions

We considered an antecedent precipitation index computed as the ratio of precipitation in the 30 days before the event to the long-term 30 days average for the same period Antecedent precipitation analysis was based on four raingauges for the 2006 and 2007 event, and nine for the 2009 event. For the three analyzed events a series of available raingauges has been analyzed, the available raingauges are reported in Tab. 9 along with some characteristic features.

Table 9: Main features of the considered raingauges for the three events analyzed with the average elevation attribute and the coefficient of variation value.

Event	**raingauges #**	**Avg. Elevation (m a.s.l.)**	**Elevation C.V.**
2006-2007	4	1374	0.31
2009	9	1091	0.29

The antecedent rainfall analysis reveals, for the considered antecedent 30 days, almost dry conditions for the 2006 event (event rainfall= 40% of average antecedent 30 days), saturation conditions close to long term average for the 2009 event (event rainfall= 82% of average antecedent 30 days), and very wet antecedent conditions for the 2007 event (event rainfall= 138% of average antecedent 30 days).

6.2 Catchment-scale analyses

The following analyses have been carried out at the watershed-scale.

6.2.1 Area over intensity threshold

This type of analysis based on eq. 15 is meant to detect, for each time step, the ratio of total basin area above a certain rainfall threshold.

The selected time step for the all events is 30 minutes, which is also the time step of radar rainfall data for the studied events. The different duration of the events did not permit the over-positioning of the graphs.

Only a selection of outputs for different basins has been here reported, highlighting the main features that characterized the events; furthermore different rainfall thresholds have been applied for the 2006-2007 and 2009 events, separately. A 10-mm threshold per time step has been chosen for the 2006-2007 events while a 5 mm threshold for the 2009 event. The differentiation of the threshold may constitute a problem when trying to compare different events in a synoptic view. The reason for this differentiation relies in the intensity values distribution. For the 2009 event in fact, as already mentioned, moderate or high values of intensity have not been registered, given the definitely more important role of the cumulative rainfall values.

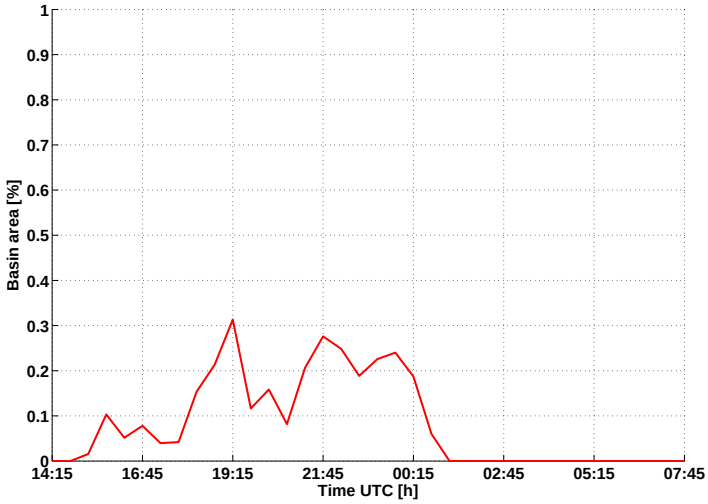

Figure 6.6: Percentage of area over 10-mm rainfall threshold for the Ridanna at Vipiteno catchment, 2006 event, time step=0.5 h.

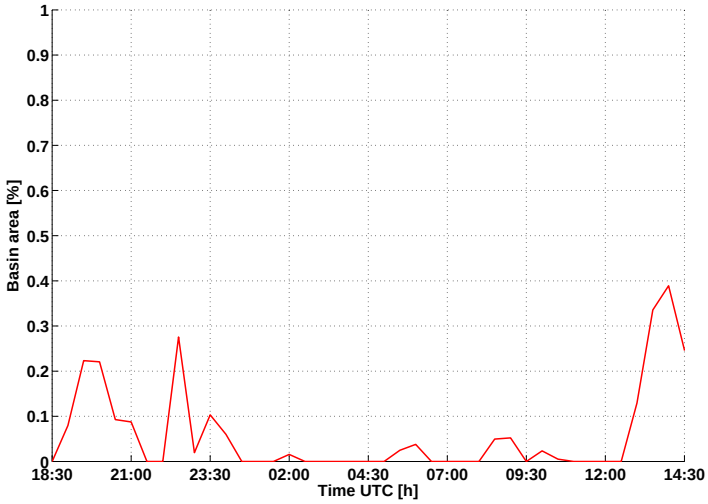

Figure 6.7: Percentage of area over 10-mm rainfall threshold for the Ridanna at Vipiteno catchment, 2007 event, time step=0.5 h.

In Figs. 6.6 and 6.7 the Ridanna catchment is analyzed for the 2006 and the 2007 events. The threshold is set at 10 mm of total rainfall.

The shape of the curves once again reflects the behavior of the different events.

In the 2006 event, the curve presents a continuum section in terms of time span over the threshold, indicating better distributed rainfall input characterizing this event in respect to the 2007, for which different severe pulsations are detectable but restricted in terms of time and not widely distributed.

Figs. 6.8 and 6.9 take in consideration a particular case happened for the 2006-2007 events: the Rio Piana catchment.

The Rio Piana is a small high elevation glacierized headwater catchment (16 km^2) characterized by the presence of almost permanent snow cover, rocky outcrops and scree deposits, and sparse high altitude herbaceous vegetation covering the 60%, 30% and 10% of the catchment respectively. The 2006 great amount of rainfall can be easily detected by such a graph (Fig. 6.8), underlying the fact that in the 2006 the severe conditions occurred at high elevation on average, and, on the opposite, in 2007 the severe conditions occurred not at high elevation (Fig. 6.9). Both the graphs confirm once more this trend and even with a not so high rainfall threshold, the 2007 curve does not show any particular severe condition. Combining this fact with the above-zero registered temperatures at the beginning of the event, also for the 2006 case leads to the hypothesis that all the basin was probably contributing at the beginning of the event and the great amount of water in the upper part of this catchments was rapidly routed the main channel network thus enhancing a possible flash flood behavior.

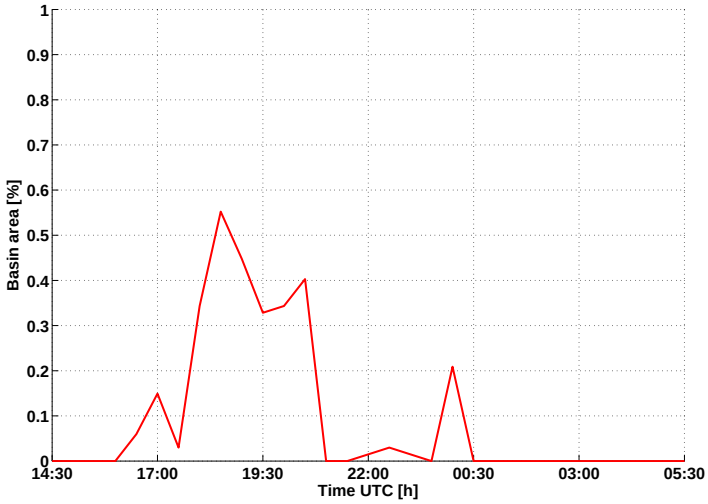

Figure 6.8: Percentage of area over 10-mm rainfall threshold for the Rio Piana catchment, 2006 event, time step=0.5 h.

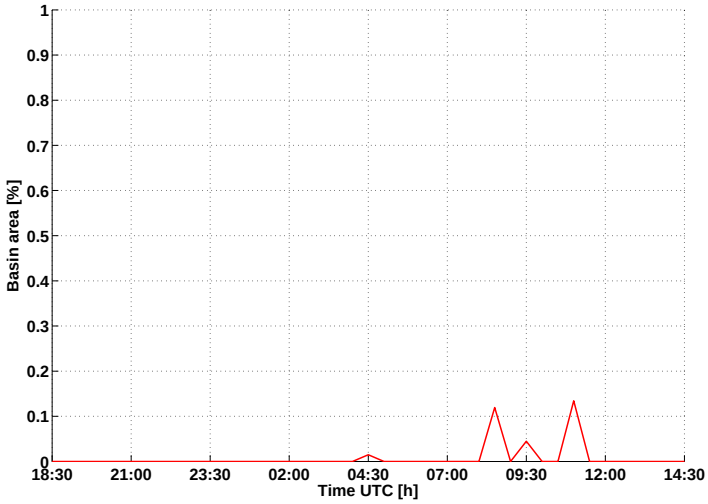

Figure 6.9: Percentage of area over 10-mm rainfall threshold for the Rio Piana catchment, 2007 event, time step=0.5 h.

Figs. 6.10 and 6.11 report the Aurino at San Giorgio ant the Talvera at Bolzano graphs for the 2009 event.

The trend emerging from the graphs reflect the most severe conditions (in terms

of cumulative rainfall values) occurred in the Aurino catchment, and also the second rainfall peak occurred with significant values mainly near the outlet of the Aurino catchment, this second peak in fact is not emerging from the analysis of the Talvera catchment, and also as a validation to this fact, the great discharges and flooding events have been registered close to the Aurino outlet area.

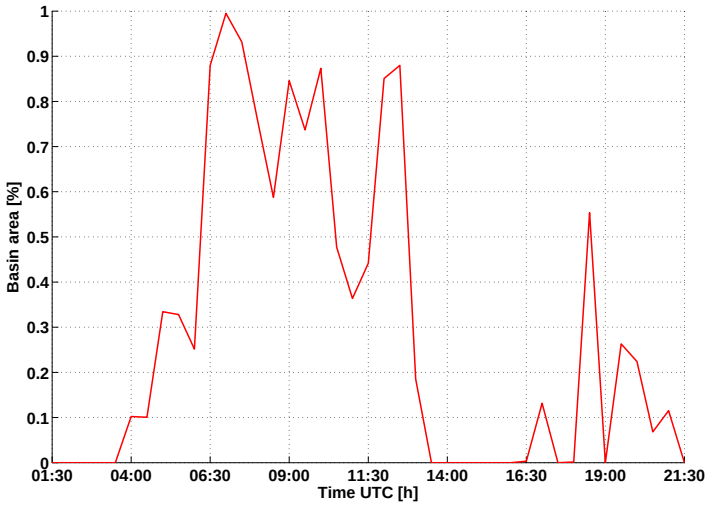

Figure 6.10: Percentage of area over 5-mm rainfall threshold for the Aurino at San Giorgio catchment, 2009 event, time step=0.5 h.

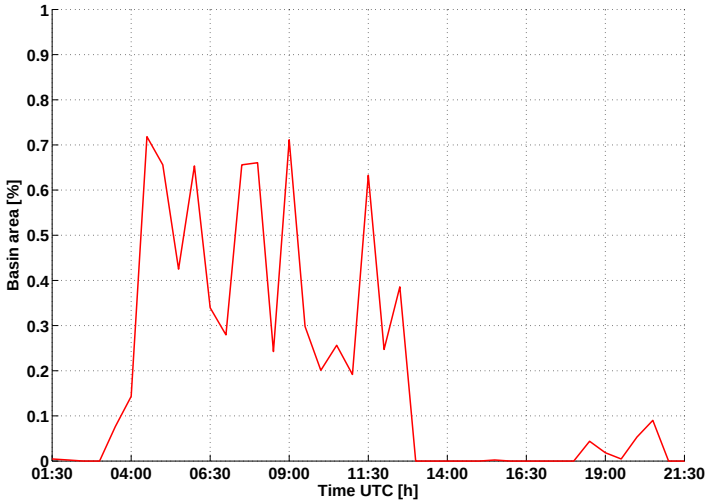

Figure 6.11: Percentage of area over 5-mm rainfall threshold for the Talvera at Bolzano, 2009 event, time step=0.5 h.

A full complete set of thresholds has been applied to the different events and, in some cases revealing important features that anyway could be summarized within the analysis of the presented graphs.

6.2.2 Cumulative rainfall - surface distribution

The plots that relate cumulative rainfall with surface distribution (eq. 16) provide information about the spatial concentration and amount of precipitation over a catchment, without considering a time series forcing trend.

Being this analysis linked only to the surface of the basin and to the cumulative rainfall values, it is possible to compare in one graph, different events occurred within the same basins.

Figs. 6.12 - 6.15 report the analysis of 2006 and 2007 events.

On average, except for the Racines basin, which has experienced both high cumulative rainfall values and intensity in 2006 and in 2007, for all the other basins

the 2006 curves presented a different trend from the 2007 ones, and within the same event similar rainfall distributions can be found over the catchments. In particular, the 2006 curve usually starts as a convex curve, meaning that there is a moderate to high widespread rainfall contribution over the all basin, then the 2006 curve usually drops down for high cumulative rainfall values, before then the 2007 curve, meaning that extremely severe conditions have not been reached in 2006 over significant portions of the basins (except for the already commented Rio Piana case).

On the opposite, the 2007 curve usually highlights a lower total rainfall contribution along with smaller portions of the catchments hit by very important rainfall, these portions of the basins are the ones where debris flows were triggered.

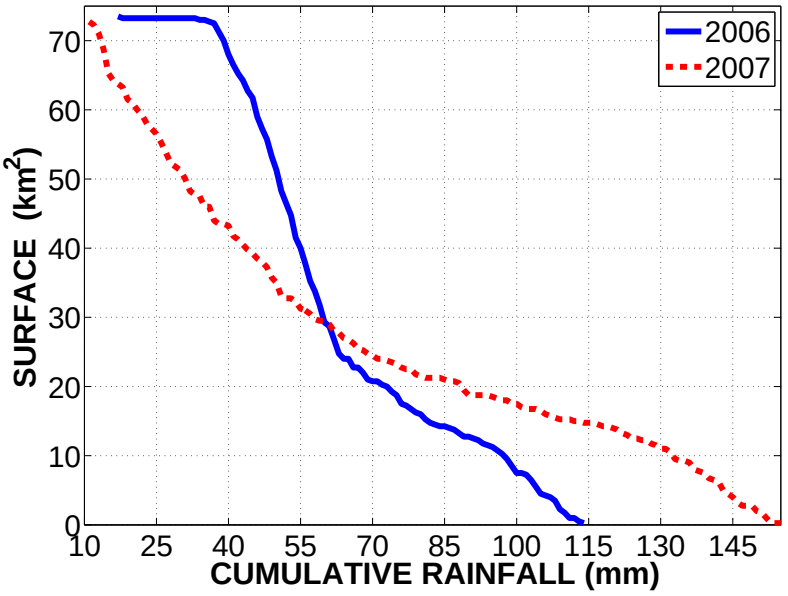

Figure 6.12: Cumulative rainfall over surface graph for 2006 2007 events: Fleres catchment

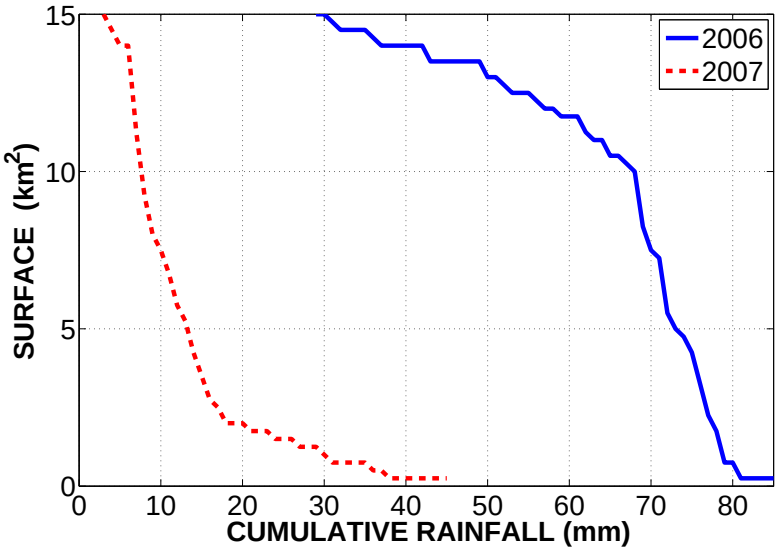

Figure 6.13: Cumulative rainfall over surface graph for 2006 2007 events: Rio Piana catchment

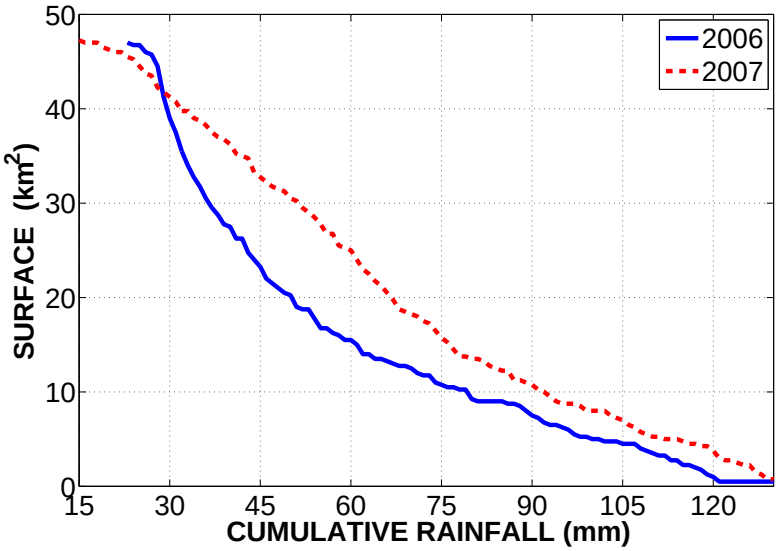

Figure 6.14: Cumulative rainfall over surface graph for 2006 2007 events: Racines catchment

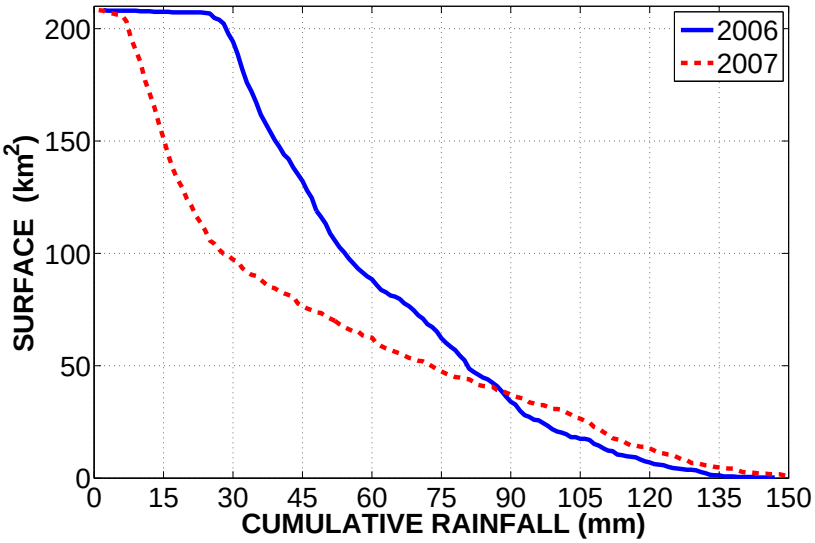

Figure 6.15: Cumulative rainfall over surface graph for 2006 2007 events: Ridanna at Vipiteno catchment

Concerning the 2009 cumulative rainfall-surface analysis only the two main basins (i.e. Aurino at San Giorgio and Talvera at Bolzano) have been reported (Figs. 6.16, 6.17).

For both the basins the curves starts as convex, as predicted, stressing the important role of widespread cumulative rainfall contributions; in the case of Aurino at San Giorgio, the graph starts at 45 mm of rainfall, meaning that all the Aurino basin received at least that amount of rainfall. This threshold for such basins represents one of the major sources of superficial instability related to soil saturation.

6.3 Debris flows and rainfall analyses

The following analyses have been carried out taking in consideration radar-calibrated rainfall maps and relative areas; this was done in order to assess

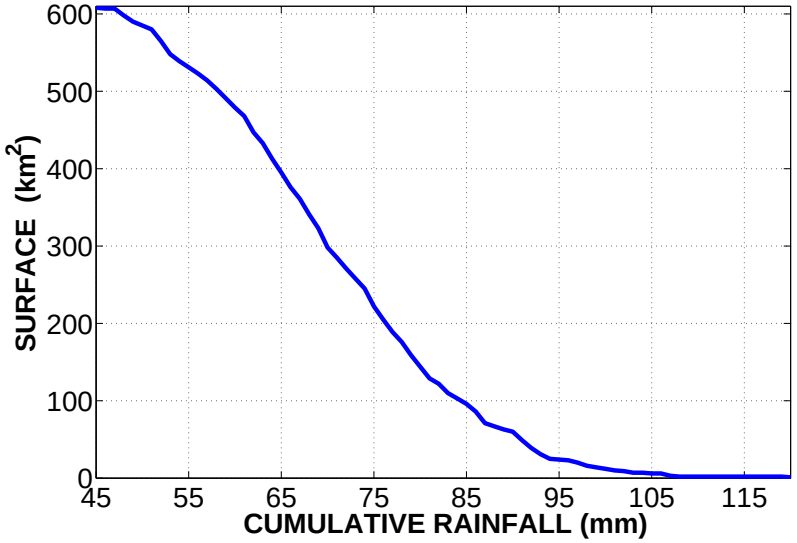

Figure 6.16: Cumulative rainfall over surface graph for 2009 event: Aurino at San Giorgio catchment

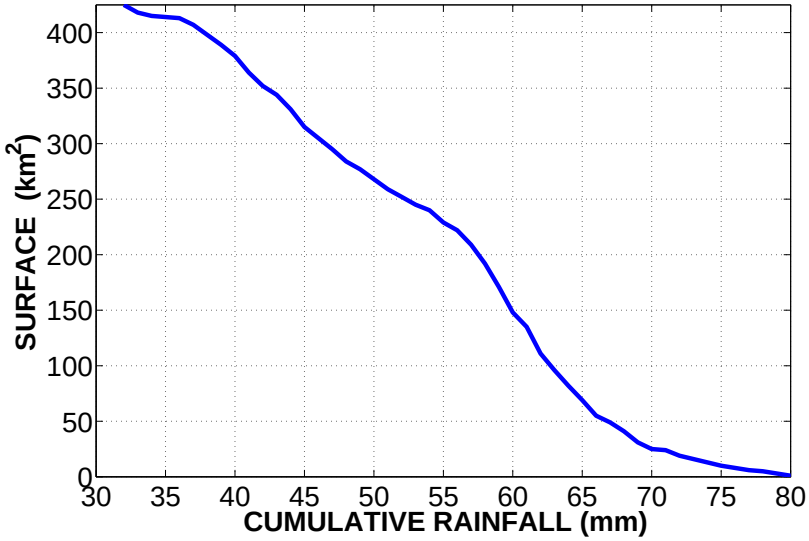

Figure 6.17: Cumulative rainfall over surface graph for 2009 event: Talvera at Bolzano catchment

the hydrologic forcing for all the registered debris flows, not only the ones occurring within the gauged catchments boundaries but also the ones occurring in interbasin areas.

6.3.1 Cumulative rainfall - intensity analysis

Figs 6.18 and 6.20 report the plots of cumulative rainfall versus intensity for the 2006, 2007 and 2009 events

It is possible to recognize important differences between the 2006 and 2007 events: in particular the 2006 points cloud shows, on average, greater values of cumulative rainfall and a more compact cloud, meaning that there has been a high contribution in terms of distributed rainfall but not so high values of intensity.

The 2007 points cloud instead is concentrated around low values of cumulative rainfall and medium to high values of intensity, but then, a sparse cluster of points spreads around extremely high values of both the variables, thus confirming and detecting the highly convective and locally extreme behavior of the event.

Such analysis is consistent with the dynamic of the storm and the location of 2007 debris flows in the most severe conditions on the plot represents a validation of the analysis' goodness.

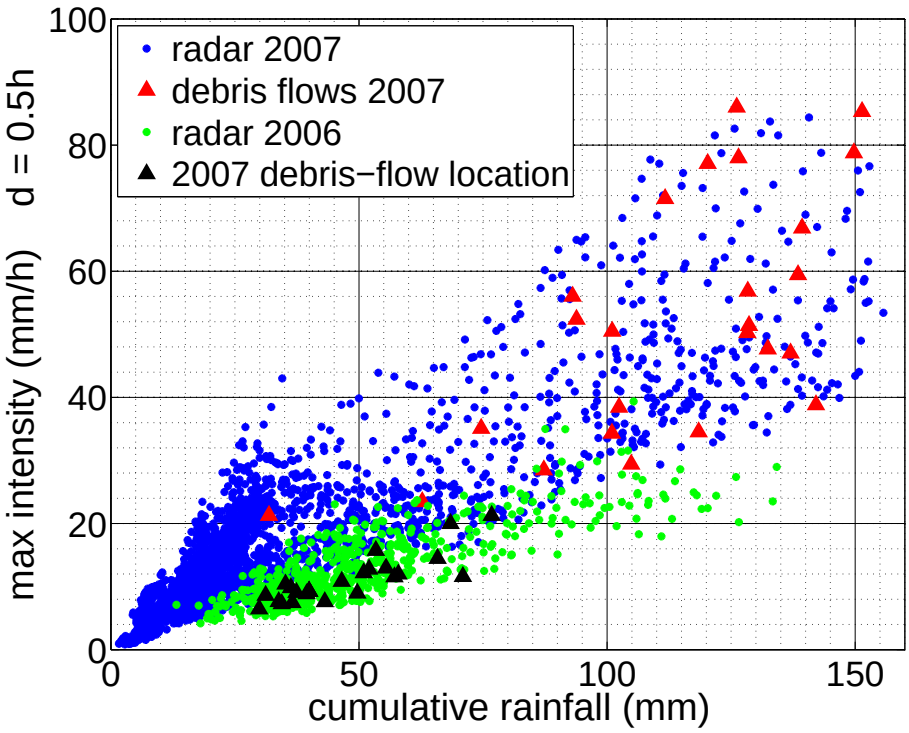

Figure 6.18: Cumulative rainfall-intensity analysis for 2006 and 2007 event; debris flow location reported in the 2006 scatter plot are actually the coordinates where, in 2007 the debris flow started, and are reported in the 2006 graph in order to better understand the local conditions over those points and the main differences between the two events.

Debris-flow initiation sites are reported with a red marker in the case of 2007; analyzing 2006 storm dynamic it was interesting to detect the conditions over the same locations in order to verify if the conditions were different from the following year ones. Cumulative rainfall and intensity values have proved to be significantly different for thee 2006 storm as stressed in the graph (Fig. 6.18) with the black marker.

The analysis of 2009 cumulative rainfall-intensity plot presents a situation of high to severe contributions in terms of rainfall but not in terms of intensity.

This suggests that probably, for this event, the major control role is played by the cumulative rainfall variable, maybe along with some considerations on the antecedent conditions.

A sort of threshold for the occurrence of debris flows, both for the 2007 and 2009 events, is present around 50 mm total rainfall value. In order to go into detail in this possible cumulative rainfall threshold behavior a simple analysis has been carried out.

The total storm selected radar target areas (as expressed in sec. 5.1) for the debris flow events (2007 and 2009) has been considered; inside this area it has been extracted the portion over 50 mm rainfall threshold and related, in percentage to the total area.

The spatial density of debris flow was assessed by means of the ratio of the number of starting points to the extent of the area with cumulated rainfall greater than 50 mm, i.e., the *"threshold"* for debris-flow occurrence resulting from Figs. 6.18 and 6.20. Results are summarized in Tab. 10.

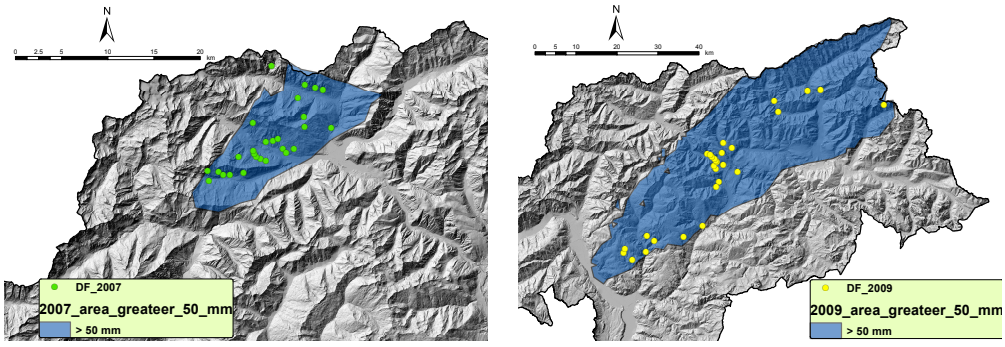

(a) (b)

Figure 6.19: 2007 (a) and 2009 (b) events; the area characterized by cumulative rainfall values > 50 mm is highlighted along with the debris-flow triggering locations.

The spatial density of debris flows appears much higher for June 2007 (0.176 events/km^2) than for September 2009 (0.012 events/km^2): this is in agreement with higher rainfall intensity of June 2007. Considering only the areas above 50 mm of total rainfall (Fig. 6.19 a and b), 23.1% in 2007 and 77.3% in 2009, the density of the events occurred over this area increases to 0.761 events/km^2 for 2007 and to 0.016 events/km^2 for 2009 case, suggesting that the majority of the 2007 collapses occurred right in the localized (23.1%) extreme-conditions area, while in 2009 once again the extensive general instability was brought by the enduring of the rainfall even without important local intensities. Fig. 6.3 shows that in September 2009 most debris flows occurred in a rather narrow sector of the area affected by the rainstorm. The analyzed event database reports repeated occurrence of debris flows in this area, referred to local morphological conditions and to the fact that this sector is the driest among the areas hit by the September 2009 event (661 mm/year on average, for the last 30 years), suggesting that the same amount of rainfall could have been more effective here than elsewhere in causing shallow instability and debris flows. This tip confirms the extreme condition and convective behavior of the 2007 event and the widespread flooding attitude of the 2009 event.

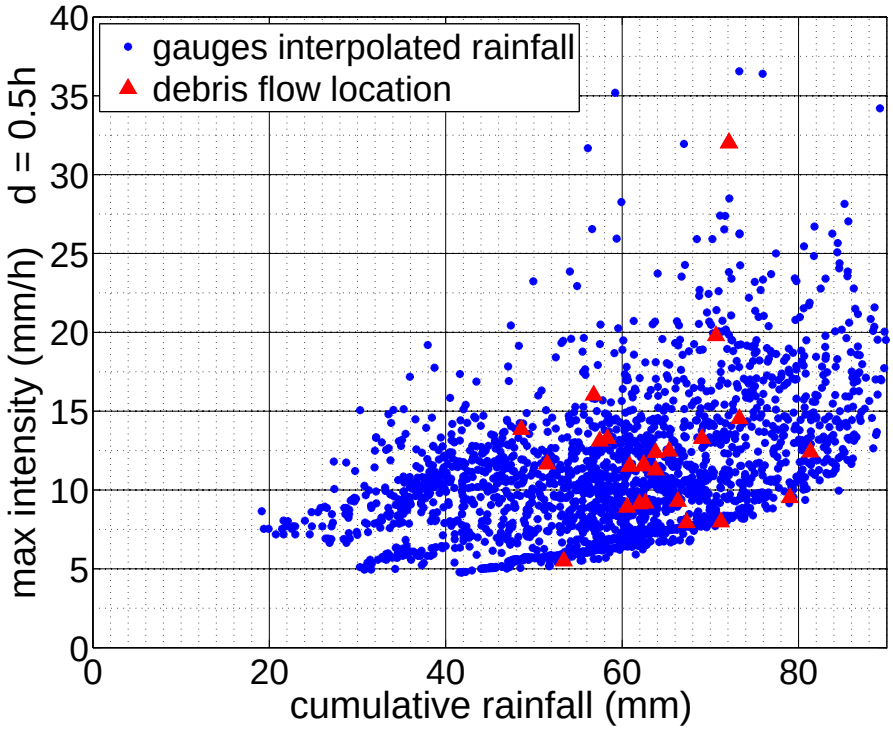

Figure 6.20: Cumulative rainfall-intensity analysis for the 2009 event

Table 10: Debris flow points density in relation to a 50 mm rainfall area threshold for the 2007 and the 2009 events.

Event	**radar target area (km^2)**	**Area >50mm (%)**	**Density pts/area (pts/km^2)**	**Density pts/area >50mm (pts/km^2)**
2007	592	23.1	0.18	0.76
2009	2208	77.3	0.012	0.016

6.3.2 Timing and variables trend

The following figures report the trend of cumulative rainfall and intensity for the 2007 and 2009 events at debris flow locations, along with the usage of some timing information. For these events the accuracy of the information on the timing of debris flows has been estimated to 2-3 hours

Considering the 2007 case (Figs. 6.21, 6.22), we need to recall the great variability that characterized the event. Analyzing cumulative rainfall and intensity trends it is possible to notice that most probable occurrence time is, for the majority of the cases, located after a sharp increase in rainfall contribution in the second part of the event. Significantly intense rainfall occurred also in the first part of the event but saturation, though presenting high values in respect to average conditions, was probably still not enough to facilitate debris-flow triggering.

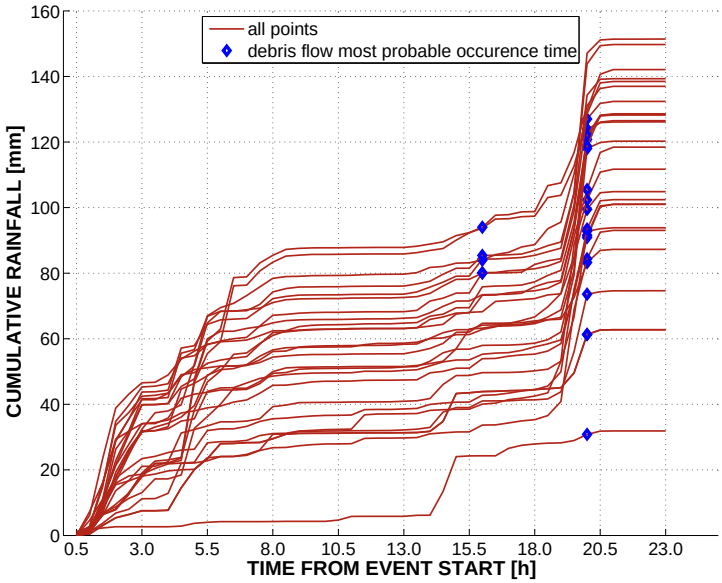

Figure 6.21: Cumulative rainfall trend over the debris flow locations for the 2007 event. Most probable occurrence time is identified with a blue marker

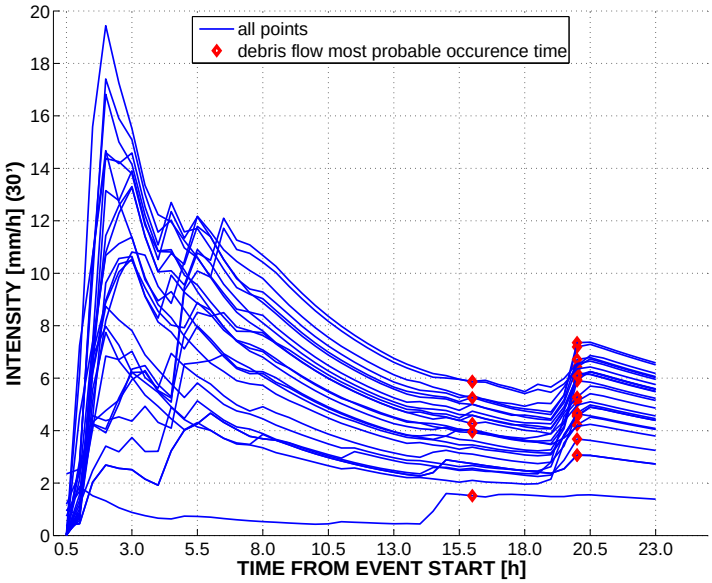

Figure 6.22: Cumulative rainfall trend over the debris flow locations for the 2007 event. Most probable occurrence time is identified with a red marker

Considering the 2009 case 6.23 and 6.24 the cumulative and the intensity rainfall graphs suggest that probably debris flows have occurred around temporary peak intensity values corresponding to flex values in the cumulative rainfall curves.

Another typical feature is related to the fact that the firs part of the storm has also a saturation role so that when the intensity increases again, towards the end of the event, on average, a lower rainfall intensity is required to trigger instabilities.

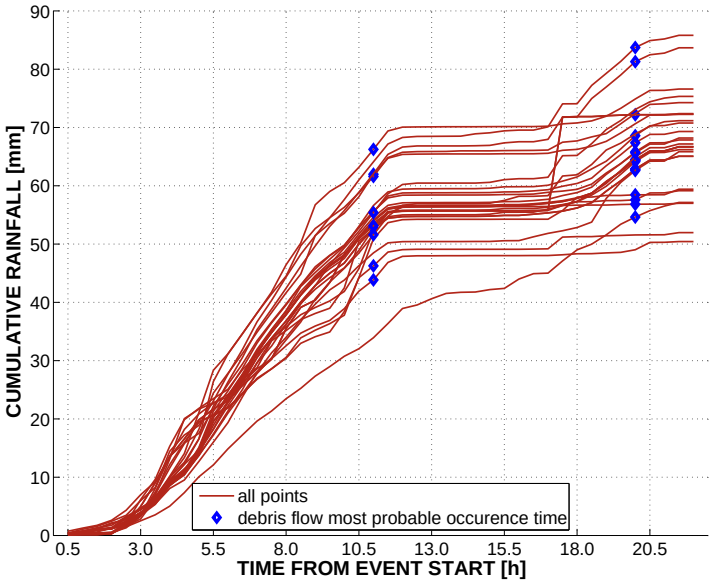

Figure 6.23: Cumulative rainfall trend over the debris flow locations for the 2009 event. Most probable occurrence time is identified with a blue marker

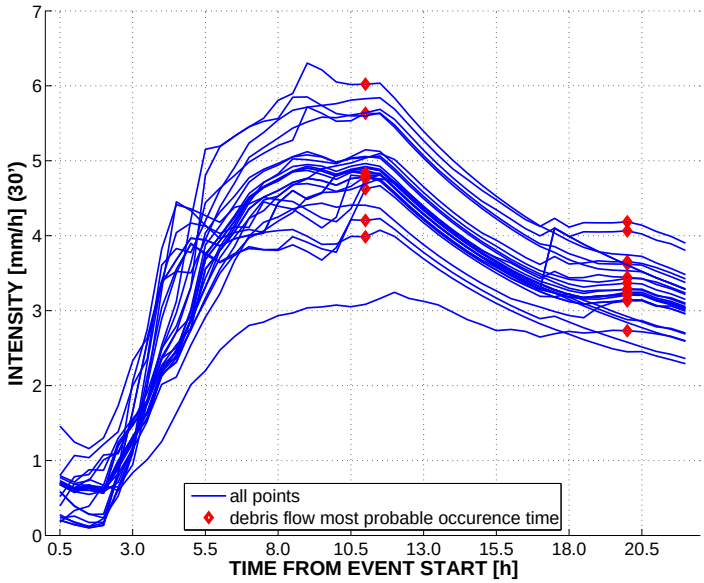

Figure 6.24: Rainfall intensity trend over the debris flow locations for the 2009 event. Most probable occurrence time is identified with a red marker

This timing information has been used also in order to retrieve rainfall volumes triggering debris flow at each single debris flow catchment and to relate these volumes to different variables such as catchment drainage area and events magnitude (volume of deposited material, sec. 6.4.1).

6.3.3 Analysis with elevation

The following analysis tries to include in the explanation of the events, the variability related to elevation range and variation.

The three variables under analysis are: cumulative rainfall, intensity and elevation. As a first attempt to give a unique elevation value to each 1-km radar pixel, the actual elevation of the central coordinates of each pixel has been chosen. For the debris flow points both the elevation values have been plotted: the

radar pixel central elevation (the radar pixel in which debris flow is included) and the actual elevation of the debris flow from DTM values. On average the radar pixel elevation value revealed higher than the actual debris-flow pixel elevation.

The mobile average operator that has been applied to the distribution was set up by recursive checking of the biggest step between two subsequent cumulative rainfall values in an ordered series. Noteworthy in the analysis of 2006 series (Fig. 6.25), is the trend of cumulative rainfall mobile average that between 50 and 60 rainfall mm crosses the 2000 m elevation line to indicate that severe conditions were located above the 2007 debris-flow band (1000-2000 m). It is also interesting that the central radar pixel elevation is usually higher than the actual debris-flow elevation (confirmed trend also for 2009).

The 2006 event was characterized by severe conditions manifested at high elevation within the basins; this issue combined with ice melt contribution (temperature records detected the thermal zero above 3000 m) helps in the explanation of the different catchment responses.

Intensity graphs are not reported here and, actually show the same trend of the cumulative rainfall ones, leading to report the same considerations.

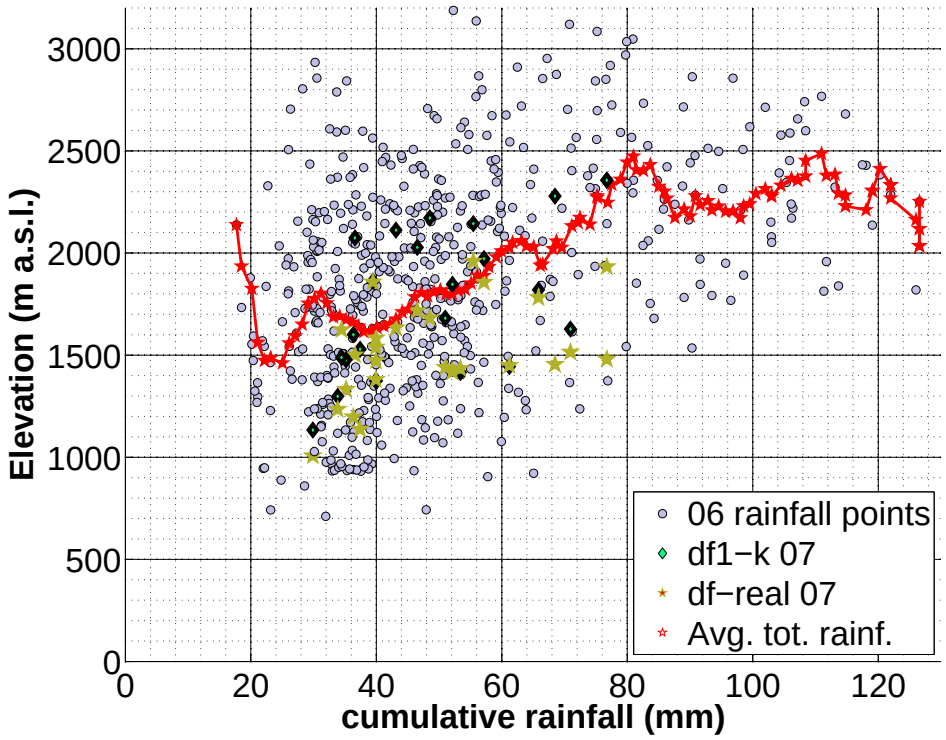

Figure 6.25: 2006 cumulative rainfall-elevation distribution and trend. 2006 3D graph rotated in 2D cumulative rainfall-elevation view.

In Fig. 6.26 noteworthy is the insistence of both medium and high rainfall average values exactly on the debris-flow elevation band (1000-2000 m) for the 2007 case, while in the 2006 event the average was moving upward.

The average trend is also characterized, differently from what happened in 2006 and 2009, by a non-stationary behavior. Both the rainfall-related variables show intermittent behavior for high values, meaning that the severe conditions were fluctuating even remaining inside the debris flow elevation band.

This variability and this intermittent behavior reflect the 2007 impact dynamics, characterized by different severe pulsations localized and not widespread within the basins.

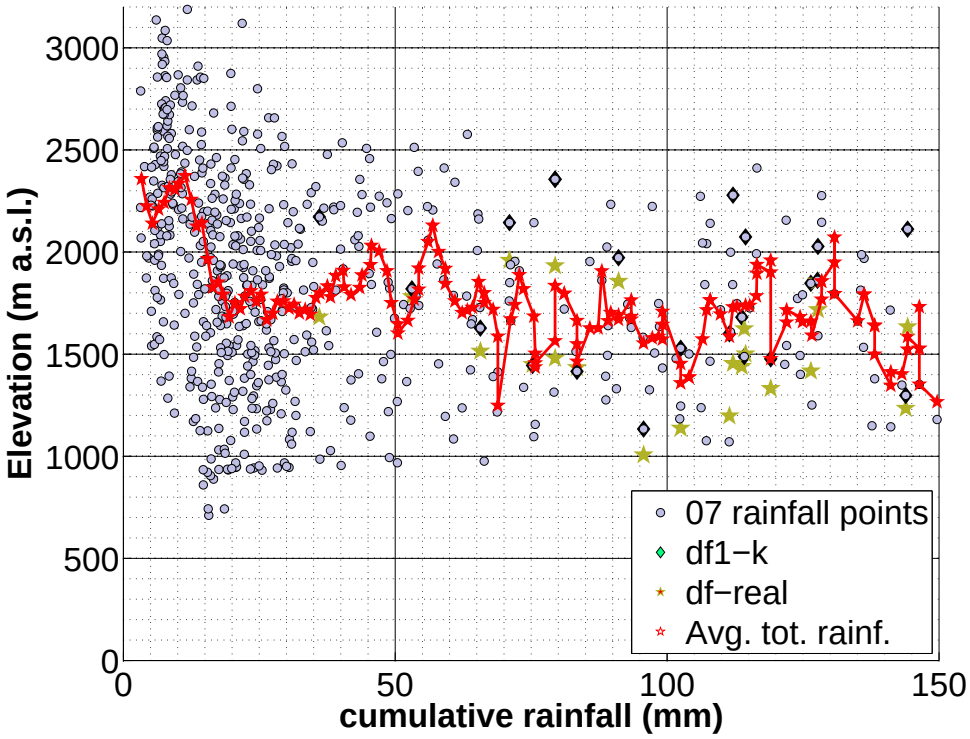

Figure 6.26: 2007 cumulative rainfall-elevation distribution and trend.

Fig. 6.27 reports the 2009 cumulative rainfall-elevation analysis.

As in the 2006 event it can be easily seen, looking at the mobile averages curves, that all the area has experienced at least 20 mm of total rainfall. This widespread value throughout the basins leads the way to the importance of the rainfall cumulative value as the major control for such events. A high lower threshold constitutes indeed an instability prone factor by means of widespread saturation effect, instead of localized kinetic energy of high intense rainfall events, as in the 2007 case.

A sort of threshold ($\sim$50 mm) for the occurrence of debris flows can be noticed, the average debris flow elevation band is in wider than the 2007 one. The mobile

average stabilizes, in terms of elevation, around the correspondent 50-80 mm of cumulative rainfall values, which is the same cumulative rainfall range of the debris flow. Except for few points, the mobile average remains below the 2000 m elevation threshold. Anyway the points cloud is much denser for this event and the mobile average may not reflect different clustering of the cloud.

Another important factor related to this graph is the centering of the points cloud around high values; debris flows occurred in fact not under very particular condition but around the center of gravity (60-80 mm of cumulative rainfall) of the event itself, meaning that the overall event has been very severe in terms of cumulative values, more than the 2007 event, for sure, but even more than the 2006 event, for which the event's cloud in centered al lower values.

2009 intensity trend showed a very similar trend remaining stable around the debris flow elevation band (except for few high intensity points), but the points cloud is mainly centered on low intensity values thus underlying, for this event, the greater importance of the cumulative rainfall variable.

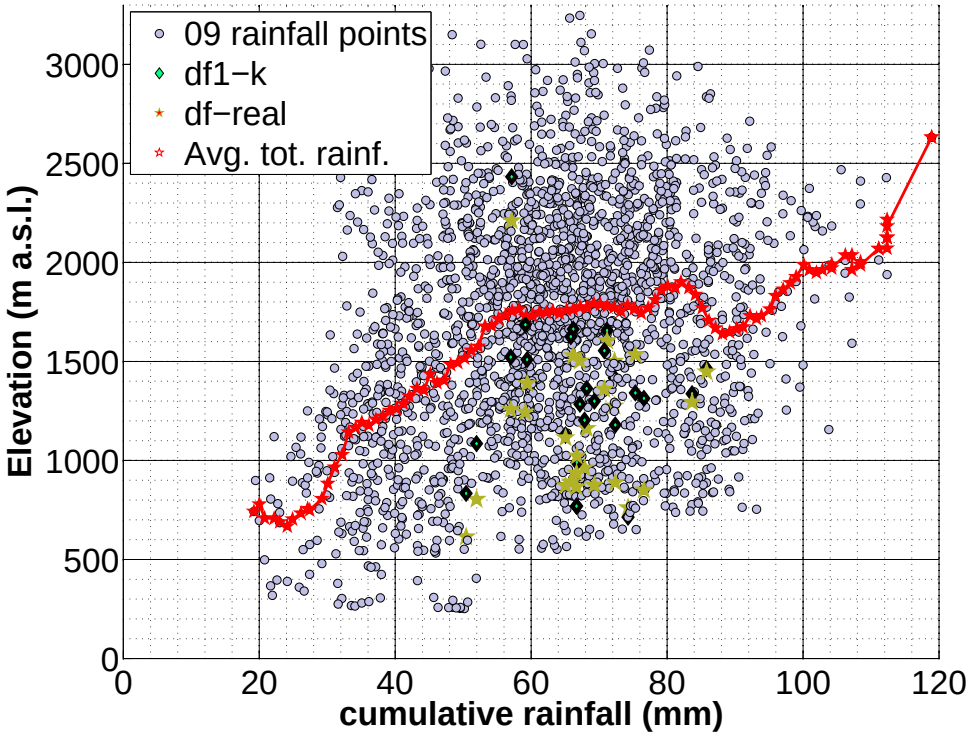

Figure 6.27: 2009 cumulative rainfall-elevation distribution and trend.

6.3.4 Frequency distribution of cumulative rainfall and intensity

The following analysis is intended to capture a picture of the three events within a unique framework.

Fig. 6.28 clearly shows that the variability of cumulative rainfall for the three studied events is particularly large for the 2007 rainstorm that shows severe conditions and debris-flow occurrences over isolated portions of the catchments. A similar pattern is observed for rainfall intensity (Fig. 6.29), with the 2007 event attaining much higher values than the 2006 and 2009 events. The distributed important cumulative rainfall over great part of the catchments comes up analyzing in particular Fig. 6.28 thus emphasizing once again the potential

instability deriving from widespread saturation (2009 event) and the 2007-2009 in between condition of the 2006 case.

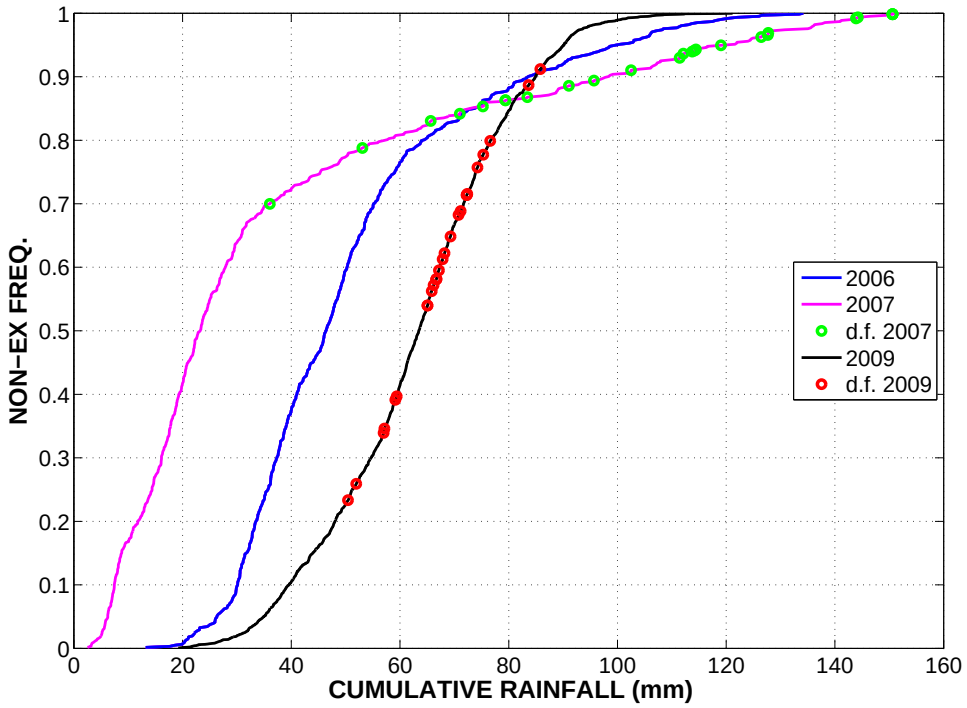

Figure 6.28: 2006 2007 2009 cumulative rainfall frequency distribution and debris-flow location: synoptic view.

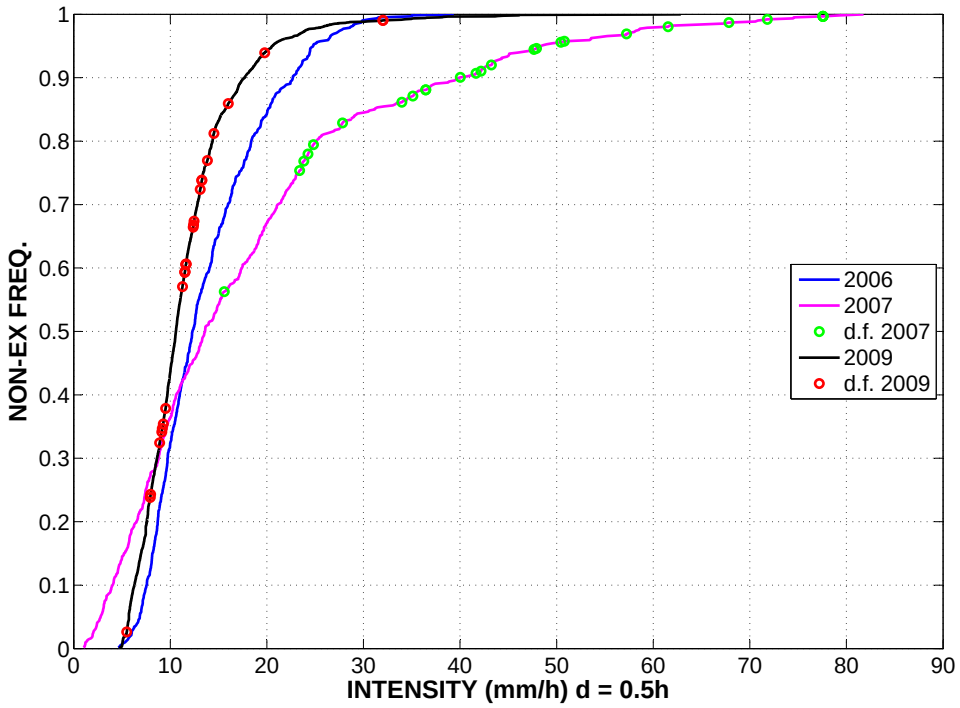

Figure 6.29: 2006 2007 2009 rainfall intensity frequency distribution and debris-flow location: synoptic view.

6.4 Hydrologic model calibration

In order to check the consistency of radar-derived rainfall fields with discharge data and to derive hydrological parameters for the analysis of debris-flow volumes, the rainfall-runoff model described in sec. 5.2 has been calibrated for the catchments listed in Tab. 11.

We used a 30-meters DTM for these hydrologic simulations at catchment scale. Figs. 6.30-6.33 report the calibrated hydrologic model outputs for the major analyzed basins related to the 2007 and 2009 events.

In the case of the Fleres catchment (Fig. 6.30), the modeling procedure was quite difficult probably due to different reasons (variability of geologic settings

and permeability within the basin, different flow paths on the opposite flanks of the valley), so we decided to synchronize the model outputs with the first significant peak, thus leading to an important overestimation of the following part of the hydrograph. The calibration carried out for the Ridanna catchment (Fig. 6.31) had an overall good performance except for a convexity on the recession limb after the peak of the hydrograph.

The Aurino at San Giorgio case (Fig. 6.32) is quite well modeled while the Talvera at Bolzano (Fig. 6.33) is well modeled for the lag time and the peak discharge but not for the rising limb that occurs later and with a faster gradient in the discharge records.

Runoff coefficients reported in Tab. 11 are coherent with the average conditions reported for the area, and usually they are greater for smaller basin characterized by rocky outcrops and glaciers (Caminata and Cadipietra), as it is expectable, and lower for larger and densely forested basins. The discharge characterized by a 2-years return period based on a Gumbel distribution applied to the maximum yearly values, was also computed (when possible) and related to the registered discharges in order to assess the magnitude of the flood. The ratios between peak registered discharge and the 2-year discharge for 2007 report usually values < 1 thus indicating the low rainfall global contribution to this event. For the case of Piana catchment it was difficult to calculate runoff coefficient and return period due to the availability of few yearly records and to the fact that the flood hydrographs were not completely registered.

The parameters obtained from the hydrologic calibration procedure have then been used in the following analyses, in particular downscaling the modeling to debris-flow basins. Peak discharge and runoff volume have been assessed for debris-flow catchments and the relations with recorded debris-flow volumes

available from ED30 database have been analyzed. This analysis will be presented in the section 6.4.1.

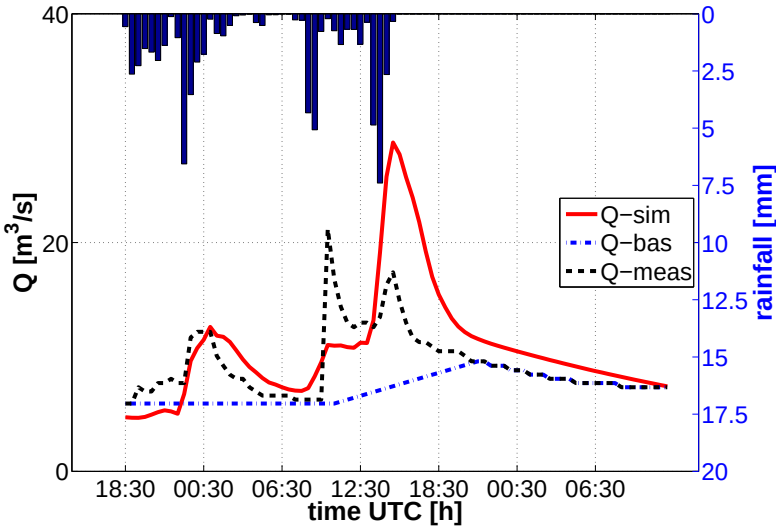

Figure 6.30: Klem model output for the Fleres basin, 2007 event.

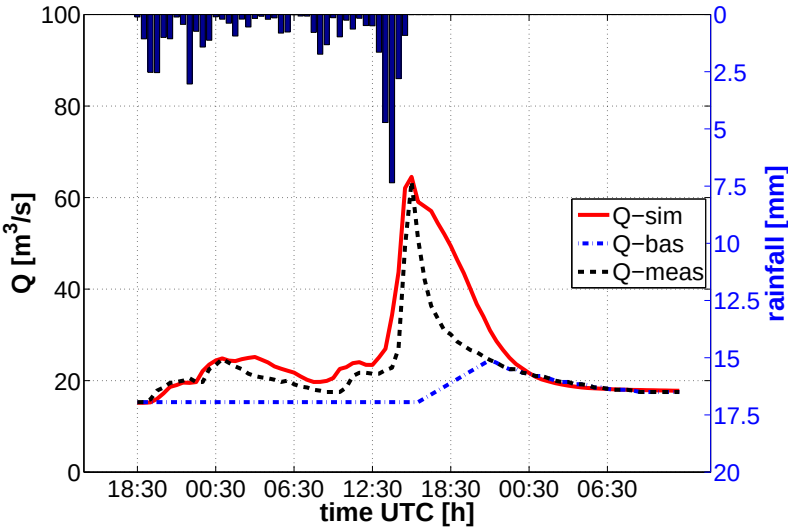

Figure 6.31: Klem model output for the Ridanna basin, 2007 event.

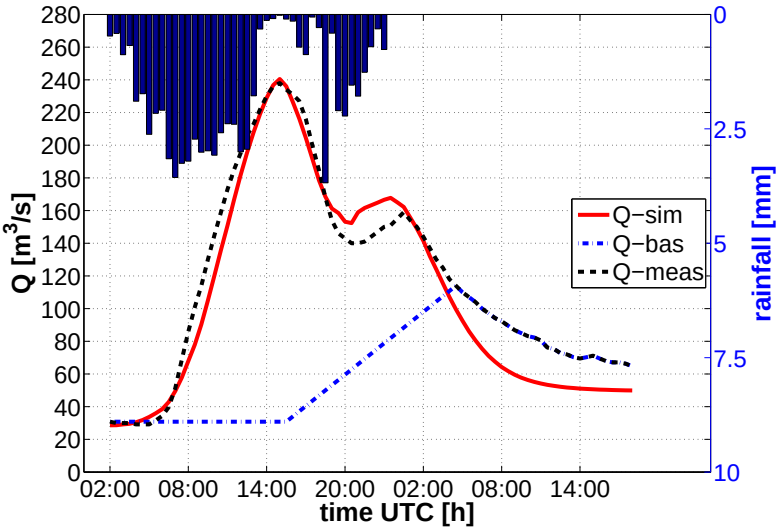

Figure 6.32: Klem model output for the Aurino at San Giorgio section, 2009 event.

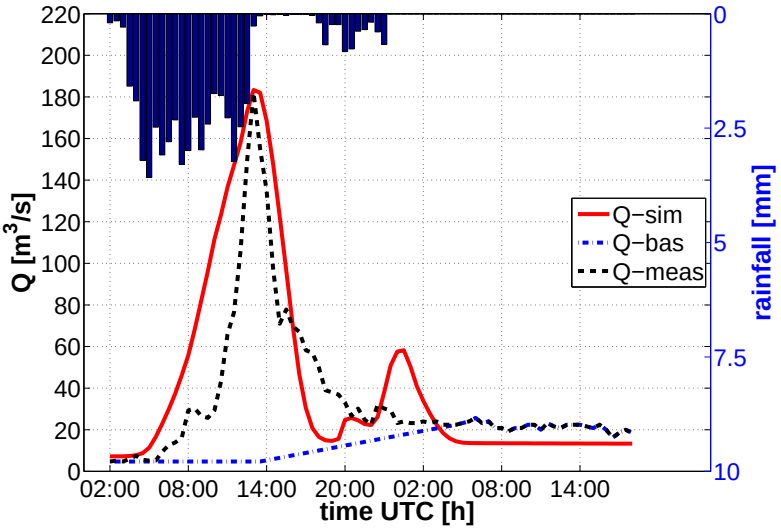

Figure 6.33: Klem model output for the Talvera at Bolzano section, 2009 event.

Table 11: For the analyzed basins, different parameters are reported: Cumulative rainfall over the watershed, registered peak discharge, the ration between peak discharge and the average discharge with a 2-year return period, the return period of the discharge based on a Gumbel distribution analysis of the registered maximum discharges and finally the runoff coefficient.

	Cumulative rainfall (mm)	**Peak discharge (m3/s)**	**Qp / Q2**	**RT Qp Gumbel**	**Runoff coefficient**
3 4 October 2006					
Fleres at Colle Isarco	63.4	76	1.84	11.63	0.15
Piana at Vedretta Piana	63.2	27.6	2.86	—	—
Racines at Stanghe	55.2	35.7	1.1	2.75	0.2
Ridanna at Vipiteno	60.7	86.8	1.2	3.03	0.11
20 21 June 2007					
Fleres at Colle Isarco	63	21.8	0.53	1.13	0.08
Piana at Vedretta Piana	11.9	9.3	0.83	—	—
Racines at Stanghe	65.3	42.2	1.26	5.1	0.12
Ridanna at Vipiteno	44.9	68.3	0.94	1.79	0.09
3 4 September 2009					
Aurino at Cadipietra	55.9	88.2	1.83	25.65	0.32
Riva at Caminata	67.4	119	1.66	8.34	0.33
Aurino at Caminata	65	160	1.55	9.16	0.21
Aurino at San Giorgio	70.9	246	1.74	23.71	0.2
Talvera at Bolzano	54.4	182	2.35	20.08	0.11

6.4.1 Analysis of rainfall and runoff response in debris-flow watersheds

Rainfall-runoff model parameters calibrated for the floods of June 21, 2007 and September 4, 2009, in different sectors of the upper Adige River basin have been applied to assess runoff response in small ungauged catchments for which data on debris-flow volume have been collected. All analyses have been carried out

using a 5-meters resolution DTM.

Data on debris-flow volumes are available from post-event field observations for 31 catchments (19 for June 2007 and 12 for September 2009).

Tab. 12 presents the linear correlation matrix between several parameters related to basin topography (catchment area and channel slope), event rainfall (total precipitation amount, rainfall volume and maximum hourly rainfall) and flood runoff (peak discharge). Basin area shows only a weak and not-significant correlation with debris-flow volume; differently from other studies (Marchi and D'Agostino, 2004), channel slope has no significant correlation with debris-flow volume. Significant correlation with debris-flow volume arise for total rainfall volume of the event, which incorporates catchment area and rainfall amount, maximum hourly rainfall rate and model-computed peak discharge. The relation between flood peak discharge and debris-flow volume is shown in Fig. 6.34

Sediment concentration has been assessed with the objective of checking the

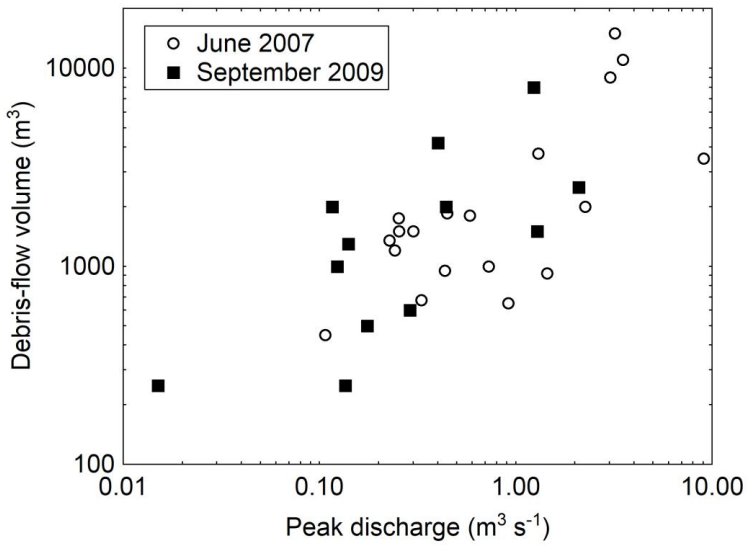

Figure 6.34: Plot of debris-flow volume versus peak discharge.

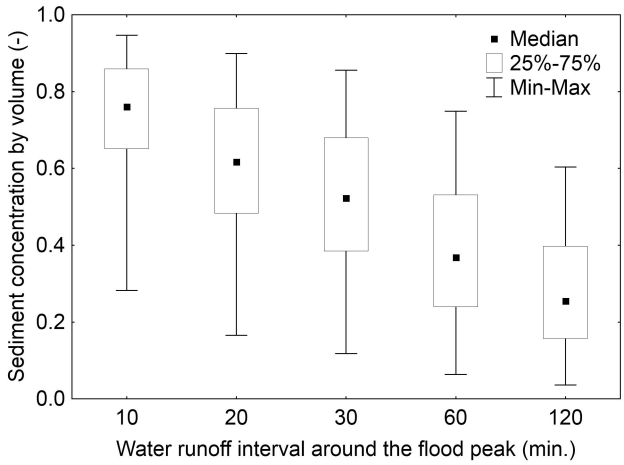

Figure 6.35: Variations of sediment concentration computed over different durations of water runoff.

consistency debris-flow volume and model-computed runoff volume. Solid volumes without voids have been assessed by assuming a porosity of 0.4 for field-estimated debris-flow volumes. The time of occurrence of debris flows is only approximately known from post-event documentation and roughly corresponds to the most intense phases of the floods. Water runoff volumes have been computed for various time intervals, ranging from 10 to 120 minutes, around the flood peak. Resulting values of sediment concentration by volume (Fig. 6.35) indicate an overall consistency between water runoff and sediment volume.

Fig. 6.36 shows the frequency distribution of sediment concentration computed considering durations of 10 and 60 minutes around the flood peak. For 10 minutes, high values of sediment concentration prevail, that are possible at debris-flow front, but are unrealistic as average values at the event scale. Most of the values of sediment concentration for a time of 60 minutes around the flood peak are in the range commonly accepted for debris flows, if also the final, more diluted parts of the surges are included. The large variability of sediment

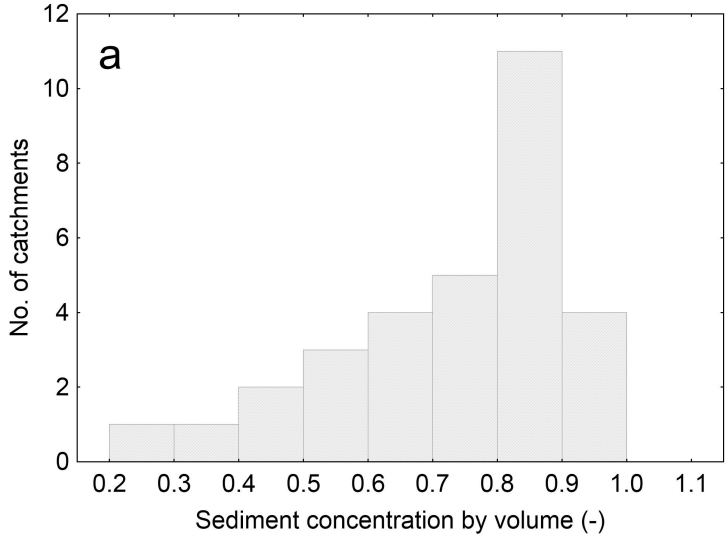

(a)

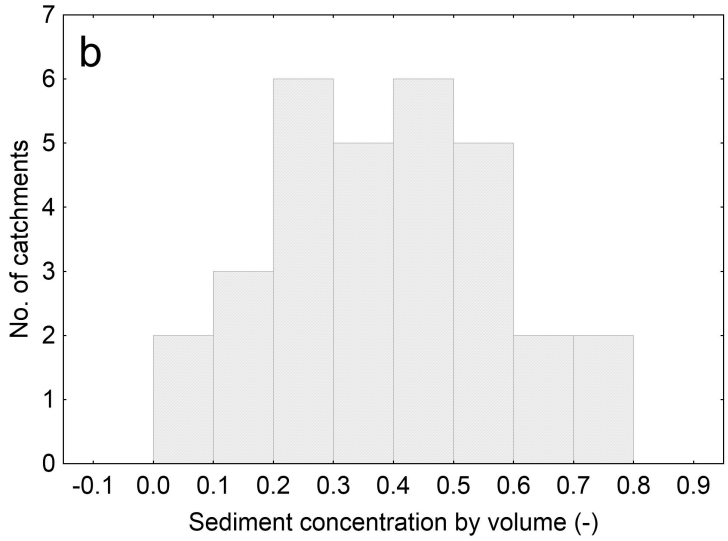

(b)

Figure 6.36: Distribution frequency of sediment concentration by volume. a) water runoff computed on a 10 minutes interval around the flood peak; b) water runoff computed on a 60-minutes interval around the flood peaks.

concentration (Fig. 6.36) can be ascribed to several factors:

- limited sediment availability in some catchments was likely the limiting factor for debris-flow volume, and resulted in low values of sediment concentration, even for short time intervals around the flood peak;
- very high values of sediment concentration can be ascribed to local sediment inputs from slope failures, not fully accounted for by the approximate balance of water and solid volumes proposed here;
- relevant approximations affect both field estimation of debris-flow volumes and water runoff modeling: opposite errors in the assessment of the two variables occur may severely bias the values of sediment concentration.

The possible impact of rainfall estimation method (radar-derived rainfall versus raingauges data interpolation) on water discharge in debris-flow catchments, and, hence, on solid concentration of debris flows and relations with observed debris-flow volumes has been investigated. The differences resulting from the two approaches to rainfall field assessment are small for the September 2009 rainstorm, whereas they are relevant for June 2007, when radar-derived rainfall is much higher than rainfall from the interpolation of raingauges data (Fig. 6.5). The influence of rainfall fields estimation method on the assessment of sediment concentration of debris flows have been tested. The application of the Mann-Whitney U test shows that the differences are significant for the debris flows of June 2007 (p-value < 0.001) whereas they are not significant for September 2009 (p-value > 0.9). For June 2007, the assessment of water runoff using raingauge data would result in unrealistically high values of sediment concentration

in debris flows (e.g. an average value of 0.6 is obtained for a duration of 60 minutes around the flood peak).

Table 12: Linear correlation matrix for topographic parameters, hydrometeorological variables and debris-flow volumes; italic indicates relations significant for p = 0.05.

	Basin area (km^2)	**Channel gradient** (%)	**Total event rainfall** (mm)	**Rainfall volume** (m^3)	**Max hourly rainfall intensity** (mm/h)	**Peak discharge** (m^3/s)	**Debris-flow volume** (m^3)
Basin area (km^2)	1.0000 p= —						
Channel gradient (%)	-.0489 p=.794	1.0000 p= —					
Total event rainfall (mm)	-.0349 p=.852	*-.3762 p=.037*	1.0000 p= —				
Rainfall volume (m^3)	*.8740 p=.000*	-.2028 p=.274	.3157 p=.084	1.0000 p= —			
Max hourly rainfall intensity (mm/h)	-.1309 p=.483	*-.3627 p=.045*	*.8218 p=.000*	.1249 p=.503	1.0000 p= —		
Peak discharge (m^3/s)	*.6814 p=.000*	-.2850 p=.120	*.4661 p=.008*	*.9401 p=.000*	.3083 p=.092	1.0000 p= —	
Debris-flow volume (m^3)	.3520 p=.052	-.2589 p=.160	.2884 p=.116	*.4206 p=.018*	*.3657 p=.043*	*.4812 p=.006*	1.0000 p= —

6.5 Discussion for the analysis at debris-flow watershed scale

A central issue of the analysis for the three selected events was to determine how the characteristics of three studied rainstorm could explain the different response observed. The comparison between the October 2006 and June 2007 events was fully homogeneous as they have hit the same catchments, thus excluding possible influence of differences in lithology, topography and land use. As to the September 2009 flood, although overall lithological and climatic settings of the areas hit by the September 2009 event are similar to those of October 2006 and June 2007 events, local differences may have affected the comparison with the effects of the event of the previous two rainstorms.

The rainstorm of October 2006 was characterized by rather low rainfall intensity and rather homogeneous spatial distribution of precipitation over the affected catchments. This resulted in a moderate flood response, which overcame the dry initial moisture conditions. The absence of debris flows can probably be ascribed to the lack of intense showers on soil and debris-mantled slopes in the central and lower parts of the catchments. It is worth reminding that the largest rainfall inputs occurred in the upper part of the Ridanna catchment, corresponding to the Rio Piana catchment (6.1, 6.13), mostly occupied by glaciers and outcropping rocks. Abundant precipitation in these impervious headwaters contributed to enhance the flood response, whereas they did not affect slopes and channels prone to debris-flow mobilization.

The rainstorm of 20-21 June 2007 was characterized by short-duration, high-intensity showers, whose spatial extent was limited to the central part of the catchments. Such precipitation triggered debris flows in small catchments, also

thank to high soil saturation due to previous rainfall and snowmelt, but was insufficient to induce appreciable water floods in the main streams. Only in the catchment of Racines at Stanghe, which lies in the sector that received the highest precipitation amounts in June 2007, peak discharge exceeded that of October 2006.

Remarkable flood response of the flood of September 2009 is consistent with spatial rainfall coverage and distribution over the catchments (Figs. 6.3, 6.16, 6.17). The reasons for the occurrence of widespread debris flows, in spite of non-extreme rainfall intensities, are rather long duration of the rainstorm, and favorable topographic conditions: a significant cluster of debris flows is located over the area in between the Talvera watershed and the Aurino valley, where repeated occurrence of debris flows is documented (Fig. 6.3).

Debris flows that occurred during two of the three studied events have been studied by considering both the control of rainstorm characteristics of debris-flow triggering and by considering possible relations between water runoff and debris flow density and volumes.

The analysis of runoff processes controlling debris flows is usually limited to instrumented catchments whereas in studies at regional scale only rainfall data are commonly used (Rickenmann and Koschni, 2010). Relating debris flows to water runoff faces difficulties in achieving a reliable representation of rainfall in debris-flow initiation areas, as well as to uncertainties in the parameterization of rainfall-runoff models (Gregoretti and Dalla Fontana, 2008). In this study, keystones for runoff assessment in debris-flow catchments were distributed rainfall fields and model parameters calibrated in downstream gauged catchments. Model-based simulation of water runoff in debris-flow catchments, together with post-event documentation of debris-flow location and magnitude, has permit-

ted estimation of sediment concentration by volume and identification of relationships between debris-flow volume and water discharge, which show better performance than the relationships between debris-flow volume and rainfall-related variables. The comparison of rainfall fields deriving from radar estimates and from rainfall data interpolation has shown that, depending on rainstorm characteristics (spatial extent, steepness of spatial gradients in rain rate), the differences can be limited or very large: this influences both rainfall threshold values for debris-flow initiation and runoff computation, required for computing concentration and analyzing relations with debris-flow volumes.

6.6 Conclusions on the selected events analysis

An integrated approach, encompassing valorization of post-event archive data, radar-rainfall analysis and rainfall-runoff modeling has been devised for the study of three selected floods, featuring different characteristics, that occurred in a sector of the Eastern Alps in 2006, 2007 and 2009. A central issue was indeed to determine how the characteristics of three studied rainstorm could explain the different observed catchment responses.

The analysis of radar-derived rainfall maps has permitted the development of several graphical tools, such as plots of maximum intensity versus cumulative or rainfall exceedance curves over catchment area, that helped outlining similarities and differences between the three rainstorm events and contributed explaining their hydrological response and geomorphic effects. Thanks to distributed hydrologic and topographic inputs it was indeed possible not only to grab the main features characterizing the storm events but also to monitor in a sort of real time the dynamic of the main hydrologic variables over the trig-

gering locations.

Occurrence and intensity of flash floods in the main streams (October 2006), debris flows in small catchments (June 2007), or both water floods and debris flows (September 2009) were controlled by space and time distribution of rainfall inputs. Rainfall-runoff modeling, in addition to enabling consistency check of precipitation and discharge data, has permitted estimating discharge and runoff volumes in a number of small ungauged catchments in which debris-flow volumes had been assessed by means of just-post-event surveys. The computation of sediment concentration by volume using model-estimated water runoff and field-observed debris-flow volumes has resulted in realistic values in most of considered catchments. The relations between water peak discharge and debris-flow volumes are significant, although not very close, and show higher correlation coefficients than those involving morphometric variables (catchment area and channel slope) and rainfall amounts. Debris flow occurrence is controlled by several factors, including topography, sediment availability and water inflows. Rate and amounts of water runoff are usually poorly known in debris-flow catchments: the results obtained in this study suggest that radar-estimated rainfall and model-computed water runoff may contribute to close this gap, improving understanding of occurrence and magnitude of debris flows.

7 Conclusions

This work has analyzed the control of hydrologic conditions on debris-flow occurrence in an alpine region. In the study area, a high-resolution digital terrain model, data from a dense raingauge network and a large database of debris-flow data were available.
In the first part of the study an analysis at regional scale, encompassing the period 2000-2010, has been carried out to characterize the morphological settings of debris-flow initiation sites and to define the rainfall intensity duration relations (including the assessment of the uncertainty related to these estimations) for the occurrence of debris flows.
In the second part the focus was on the analysis of the hydrologic response of some watersheds for a selection of events. The hydrometeorological and hydrological controls of debris-flow triggering events were examined through the analysis of three storm systems occurred on October 3-4, 2006, June 20-21 2007 and September 3-4, 2009. The purpose of the analysis was to relate the variability of the hydrological responses of the catchments to the different features that characterized the storm systems thanks to the availability of detailed and distributed input information.

The morphology of debris-flow initiation sites was analyzed by examining local slope and drainage area distributions. Slope-area relation have been analyzed also considering sites located over different lithologies. Some differences in the contributing areas especially for small size watersheds were detected; in calcareous and dolomitic setting it appears that a larger minimum area is needed for the debris flow to occur. Regarding the local slope, the two distri-

butions differ, with the debris-flow initiation points located at steeper slopes on igneous and metamorphic lithologies. This could be ascribed to the frequent occurrence of debris flows in steep channelized upper part of the catchments over metamorphic lithologies and at the interface between rocky headwaters and scree deposits, characterized by a sudden decrease of slope, on dolomitic and limestone lithologies.

The further step involved the assessment of rainfall thresholds for debris flow estimation. Rainfall intensity-duration thresholds were derived adopting a frequentist approach and filtering the series according to thresholds on cumulative rainfall, intensity, duration and distance from the reference gauge. The outcomes were compared to selected reference equations to assess the performance of the various derived thresholds. Triggering locations were also divided based on the main lithologies.

It emerged that discrimination between carbonate (calcareous and dolomitic) and other lithologies seems not to differentiate specific combinations of rainfall duration and intensity; similarly, the occurrences characterized by greater distances between the initiation sites and the reference gauges seem to be located, in higher percentage, below the reference thresholds but a clear trend is not visible.

For all the non filtered cases, part of the sample (12-18%), is located below the global threshold selected as a reference. This could be ascribed partially to the strong climatic regional variability. Part of the western portion of the study area belongs in fact, to the dry inner alpine region, with a mean annual precipitation (MAP) ranging between 400 mm and 700 mm, the result of sheltering of the mountain range to southerly and northerly winds. The MAP increases to 1300 mm in the Northern portion of the region.

Regarding the thresholds assessment, it appears that the most efficient filter applied to the series, in order to have both a good score to the reference equation and to preserve a good dataset size, is the 5-mm threshold on the intensity, i.e. at least one hour time increment with rainfall intensity > 5 mm/h.
Thresholds on rainfall intensity have shown a higher impact on the ID equation, compared to thresholds on raingauges percentage contribution and thresholds on inter distances or search radius.
The regional-scale analysis was extended to investigate the impact of the uncertainty associated with the estimation of the rainfall in the definition and the exploitation of rainfall thresholds for the forecast of possible debris-flow occurrence. An experiment was carried out at regional scale, by selecting two sets of raingauges, one assumed to represent debris-flow initiation point (DFR), the second representing the closest rainfall measurement point (MR) used for thresholds estimation. Rainfall characteristics of the events that have resulted in debris flows can be significantly different from that measured at nearby raingauges. Comparison between DFR and MR showed that lower rainfall accumulation quantiles of rainfall events above a reference ID threshold (i.e., assumed to be debris-flow triggering events) was systematically underestimated. The differences in the rainfall characteristics of the events that have resulted in debris flows estimated at the locations of the debris flows (DFR), and measured at the nearby raingauges (MR), bias the constant α and the exponent β of the ID threshold. The Critical Success Index (CSI), depends on the threshold, and decreases for higher (more severe) thresholds. The Probability of Detection (POD) was found slightly affected by the level of the threshold, whereas the False Alarm Ratio (FAR) increases significantly with increasing thresholds. It has been shown that the choice of exceedance level applied in the frequentist

method affects the error in ID estimation and the performance in debris-flow prediction. However, it was shown that optimum performance is not achieved for unbiased ID. Finally, estimation of ID thresholds based only on long duration ($>$ 12 hrs) events can improve bias and performance of estimated ID but only for high ($\alpha > 4$) rainfall thresholds. In this analysis only the natural variability of rainfall was considered as source of uncertainty. Measurement error can be an additional source of uncertainty not accounted herein. In addition, the uncertainty introduced by the method adopted to determine the threshold model is not considered from the empirical rainfall data.

The conclusions of this analysis are potentially applicable to different types of thresholds, including cumulative event rainfall-rainfall duration thresholds, and other thresholds that consider the antecedent rainfall conditions to forecast the possible occurrence of debris flows and other shallow landslides.

Using the same source of information (raingauges network records) an effort was made to improve thresholds assessment done using the nearest available record, by comparing this (DFR-MR) estimation with an interpolation of selected (max. 5) nearest gauges. Interpolations have shown correlation improvement, though limited to the case of bad correlation between DFR and MR, thus being important source of information when MR estimation is poor. The choice of the 5 nearest gauges was anyway suffering from a bias probably linked to the distance values as a matter of fact the relation to distances for the different interpolations, showed a clear trend, thus emphasizing the explanatory role of distance. The influence on the POD, FAR and CSI and the ratio of estimated/theoretical α and β has been almost negligible thus leading to the general conclusion of a moderate improvement given by the interpolation technique, but still significant especially in the case of poor DFR-MR correlation.

In the second part of the thesis the hydrometeorological and hydrological controls of debris-flow triggering have been examined in detail through the analysis of three storm systems occurred on October 3-4, 2006, June 20-21 2007 and September 3-4, 2009. The purpose of the analysis was to determine how the characteristics of three studied rainstorm could explain the different observed catchment responses.

An integrated approach, including the valorization of post-event archive data, radar-rainfall analysis and rainfall-runoff modeling has been devised for the three selected floods. The analysis of radar-derived rainfall maps has permitted the development of several graphical tools, such as plots of maximum intensity versus cumulative or rainfall exceedance curves over catchment area, that helped outlining similarities and differences between the three rainstorm events and contributed explaining their hydrological response and geomorphic effects. Occurrence and intensity of flash floods in the main streams (October 2006), debris flows in small catchments (June 2007), or both water floods and debris flows (September 2009) were controlled by space and time distribution of rainfall inputs. The role of antecedent conditions was also assessed by means of gauges data analysis and the outputs of this analysis stressed the almost dry antecedent conditions in the case of 2006, moderately wet for 2009 event and very wet for 2007, thus contributing significantly it the explanation of the different responses.

Rainfall-runoff modeling, in addition to enabling consistency check of precipitation and discharge data, has permitted estimating discharge and runoff volumes in a number of small ungauged catchments in which debris-flow volumes had been assessed by means of post-event surveys. The computation of sediment

concentration by volume using model-estimated water runoff and field-observed debris-flow volumes has resulted in realistic values in most of considered catchments. The relations between water peak discharge and debris-flow volumes are significant, although not very close, and show higher correlation coefficients than those involving morphometric variables (catchment area and channel slope) and rainfall amounts. Debris-flow occurrence is controlled by several factors, including topography, sediment availability and water inflows. Rate and amounts of water runoff are usually poorly known in debris-flow catchments: the results obtained in this study suggest that radar-estimated rainfall and model-computed water runoff may contribute to close this gap, improving understanding of occurrence and magnitude of debris flows.

Acknowledgements

The author thanks the supervisors for the patient and constant support and for having been a fundamental reference to increase the scientific strength of the research.

Rudolf Pollinger, director of the 30^{th} Division of the Autonomous Province of Bolzano is aknowledged for making available the database on the occurrence of instability phenomena that has been one of the major sources of information of the present work. Pierpaolo Macconi and Omar Formaggioni kindly provided technical information on the GIS management of the database.

The collaboration with Efthymios Nikolopoulos on the assessment of the uncertainty related to rainfall thresholds for debris flows initiation has been intense and has brought to a fertile exchange.

Francesco Marra and Davide Zoccatelli kindly provided me with hydrologic data, models and suggestions for the research activity.

Sue Cannon and the Landslide Hazard Program team at USGS in Golden, Colorado, deserve a particular mention for the advices related to the ongoing research activity and for having kindly worked together on the interpretation of the variability leading to debris-flow initiation.

Lastly the author wants to thank Marco Cavalli and Luca Schenato for the huge help across these years, for being mentors and for having transmitted passion for research.

List of Figures

List of Tables

References

Aleotti, P. (2004). A warning system for rainfall-induced shallow failures. *Engineering Geology*, *73*, 247–265.

Anderson, M. G., and Burt, T. P. (1978). The role of topography in controlling throughflow generation. *Earth Surface Processes*, *3*, 331344.

Badoux, A., Graf, C., Rhyner, J., Kuntner, R., and McArdell, B. W. (2009). A debris-flow alarm system for the Alpine Illgraben catchment: design and performance. *Natural Hazards*, *49*, 517–539.

Baum, R. L., Godt, J. W., and Savage, W. Z. (2010). Estimating the timing and location of shallow rainfall-induced landslides using a model for transient, unsaturated infiltration. *Journal of Geophysical Research: Earth Surface*, *115-F03013*.

Berne, A., and Krajewski, W. (2013). Radar for hydrology: Unfulfilled promise or unrecognized potential? *Advances in Water Resources*, *51*, 357–366.

Berti, M., Martina, M. L. V., Franceschini, S., Pignone, S., Simoni, A., and Pizziolo, M. (2012). Probabilistic rainfall thresholds for landslide occurrence using a Bayesian approach. *Journal of Geophysical Research*, *117*.

Borga, M., Dalla Fontana, G., Gregoretti, C., and Marchi, L. (2002). Assessment of shallow landsliding by using a physically based model of hillslope stability. *Hydrological Processes*, *16*, 2833–2851.

Brand, E. (1981). Some thoughts on rain-induced slope failures. *Proceedings of the International Conference on Soil Mechanics and Foundation Engineering*, *3*, 373–376.

Brardinoni, F., Church, M., Simoni, A., and Macconi, P. (2012). Lithologic and glacially conditioned controls on regional debris-flow sediment dynamics. *Geology*, *40*, 455–458.

Brunetti, M. T., Peruccacci, S., Rossi, M., Luciani, S., Valigi, D., and Guzzetti, F. (2010). Rainfall thresholds for the possible occurrence of landslides in Italy. *Nat. Hazards Earth Syst. Sci.*, *10*, 447–458.

Caine, N. (1980). The Rainfall Intensity: Duration Control of Shallow Landslides and Debris Flows. *Geografiska Annaler. Series A, Physical Geography*, *62*, 23–27. ArticleType: research-article / Full publication date: 1980 / Copyright 1980 Swedish Society for Anthropology and Geography.

Cannon, S., Boldt, E., Laber, J., Kean, J., and Staley, D. (2011). Rainfall intensity-duration thresholds for postfire debris-flow emergency-response planning. *Natural Hazards*, *59*, 209–236.

Cannon, S. H., and Gartner, J. E. (2005). Wildfire-related debris flow from a hazards perspective. In *Debris-flow Hazards and Related Phenomena* Springer Praxis Books (pp. 363–385). Springer Berlin Heidelberg.

Cannon, S. H., Kirkham, R. M., and Parise, M. (2001). Wildfire-related debris-flow initiation processes, Storm King Mountain, Colorado. *Geomorphology*, *39*, 171–188.

Cazorzi, F. (2002). *HyGrid2k2, Guida di Riferimento*. Technical Report Università degli Studi di Udine.

Coe, J. A., Glancy, P. A., and Whitney, J. W. (1997). Volumetric analysis and hydrologic characterization of a modern debris flow near Yucca Mountain, Nevada. *Geomorphology*, *20*, 11–28.

Coe, J. A., Kinner, D. A., and Godt, J. W. (2008). Initiation conditions for debris flows generated by runoff at Chalk Cliffs, central Colorado. *Geomorphology*, *96*, 270–297.

Comiti, F., Marchi, L., Macconi, P., Arattano, M., Bertoldi, G., Borga, M., Brardinoni, F., Cavalli, M., D'Agostino, V., Penna, D., and Theule, J. (2014). A new monitoring station for debris flows in the European Alps: first observations in the Gadria basin. *Natural Hazards, under revision*, *xx*.

Costa, J. E. (1984). Physical Geomorphology of Debris Flows. In D. J. E. Costa, and P. D. P. J. Fleisher (Eds.), *Developments and Applications of Geomorphology* (pp. 268–317). Springer Berlin Heidelberg.

Coussot, P., and Meunier, M. (1996). Recognition, classification and mechanical description of debris flows. *Earth-Science Reviews*, *40*, 209–227.

Crosta, G. B., and Frattini, P. (2001). Rainfall thresholds for the triggering of soil slips and debris flows. In *Mediterranean Storms Conference 2000* (pp. 463–488). Siena, Italy: GNDCI. EGS.

Deganutti, A., Marchi, L., and Arattano, M. (2000). Rainfall and debris flow occurrence in the Moscardo basin (Italian Alps). In *proceddings of Second International Conference on Debris-flow Hazard Mitigation: Mechanics, Prediction, and Assessment* (pp. 67–72). Rotterdam.

Del Favero, R. (2004). *I boschi delle regioni alpine italiane: tipologia, funzionamento, selvicoltura*. Padova: CLUEP.

Godt, J. W., and Coe, J. A. (2007). Alpine debris flows triggered by a 28 July 1999 thunderstorm in the central Front Range, Colorado. *Geomorphology*, *84*, 80–97.

Gregoretti, C., and Dalla Fontana, G. (2008). The triggering of debris flow due to channel-bed failure in some alpine headwater basins of the Dolomites: analyses of critical runoff. *Hydrological Processes*, *22*, 22482263.

Guzzetti, F., Peruccacci, S., Rossi, M., and Stark, C. P. (2007). Rainfall thresholds for the initiation of landslides in central and southern Europe. *Meteorology and Atmospheric Physics*, *98*, 239–267.

Guzzetti, F., Peruccacci, S., Rossi, M., and Stark, C. P. (2008). The rainfall intensityduration control of shallow landslides and debris flows: an update. *Landslides*, *5*, 3–17.

Guzzetti, F., Reichenbach, P., Cardinali, M., Galli, M., and Ardizzone, F. (2005). Probabilistic landslide hazard assessment at the basin scale. *Geomorphology*, *72*, 272–299.

Hungr, O., Morgan, G. C., and Kellerhals, R. (1984). Quantitative analysis of debris torrent hazards for design of remedial measures. *Canadian Geotechnical Journal*, *21*, 663–677.

Innes, J. L. (1983). Debris flows. *Progress in Physical Geography*, *7*, 469–501.

Iverson, R. M., Reid, M. E., and LaHusen, R. G. (1997). Debris-Flow Mobilization from Landslides1. *Annual Review of Earth and Planetary Sciences*, *25*, 85–138.

Jakob, M. (2005). A size classification for debris flows. *Engineering Geology*, *79*, 151–161.

Jakob, M., Owen, T., and Simpson, T. (2012). A regional real-time debris-flow warning system for the District of North Vancouver, Canada. *Landslides*, *9*, 165–178.

Jakob, M., and Weatherly, H. (2003). A hydroclimatic threshold for landslide initiation on the North Shore Mountains of Vancouver, British Columbia. *Geomorphology*, *54*, 137–156.

Jibson, R. W. (1989). Debris flows in southern Puerto Rico. *Geological Society of America Special Papers*, *236*, 2956.

Johnson, A., and Rodine, J. (1984). Debris flow. In *Slope instability*. D. Brunsden & D.B. Prior., New York.

Li, M., and Shao, Q. (2010). An improved statistical approach to merge satellite rainfall estimates and raingauge data. *Journal of Hydrology*, *385*, 51–64.

Macconi, P., and Sperling, M. (2008). Il sistema di documentazione eventi ED30. In *IHR- Sistema Informativo sui rischi idrogeologici*. Bolzano. (Provincia Autonoma di Bolzano - Alto Adige, Ripartizione Opere Idrauliche ed.).

Marchi, L., Cavalli, M., and Goldin, B. (2014). *Progetto GESTO: Gestione del trasporto di sedimento nei piccoli bacini montani - Final report contribution of CNR-IRPI, unpublished*. Technical Report.

Marchi, L., and D'Agostino, V. (2004). Estimation of debris-flow magnitude in the Eastern Italian Alps. *Earth Surface Processes and Landforms*, *29*, 207220.

Marra, F. (2013). *Procedura integrata di analisi e correzione delle osservazioni radarper la stima di precipitazioni intense in ambiente alpino*. PhD thesis University of Padova.

Marra, F., Borga, M., and Creutin, J.-D. (2013). Precipitation thresholds and debris flow warning: comparing gauge versus weather radar detection. In *EGU General Assembly Conference Abstracts* (p. 11628). volume 15.

Matheron, G. (1963). *Trait de gostatistique applique...: Georges Matheron. Prface de F. [Fernand] Blondel. Le Krigeage....* ditions Technip.

Montgomery, D. R. (2001). Slope Distributions, Threshold Hillslopes, and Steady-state Topography. *American Journal of Science*, *301*, 432–454.

Montgomery, D. R., and Foufoula-Georgiou, E. (1993). Channel network source representation using digital elevation models. *Water Resources Research*, *29*, 39253934.

Nikolopoulos, E. I., Crema, S., Marchi, L., Marra, F., Guzzetti, F., and Borga, M. (2014). Impact of uncertainty in rainfall estimation on the identification of rainfall thresholds for debris-flow occurrence. *Geomorphology, under revision*, *xx-2014*.

Norbiato, D., Borga, M., and Dinale, R. (2009). Flash flood warning in ungauged basins by use of the flash flood guidance and model-based runoff thresholds. *Meteorological Applications*, *16*, 6575.

Norbiato, D., Borga, M., Sangati, M., and Zanon, F. (2007). Regional frequency analysis of extreme precipitation in the eastern Italian Alps and the August 29, 2003 flash flood. *Journal of Hydrology*, *345*, 149–166.

Panziera, L., Germann, U., Gabella, M., and Mandapaka, P. V. (2011). NORA-Nowcasting of Orographic Rainfall by means of Analogues. *Quarterly Journal of the Royal Meteorological Society*, *137*, 2106–2123.

Peruccacci, S., Brunetti, M. T., Luciani, S., Vennari, C., and Guzzetti, F. (2012). Lithological and seasonal control on rainfall thresholds for the possible initiation of landslides in central Italy. *Geomorphology*, *139140*, 79–90.

Phillips, C. J., and Davies, T. R. (1991). Determining rheological parameters of debris flow material. *Geomorphology*, *4*, 101–110.

Reichenbach, P., Cardinali, M., Vita, P. D., and Guzzetti, F. (1998). Regional hydrological thresholds for landslides and floods in the Tiber River Basin (central Italy). *Environmental Geology*, *35*, 146–159.

Rickenmann, D. (1999). Empirical Relationships for Debris Flows. *Natural Hazards*, *19*, 47–77.

Rickenmann, D., and Koschni, A. (2010). Sediment loads due to fluvial transport and debris flows during the 2005 flood events in Switzerland. *Hydrological Processes*, *24*, 9931007.

Rossi, M., Kirschbaum, D., Luciani, S., Mondini, A. C., and Guzzetti, F. (2012). TRMM satellite rainfall estimates for landslide early warning in Italy: preliminary results. (pp. 85230D–85230D–7). volume 8523.

Salvati, P., Bianchi, C., Rossi, M., and Guzzetti, F. (2010). Societal landslide and flood risk in Italy. *Natural Hazards and Earth System Science*, *10*, 465–483.

Scheidl, C., Rickenmann, D., and McArdell, B. W. (2013). Runout Prediction of Debris Flows and Similar Mass Movements. In C. Margottini, P. Canuti, and K. Sassa (Eds.), *Landslide Science and Practice* (pp. 221–229). Springer Berlin Heidelberg.

Schneuwly-Bollschweiler, M., and Stoffel, M. (2012). Hydrometeorological triggers of periglacial debris flows in the Zermatt valley (Switzerland) since 1864. *Journal of Geophysical Research*, *117*.

Shepard, D. (1968). A Two-dimensional Interpolation Function for Irregularly-spaced Data. In *Proceedings of the 1968 23rd ACM National Conference* ACM '68 (p. 517524). New York, NY, USA: ACM.

Simoni, A. (2005). Hydrologic prediction and geologic reality in debris flow triggering. *proceedings of the International Symposium on Landslide Hazard in Orogenic Zone from the Hymalaya to Island Arc in Asia, Kathmandu, Nepal*, (pp. 185–195).

Staley, D. M., Kean, J. W., Cannon, S. H., Schmidt, K. M., and Laber, J. L. (2013). Objective definition of rainfall intensityduration thresholds for the initiation of post-fire debris flows in southern California. *Landslides*, *10*, 547–562.

Stoffel, M., Bollschweiler, M., and Beniston, M. (2011). Rainfall characteristics for periglacial debris flows in the Swiss Alps: past incidencespotential future evolutions. *Climatic Change*, *105*, 263–280.

Strangeways, I. (2006). *Precipitation: Theory, Measurement and Distribution*. Cambridge University Press.

Tarolli, P., and Dalla Fontana, G. (2009). Hillslope-to-valley transition morphology: New opportunities from high resolution DTMs. *Geomorphology*, *113*, 47–56.

Tecca, P. R., Galgaro, A., Genevois, R., and Deganutti, A. M. (2003). Development of a remotely controlled debris flow monitoring system in the Dolomites (Acquabona, Italy). *Hydrological Processes*, *17*, 17711784.

Wieczorek, G. F. (1996). Landslides: investigation and mitigation. chapter 4 - Landslide triggering mechanisms. *Transportation Research Board Special Report*, *ch 4*.

Wieczorek, G. F., and Glade, T. (2005). Climatic factors influencing occurrence of debris flows. In *Debris-flow Hazards and Related Phenomena* Springer Praxis Books (pp. 325–362). Springer Berlin Heidelberg.

Zangl, G. (2007). Small-scale variability of orographic precipitation in the Alps: Case studies and semi-idealized numerical simulations. *Quarterly Journal of the Royal Meteorological Society*, *133*, 1701–1716.

Zanon, F., Borga, M., Zoccatelli, D., Marchi, L., Gaume, E., Bonnifait, L., and Delrieu, G. (2010). Hydrological analysis of a flash flood across a climatic and geologic gradient: The September 18, 2007 event in Western Slovenia. *Journal of Hydrology*, *394*, 182–197.

Zoccatelli, D., Borga, M., Zanon, F., Antonescu, B., and Stancalie, G. (2010). Which rainfall spatial information for flash flood response modelling? A numerical investigation based on data from the Carpathian range, Romania. *Journal of Hydrology*, *394*, 148–161.